

Marquette University

e-Publications@Marquette

---

Dissertations (1934 -)

Dissertations, Theses, and Professional  
Projects

---

## A Study on the Hierarchical Control Structure of the Islanded Microgrid

Fahad Shumran Alshammari  
*Marquette University*

Follow this and additional works at: [https://epublications.marquette.edu/dissertations\\_mu](https://epublications.marquette.edu/dissertations_mu)



Part of the [Engineering Commons](#)

---

### Recommended Citation

Alshammari, Fahad Shumran, "A Study on the Hierarchical Control Structure of the Islanded Microgrid" (2022). *Dissertations (1934 -)*. 2052.

[https://epublications.marquette.edu/dissertations\\_mu/2052](https://epublications.marquette.edu/dissertations_mu/2052)

A STUDY ON THE HIERARCHICAL CONTROL  
STRUCTURE OF THE ISLANDED  
MICROGRID

by

Fahad Alshammari

A Dissertation submitted to the Faculty of the Graduate School,  
Marquette University,  
in Partial Fulfillment of the Requirements for  
the Degree of Doctor of Philosophy

Milwaukee, Wisconsin

December 2022

ABSTRACT  
A STUDY ON THE HIERARCHICAL CONTROL  
STRUCTURE OF THE ISLANDED  
MICROGRID

Fahad Alshammari

Marquette University, 2022

The microgrid is essential in promoting the power system's resilience through its ability to host small-scale DG units. Furthermore, the microgrid can isolate itself during main grid faults and supply its demands. However, islanded operation of the microgrid is challenging due to difficulties in frequency and voltage control. In islanded mode, grid-forming units collaborate to control the frequency and voltage. A hierarchical control structure employing the droop control technique provides these control objectives in three consecutive levels: primary, secondary, and tertiary. However, challenges associated with DG units in the vicinity of distribution networks limit the effectiveness of the islanded mode of operation.

In MV and LV distribution networks, the X/R ratio is low; hence, the frequency and voltage are related to the active and reactive power by line parameters. Therefore, frequency and voltage must be tuned for changes in active or reactive powers. Furthermore, the line parameters mismatch causes the voltage to be measured differently at each bus due to the different voltage drops in the lines. Hence, a trade-off between voltage regulation and reactive power sharing is formed, which causes either circulating currents for voltage mismatch or overloading for reactive power mismatch. Finally, the economic dispatch is usually implemented in tertiary control, which takes minutes to hours. Therefore, an estimation algorithm is required for load and renewable energy quantities forecasting. Hence, prediction errors may occur that affect the stability and optimality of the control.

This dissertation aims to improve the power system resilience by enhancing the operation of the islanded microgrid by addressing the above-mentioned issues. Firstly, a linear relationship described by line parameters is used in droop control at the primary control level to accurately control the frequency and voltage based on measured active and reactive power. Secondly, an optimization-based consensus secondary control is presented to manage the trade-off between voltage regulation and reactive power sharing in the inductive grid with high line parameters mismatch. Thirdly, the economic dispatch-based secondary controller is implemented in secondary control to avoid prediction errors by depending on the measured active and reactive powers rather than the load and renewable energy generation estimation. The developed methods effectively resolve the frequency and voltage control issues in MATLAB/SIMULINK simulations.

## ACKNOWLEDGMENTS

Fahad Alshammari

First praise is to Allah, the Almighty, on whom ultimately I depend for sustenance and guidance.

I would like to thank my advisor Prof. Ayman EL-Refaie for his help, guidance, support, and patience. He is one of the most intelligent people I have ever met. I always learn something every time we meet. I still remember some of his questions during our meetings that brought new ideas while I was trying to find answers. His guidance helped this work to be done and published. I enjoyed taking courses with him.

It is also my pleasure to thank my committee members, Prof. Hayat, Majeed, Prof. Yaz, Edwin, and Prof. Weise, Nathan, for their valuable comments about my research and encouraging words to start my career after.

A special thanks to my professors during my Ph. D courses, including Prof. Yaz, Edwin, who I learned from him about linear algebra beyond basic and engineering mathematics in general. Also, Prof. Josse, Fabien for teaching me the probability and random variable course. In addition to Dr. Tallam, Rangarajan who inspired me to dig more into Microgrid's state of art technologies.

I would also like to thank my retired professors, Prof. Demerdash, Nabeel, and Dr. Brown, Ronald. I have learned a lot from their knowledge of electrical machines and control. I am grateful to have most of their last courses offered by the university.

My sincere gratitude goes out to my colleagues and friends at Marquette, including Mr. Ali Alqarni, Mr. Musehaf Mudwah, and Mr. Hesham Badahdah for always being around me in tough times.

To all my friends and colleagues in Werner's Sustainable Energy lab, including Mr. Vahid, Sina, and Dr. Ma Qingqing.

I am also so grateful to have such a supportive family back home for their ongoing support and encouragement, especially my siblings Mohammad, Ahmed, Abdullah, and Merriam.

## DEDICATION

I would like to dedicate this work to my parents, Mr. Shumran and Mrs. Talia. You're always living in my heart and memories. Also, to my wife Mona and children Juri and Faisal.

## TABLE OF CONTENTS

ACKNOWLEDGMENTS . . . . .	i
DEDICATION . . . . .	ii
LIST OF TABLES . . . . .	viii
LIST OF FIGURES . . . . .	ix
Nomenclature . . . . .	xiii
<b>1 INTRODUCTION . . . . .</b>	<b>1</b>
1.1 Significance of the Research Topic . . . . .	1
1.2 Problem Statements . . . . .	8
1.3 Dissertation Organization . . . . .	9
<b>2 LITERATURE REVIEW . . . . .</b>	<b>11</b>
2.1 Microgrid Role in Improving Power System Resilience . . . . .	11
2.1.1 Resilience-based Planning . . . . .	13
2.1.2 Resilience-based Response . . . . .	14
2.1.3 Resilience-based Restoration . . . . .	15
2.2 The Concept of Microgrid . . . . .	16
2.2.1 Microgrid Architectures and Components . . . . .	17
2.2.2 Microgrid Operation . . . . .	20
2.2.3 Microgrid Control . . . . .	23
2.2.4 Microgrid Protection . . . . .	25
2.2.5 Microgrid Economic Operation . . . . .	26
2.2.6 Microgrid Cybersecurity . . . . .	27

2.3	Hierarchical Control Structure in Islanded AC Microgrid . . . . .	29
2.3.1	Voltage and Current Control . . . . .	30
2.3.2	Power Quality Control . . . . .	34
2.3.3	Primary Control Level . . . . .	36
2.3.4	Secondary Control Level . . . . .	40
2.3.5	Tertiary Control Level . . . . .	43
3	GENERALIZED DROOP CONTROL . . . . .	45
3.1	Introduction . . . . .	45
3.2	Primary Control in Islanded Microgrid . . . . .	46
3.2.1	Droop Control in Mixed Impedance Microgrid . . . . .	48
3.2.2	Droop Control Equations . . . . .	50
3.3	The Proposed Generalized Droop Control . . . . .	51
3.3.1	Derivation of Normalized Dependency Matrix . . . . .	52
3.3.2	Identify the Normalized Dependency Matrix Elements . . . . .	52
3.4	Simulations Results . . . . .	54
3.4.1	Resistive Grid . . . . .	56
3.4.2	Mixed Impedance Grid . . . . .	56
3.4.3	Inductive Grid . . . . .	56
3.5	Conclusions . . . . .	60
4	CONSENSUS OPTIMIZATION-BASED SECONDARY CONTROL . . . . .	61
4.1	Introduction . . . . .	61
4.2	Secondary Control in Islanded Microgrid . . . . .	63

4.2.1	Reactive power-sharing . . . . .	65
4.2.2	Sensitivity Analysis . . . . .	67
4.3	Analysis of Optimization-Based Control for Uniform Power-Sharing between Units . . . . .	69
4.4	Proposed Optimization-based Consensus Control . . . . .	70
4.4.1	Objective Function . . . . .	71
4.4.2	Nominal Frequency Constraint . . . . .	71
4.4.3	Terminal Voltage constraint . . . . .	72
4.4.4	Minimization Algorithm . . . . .	72
4.5	Simulation Results . . . . .	73
4.5.1	Control Objective . . . . .	74
4.5.2	Communication Channel Comparison . . . . .	81
4.5.3	Controller Behavior Under Line Parameters Mismatch . . . . .	83
4.5.4	Resilience-based Cybersecurity . . . . .	84
4.6	Conclusions . . . . .	89
5	ECONOMIC DISPATCH-BASED SECONDARY CONTROL . . . . .	90
5.1	Introduction . . . . .	90
5.2	Tertiary Control in islanded Microgrid . . . . .	91
5.2.1	Optimal Power Flow . . . . .	91
5.2.2	Economic Dispatch . . . . .	95
5.3	Proposed Economic Dispatch-based Secondary Control . . . . .	95
5.3.1	Cost Minimization . . . . .	96
5.3.2	Active and Reactive power management . . . . .	96

5.3.3	Frequency and Voltage restorations . . . . .	97
5.4	Simulation Results . . . . .	99
5.4.1	Performance of Controller . . . . .	100
5.4.2	Comparison with decentralized secondary control . . . . .	102
5.5	Conclusions . . . . .	104
6	SCALABILITY VALIDATION ON CIGRE NORTH AMERICA MICROGRID BENCHMARK SYSTEM . . . . .	105
6.1	Introduction . . . . .	105
6.2	CIGRE North America LV Distribution System . . . . .	105
6.3	Generalized Droop Control . . . . .	109
6.4	Optimization-Based Consensus Secondary Control . . . . .	111
6.5	Economic Dispatch Secondary Control . . . . .	114
6.5.1	The effect of conductivity on economic dispatch. . . . .	114
6.6	Conclusions . . . . .	117
7	CONCLUSIONS . . . . .	118
7.1	Summary and Contributions . . . . .	118
7.1.1	Key Contributions . . . . .	120
7.2	Recommendation and Future work . . . . .	121
	BIBLIOGRAPHY . . . . .	123
A	PRELIMINARY ON GRAPH THEORY . . . . .	140
A.1	Definitions and Connectivity . . . . .	140
A.2	Graph Matrices . . . . .	141
A.3	Directed Graph Example . . . . .	142

B	CVX/CVXGEN . . . . .	143
B.1	An Overview . . . . .	143
B.2	Generating the Custom Code . . . . .	144
C	CIGRE NORTH AMERICA MICROGRID BENCHMARK . . . . .	146
C.1	An Overview . . . . .	146
C.2	System specifications . . . . .	146
C.3	Network Data . . . . .	146
C.4	Loads Data . . . . .	147

**LIST OF TABLES**

2.1	Maximum odd harmonic current distortion . . . . .	36
3.1	Specifications of the test system . . . . .	55
4.1	Specifications of the test system . . . . .	75
5.1	Examples of constraints applied to OPF. . . . .	93
5.2	Specifications of the test system . . . . .	101
6.1	The modified commercial feeder parameters . . . . .	108
C.1	Connections and line parameters of the commercial feeder of North American LV distribution network benchmark . . . . .	148
C.2	Primitive impedance matrices of three-phase overhead lines of North American LV distribution network benchmark . . . . .	148
C.3	Primitive impedance matrices of three-phase underground lines of North American LV distribution network benchmark . . . . .	149
C.4	Load parameters of North American LV distribution network benchmark	149

## LIST OF FIGURES

1.1	Annual number of reported weather- and non-weather-related power outages in the U.S., 1984–2012. . . . .	2
1.2	Classification of power system resilience in terms of the time of an event’s occurrence. . . . .	3
1.3	The microgrid world market by region from 2015 to 2024. . . . .	4
1.4	The hierarchical control structure. . . . .	5
2.1	The performance levels of a resilient power system in the face of a disruptive event. . . . .	12
2.2	Microgrid architectures. . . . .	18
	(a) AC microgrid . . . . .	18
	(b) DC microgrid . . . . .	18
	(c) Hybrid microgrid . . . . .	18
2.3	Power and energy densities of different energy storage devices. . . . .	20
2.4	Microgrid transition status . . . . .	23
2.5	Challenges in protection associated with AC microgrids . . . . .	26
2.6	Hierarchical control structure. . . . .	31
2.7	Grid-following unit . . . . .	33
2.8	Grid-forming unit . . . . .	34
3.1	The hierarchical control structure of grid-forming units. . . . .	48
3.2	Inverter-based unit connected to a grid bus. . . . .	49
3.3	The block diagram of the proposed droop controller. . . . .	54
3.4	Single line diagram of the test system. . . . .	55

3.5	System behavior under a resistive grid. . . . .	57
3.6	System behavior under a mixed impedance grid. . . . .	58
3.7	System behavior under an inductive grid. . . . .	59
4.1	Grid-forming unit in the hierarchical control structure. . . . .	65
4.2	Droop characteristics of two grid-forming units . . . . .	67
	(a) $P - \omega$ droop with similar droop coefficients . . . . .	67
	(b) $Q - V$ droop with equal droop coefficients. . . . .	67
4.3	Two units are supplying a common load. . . . .	68
4.4	Sensitivity analysis of the line impedance mismatch to the reactive power mismatch. . . . .	68
4.5	An example of constructing an adjacency matrix for four nodes. . . . .	69
4.6	Optimization-based consensus secondary control. . . . .	73
4.7	Single-line diagram of the microgrid test system . . . . .	74
4.8	Communication topology employed for the optimization-based secondary controller. . . . .	76
	(a) Consensus-based communication topology. . . . .	76
	(b) Centralized-based communication topology. . . . .	76
4.9	System variables for the unconstrained problem. . . . .	78
4.10	System variables for constrained problem for voltage regulation. . . . .	79
4.11	System variables for constrained problem for reactive power-sharing. . . . .	80
4.12	Active and reactive power-sharing generated from the optimization-based secondary controller with different communication topologies. . . . .	82
4.13	The controller behavior under different line parameter values. . . . .	84

4.14	Undirected graph connectivity for the proposed controller. . . . .	85
4.15	System variables for disconnection of the communication link between units 3 & 4. . . . .	86
4.16	System variables for disconnection of the communication link between units 3 & 4. . . . .	87
4.17	System variables for disconnection of the communication link between units 3 & 4. . . . .	88
4.18	System variables for disconnection of unit 3. . . . .	88
5.1	Hierarchical control structure. . . . .	92
	(a) Consensus-based communication topology. . . . .	92
	(b) Centralized-based communication topology. . . . .	92
5.2	Economic dispatch-based secondary controller . . . . .	99
5.3	Single-line diagram of the microgrid test system. . . . .	100
5.4	Economic dispatch-based secondary control. . . . .	102
5.5	Decentralized secondary controller. . . . .	103
5.6	Comparison with the decentralized secondary controller. . . . .	103
6.1	The modified commercial feeder of LV North America distribution system benchmark. . . . .	107
6.2	The unit variables with generalized droop control applied to the CIGRE LV benchmark. . . . .	110
6.3	Constrained for voltage regulation . . . . .	112
6.4	Constrained for reactive power-sharing . . . . .	113
6.5	System behavior with the economic dispatch-based secondary controller.	115
6.6	System behavior with the decentralized secondary controller. . . . .	116
6.7	Cost of generation comparison. . . . .	116

A.1	An example of a directed graph. . . . .	142
(a)	A directed graph. . . . .	142
(b)	Spanning tree in the directed graph. . . . .	142
B.1	The process of generating a custom solver in CVX/CVXGEN. . . . .	143
B.2	Optimization problem of Chapter 4 converted to DCP. . . . .	144
B.3	Optimization problem of Chapter 5 converted to DCP. . . . .	145
C.1	CIGRE North America LV distribution network benchmark . . . . .	147

## NOMENCLATURE

### A

- $A$  Adjacency matrix
- $a_{11}$  Element 1x1 of the dependency matrix
- $a_{12}$  Element 1x2 of the dependency matrix
- $a_{21}$  Element 2x1 of the dependency matrix
- $a_{22}$  Element 2x2 of the dependency matrix
- $a_i$  Quadratic fuel cost coefficient for unit  $i$  [ $\$/MW^2hr$ ]

### B

- $B_{ik}$  Susceptance between line  $i$  and  $k$  [ $\Omega^{-1}$ ]
- $b_i$  Linear fuel cost coefficient for unit  $i$  [ $\$/MWhr$ ]

### C

- $C_f$  Filter capacitance [F]
- $C_i(P)$  Operating cost [\$]
- $c_i$  Constant fuel cost coefficient for unit  $i$  [ $\$/hr$ ]

### F

- $f_{nom}$  Nominal frequency [Hz]
- $f_{sw}$  Switching frequency [Hz]

### G

- $G_{ik}$  Conductance between line  $i$  and  $k$  [ $\Omega^{-1}$ ]

### H

- $h$  Harmonic order

$H(x)$  Hessian matrix

## **I**

$i_o$  Output current [Amps]

$i_{ik}$  Current flow through line  $i$  to  $k$  [Amps]

## **K**

$K_{p_i}$  Active power droop control coefficient at unit  $i$  [ $rad/sec.W$ ]

$K_{q_i}$  Reactive power droop control coefficient at unit  $i$  [ $Volts/VAR$ ]

## **L**

$L_c$  Coupling inductance [ $H$ ]

$L_f$  Filter inductance [ $H$ ]

$L_l$  Line inductance [ $H$ ]

$L_v$  Virtual inductance [ $H$ ]

## **P**

$\bar{P}_i$  Rated active power [Watts]

$P_i$  Active power at unit  $i$  [Watts]

$P_{ik}$  Line active power [Watts]

$P_{line}$  Line active power [Watts]

$P_{load}$  Load active power [Watts]

$P_m$  Measured active power [Watts]

$P_{ref}$  Active power reference [Watts]

## **Q**

$\bar{Q}_i$  Rated reactive power [VAR]

$Q_i$  Reactive power at unit  $i$  [VAR]

$Q_{ik}$  Line reactive power [VAR]

$Q_{line}$  Line reactive power [VAR]

$Q_{load}$  Load reactive power [VAR]

$Q_m$  Measured reactive power [VAR]

$Q_{ref}$  Reactive power reference [VAR]

## **R**

$R_c$  Coupling resistance [ $\Omega$ ]

$R_f$  Filter resistance [ $\Omega$ ]

$R_l$  Line resistance [ $\Omega$ ]

## **S**

$S_{ref}$  Reference apparent power [VA]

## **V**

$V_{ref}^*$  Voltage reference with virtual impedance [Volts]

$V_g$  Grid voltage [Volts]

$V_i$  Voltage at unit  $i$  [Volts]

$V_s$  Source voltage [Volts]

$V_{DC}$  DC voltage [Volts]

$V_{max}$  Maximum voltage [Volts]

$V_{min}$  Minimum voltage [Volts]

$V_{nom}$  nominal voltage [Volts]

$V_{ref}$  Voltage reference without virtual impedance [Volts]

$V_{RMS}$  RMS voltage [Volts]

## **W**

$W$  Lyapunov function candidate

## **X**

$x_l$  Line reactance [ $\Omega$ ]

$x_{\omega_i}$  Active power sharing for unit  $i$  [ $\text{rad}/\text{Watts}\cdot\text{sec}$ ]

$x_{V_i}$  Reactive power sharing for unit  $i$  [ $\text{Volts}/\text{VAR}$ ]

## **Z**

$Z_l$  Line impedance [ $\Omega$ ]

$Z_v$  Virtual impedance [ $\Omega$ ]

## **Greek Letters**

$\Delta\omega$  Change of angular frequency [ $\text{rad}/\text{sec}$ ]

$\Delta\omega_{max}$  Maximum allowable change of angular frequency [ $\text{rad}/\text{sec}$ ]

$\Delta f$  Change of frequency [ $\text{Hz}$ ]

$\Delta V$  Change of voltage [ $\text{Volts}$ ]

$\Delta V_{max}$  Maximum allowable change of voltage [ $\text{Volts}$ ]

$\delta$  Voltage phase angle [ $\text{rad}$ ]

$\delta_{\omega_i}$  Secondary corrective term for angular frequency at unit  $i$  [ $\text{rad}/\text{sec}$ ]

$\delta_{V_i}$  Secondary corrective term for voltage at unit  $i$  [ $\text{Volts}$ ]

$\omega_i$  Angular frequency at unit  $i$  [ $\text{rad}/\text{sec}$ ]

$\omega_{nom}$  nominal angular frequency [ $\text{rad}/\text{sec}$ ]

$\theta$  Line impedance phase angle [ $\text{rad}$ ]

$\tau$  Step size

## CHAPTER 1 INTRODUCTION

### 1.1 Significance of the Research Topic

Today's modern societies are heavily dependent on the electrical power sector. It is considered a critical infrastructure that provides an "Enabling function" to other critical infrastructures such as water, gas, transportation, telecommunication, and safety. Therefore, a large-scale power outage has catastrophic consequences and costs the economy tens of billions of dollars.

There are three main causes of power outages: natural disasters, technical problems, and human-made power outages [1]. Climate change drives an increase in major weather-related power outages. Figure 1.1 shows the major power outages for the weather- and non-weather-related power outages. Extreme weather conditions are considered high-impact and low-probability (HILP) events that impact the power system's resilience. Severe weather conditions are expected to increase in the future [2]. Such events are usually ignored in reliability-based studies. Therefore, the concept of resilience was introduced into power system studies to provide more realistic modeling of the power system. The power system is not only supposed to be reliable but also resilient against major power outages.

The IEEE Technical Report PES-TR65 defines resilience as "The ability to withstand and reduce the magnitude and/or duration of a disruptive event." [3]. It also comments on the key features that differentiate between resilience and reliability as follows:

- Resilience involves all events, including HILP events, that are normally excluded from reliability calculations.

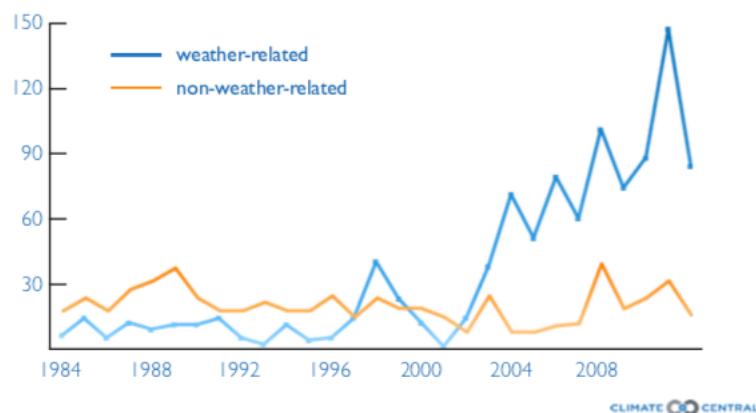


Figure 1.1: Annual number of reported weather- and non-weather-related power outages in the U.S., 1984–2012.

- Resilience considers the transition time between the power system states, while reliability focuses only on the states where the power system ends up. Therefore, resilience requires the characterization of the preparation before events, the operational processes during them, and the response after them.
- Resilience captures the effects on the customer (similar to reliability), operators, and infrastructure.

For an occurrence of an event, the resilience of the power system includes short- and long-term features. Therefore, the resilience evaluation is classified according to the time of occurrence relative to the event in terms of planning, response, and restoration [4]. Resilience-based planning covers all long-term measures, including plant management, underground cables, and the design of power system hardware. The resilience-based response focuses on preventive and emergency responses, including day-to-day and real-time measures. Resilience-based restoration concentrates on recovery measures in the system. Figure 1.2 shows the classification of the power system's resilience relative to the time of event occurrence [1].

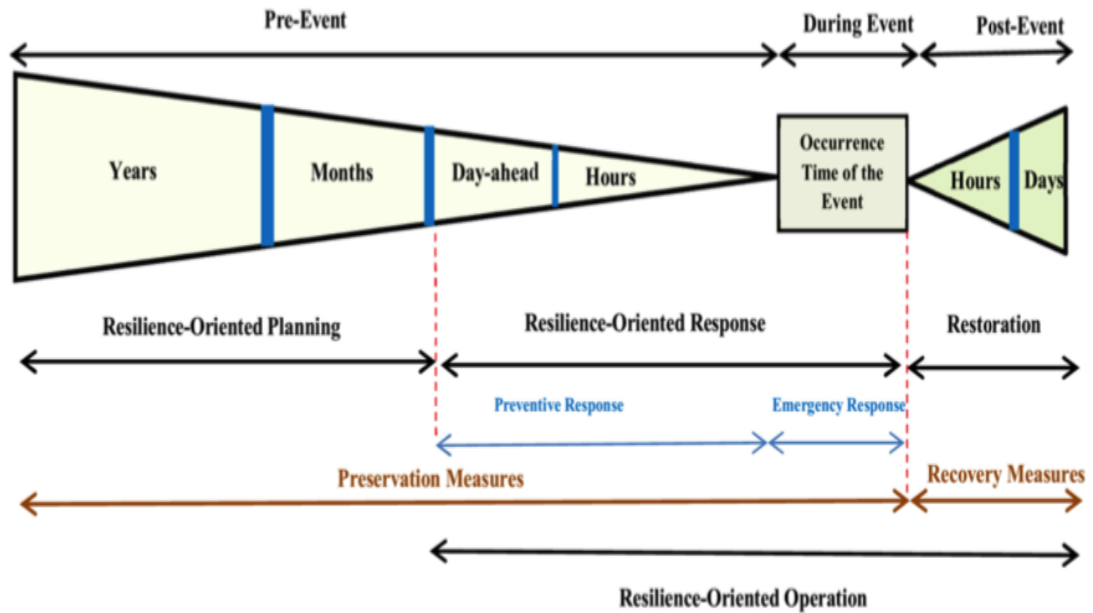


Figure 1.2: Classification of power system resilience in terms of the time of an event's occurrence.

The microgrid is a crucial solution to improve the power system's resilience in all aspects [1]. For example, the ability of the microgrid to integrate small-scale DG units enhances the power system's resilience with resilience-based planning. Furthermore, the ability of the microgrid to isolate itself during faults in the main grid improves resilience through a resilience-based response [5]. The microgrid also improves resilience-based restoration through black-start algorithms that consider the microgrid as a black-start power supply. Furthermore, the improvement in the resilience of the power system through microgrids was proven during Hurricane Sandy, and the Sendai microgrid during the Great East Japan Earthquake [6].

The global market for microgrids is growing from \$19.3 billion in 2018 and is expected to reach \$36.3 billion in 2024, representing a growth of 10.9 %, as shown in Figure 1.3 [7]. A new report by Guidehouse Insights predicts the growth of clean energy microgrid capacity from 4,288.8 MW in 2022 to 20,053.9 MW in 2031



Figure 1.3: The microgrid world market by region from 2015 to 2024.

[8]. According to the report, the main drivers of growth include the reduction of energy storage costs, upgrades of microgrid controllers, the overall impulsion for modular microgrids, and the potential energy offsets that remote microgrids can provide. However, the main barriers are complications with renewable energy deployments, a lack of agreement on the value of resilience, long delays during microgrid interconnections, and compatibility issues.

The islanded microgrid is a challenging mode of operation that can limit the advantages of microgrids to improve the resilience of the power system. In an islanded microgrid, the frequency and voltage are controlled within the microgrid itself. Grid-forming units collaborate to provide these functionalities using droop control characteristics in a hierarchical control structure [9]. The control system of the grid-forming units contains primary, secondary, and tertiary levels of hierarchy. The functions of each level in the islanded microgrid are shown in Figure 1.4. The primary control, which has the fastest response, maintains the stability of frequency and voltage control and ensures appropriate power-sharing between units. Secondary control is required to compensate for the deviations in frequency

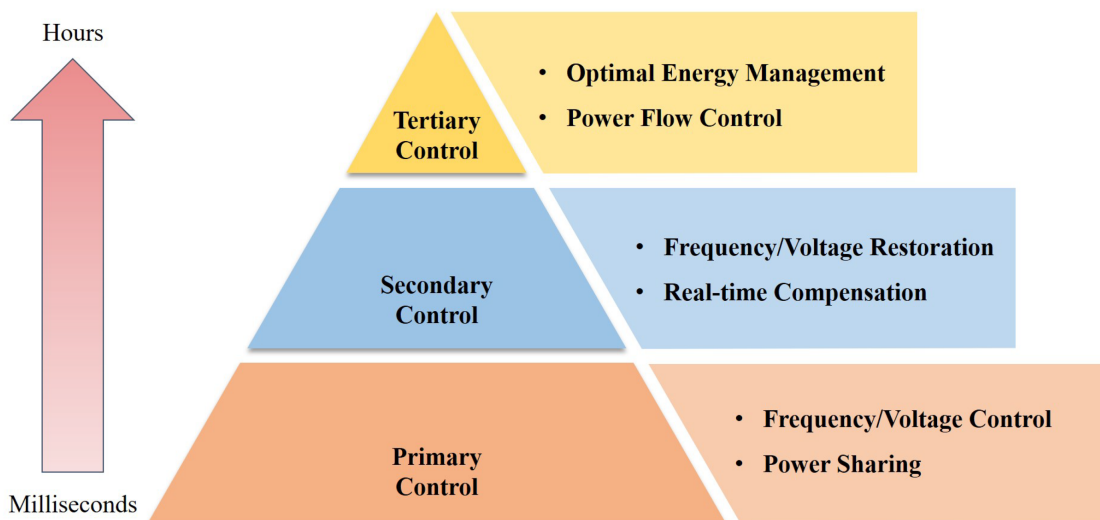


Figure 1.4: The hierarchical control structure.

and voltage caused by primary control. Tertiary control is mainly dedicated to the microgrid energy management system, which provides economical operation of the microgrid with the use of various optimization methods [10].

The application of the hierarchical control structure in the microgrid, which is usually located in distribution systems, limits the effectiveness of an islanded microgrid during a power outage on the main grid. These limitations include instability in frequency and voltage control, unequal power-sharing between units, and the lack of economic consideration for grid-forming units during the island mode of operation [10]. This dissertation focuses on improvements in the hierarchical control structure through improvements in these three aspects of operation in islanded microgrids.

At the primary control level, the droop control is utilized to set the frequency and control level based on changes in the measured active and reactive power. In an inductive grid, the frequency is related to the active power and the voltage to the reactive power. However, the grid has a mixed impedance in the distribution network, and coupling between voltage and frequency occurs. Virtual

impedance is used by feeding the output current through an artificial impedance, in which the grid is considered inductive and then added to the reference voltage [11, 12]. A similar technique is used to show the grid as resistive in a low-voltage grid [13]. However, virtual impedance techniques are designed for static systems where modification of the system configuration is not considered. Furthermore, virtual impedance elements require a thorough design to avoid current spikes at the initial connection of the DG unit [14]. Furthermore, a virtual frame transformation method is utilized by transferring the active and reactive power to a new reference frame to eliminate the coupling between them. The droop control is then applied using the transformed power quantities [15, 16]. However, the line parameters are required to be given in advance or can be estimated. In addition, transformed quantities of active and reactive power are a function of real active and reactive power. Therefore, the droop control coefficients are designed to share transformed quantities rather than real quantities, degrading the power-sharing accuracy.

At the secondary control level, the secondary control restores the voltage and frequency to their nominal values. However, when there is a line parameter mismatch in the inductive grid, the voltage drop in the lines causes the grid-forming units to contribute reactive power differently. Therefore, when the secondary control objective is designed to restore the voltage to its nominal value, reactive power sharing is mismatched, and the units share reactive power beyond their ratings. When the secondary control objective is to share the reactive power equally between units, the voltage is mismatched, and the circulating currents flow between units. Some work has been done on accurately sharing reactive power while bounding the voltage to limits in a consensus manner [17, 18, 19, 20]. In [20], two alternative output limitation methods were used to deal with voltage or reactive power-sharing limits for a consensus-based approach. However,

all DGs must be connected to a common critical bus. The authors in [19] used a predictive model control (MPC) to predict the optimal behavior of DG units in terms of voltage regulation and power-sharing and to share it with neighboring units described by the communication graph. Power transfer equations were used to predict active and reactive power generation in coupling elements, and droop control equations were used to predict the optimal behavior of the DG units. The technical constraints, including limits for voltage and power capacity, were enforced by the MPC. However, the average voltage and frequency values for all units are required, which requires the unit to communicate with all other units to share extensive information. In [18], an optimization function was implemented to minimize the trade-off between voltage regulation and the sharing of reactive power subject to technical constraints of the DG output, including voltage limits and reactive power capacity. However, the controller requires the line parameters between the connected DGs, which is not practical in distribution systems. The work in [17] implements two PI controllers for the secondary control level to keep the voltage within a predefined range (containment-based controller) and maintain precise reactive power-sharing (consensus-based controller). However, when precise reactive power-sharing cannot be maintained for the given voltage range, settings are required to either enlarge the voltage range of the containment-based controller to maintain precise reactive power-sharing or set the error saturation for the consensus-based controller to allow a reactive power-sharing mismatch while keeping the voltage range intact. Only the leader units can access the lower and upper bounds of the voltage.

For the tertiary control level, the economic aspects are incorporated into islanded microgrid operation with either economic dispatch-based or optimal power flow-based methods. Optimal power flow considers a variety of objective functions subject to a range of constraints for all buses [21, 22, 23]. Optimal power

flow-based techniques are usually done offline due to the non-convexity of optimal power flow and the need for linear approximation or convex relaxation techniques [24]. In contrast, in economic dispatch [25, 26, 27], units with different cost coefficients are dispatched based on the lowest price, considering the maximum capacity of the committed units and satisfying the equality of power balance. Economic dispatch methods only consider generation units. Therefore, the economic dispatch approach is more suitable for real-time applications. In [25], an economic dispatch algorithm was proposed to dispatch active power in real-time; however, grid-forming units were not considered. The authors in [27] propose a secondary controller based on economic dispatch in real time for an islanded microgrid that dispatches active power in correlation with frequency without considering reactive power generation and voltage control.

## 1.2 Problem Statements

This dissertation aims to improve the operation of the islanded microgrid by addressing three issues at all three levels of the hierarchical control structure, including the primary, secondary, and tertiary levels, as follows

At the primary control level, the frequency and voltage are related to the active and reactive power through a nonlinear relationship because of the mixed impedance of the line. Thus, the accuracy of droop control equations is reduced, causing instability of frequency and voltage control. This dissertation aims to implement a linear relationship described by line parameters to be used in droop control to improve the accuracy of power-sharing, thereby enhancing the stability of frequency and voltage controls.

At the secondary control level applied to the inductive grid, line parameter mismatches cause the voltage to be measured differently in each grid-forming unit. Therefore, there is a trade-off between voltage regulation and reactive power-

sharing. This dissertation aims to employ an optimization method to manage the trade-off between these variables in the minimum communication link between the grid-forming units.

The tertiary control level is responsible for the economic operation of the islanded microgrid. It has a time constant of minutes to hours. Therefore, an estimation algorithm is required to estimate the load and generation of renewable energy. Therefore, an estimation error may occur and affect the efficiency of the economic dispatch algorithm. This dissertation aims to eliminate the prediction error in an economic dispatch by integrating the economic dispatch algorithm in the secondary control level and eliminating the need for an estimation algorithm.

### **1.3 Dissertation Organization**

This dissertation includes three independent topics to improve the islanded operation of the microgrid through a hierarchical control structure. The first topic is to improve the frequency and voltage stability in the microgrid at the primary control level. The second topic focuses on the power-sharing issue that occurs in secondary control. Finally, the issue of prediction error in economic dispatch is the subject of the third topic.

Chapter 2 surveys the literature on the role of microgrids in improving the resilience of the power system, the concept of microgrids, and the hierarchical control structure applied to the islanded microgrid. Furthermore, it discusses issues related to hierarchical control structures.

Chapter 3 explains the primary control level of the islanded microgrid in the context of hierarchical control structures. Furthermore, it shows the implementation of the generalized droop controller that solves the issue of the non-linear coupling control between frequency and voltage at the primary control level.

In Chapter 4, the role of secondary control is demonstrated in the hierarchical control structure of the islanded microgrid. In addition, distributed secondary controllers based on averaging and consensus optimization are presented to manage the trade-off between voltage regulation and reactive power-sharing in the inductive grid of the microgrid.

Chapter 5 demonstrates the economic operation applied by the tertiary control level to the islanded microgrids. Consequently, it shows the implementation of the economic dispatch-based secondary controller to overcome the economic dispatch prediction error in the islanded microgrid.

Chapter 6 validates the scalability of the proposed controllers by evaluating their functionalities with the CIGRE North America Microgrid Benchmark System.

Chapter 7 concludes the dissertation by summarizing the content and presenting future work and recommendations.

Finally, Appendices A, B, and C serve as supporting material for the content of this dissertation.

## CHAPTER 2 LITERATURE REVIEW

This chapter provides an overview of the relevant literature that focuses on the topic of the dissertation. The importance of microgrids in improving the resilience of the power system is reviewed in the first section. Then, the concept and related literature on microgrids are presented. Finally, the hierarchical control structure of the microgrid and related issues in islanded mode are discussed and reviewed.

### 2.1 Microgrid Role in Improving Power System Resilience

The resilience of power systems is defined by the North America Transmission Forum (NATF) as “The ability of the system and its components (i.e., both the equipment and human components) to minimize damage and improve recovery from non-routine disruptions, including high impact, low probability (HILP) events, in a reasonable amount of time.” [28]. Events such as cyber-attacks, physical attacks, severe weather, wildfires, and fuel delivery failures are examples of the HILP intended in resilience studies. Resilience aims to enable the power system to handle such events. The U.S. Department of Energy addresses some challenges associated with resilience in grid modernization initiatives as follows[29]:

- Ensuring a safe energy supply chain and delivery systems.
- Mitigating vulnerabilities related to interdependencies between the electricity grid and other infrastructure.
- Increasing the availability of the system through current technologies, architectures, and computing tools as the grid continues to evolve with the addition of new technologies.

- Understanding the human-machine interface and the effect of human behavior, including social, physical, and economic impacts.
- Facilitate decisions and visualization tools for disaster prevention and recovery by developing new analytical methods.

The typical performance of a more resilient power system during events compared to a traditional one is shown in Figure 2.1. Improvement in the resilience of the power system can be made according to three time-based categories, known as resilience-based planning, response, and restoration [4]. Resilience-based planning is a long-term factor that concentrates on the infrastructure of the power system and includes hardware- and software-based approaches [30]. The resilience-based response focuses on the adaptability of the power system, including preventive and emergency responses. Resilience-based restoration tends to restore the power system to its pre-event state with minimum restoration time, such as black-start algorithms [31].

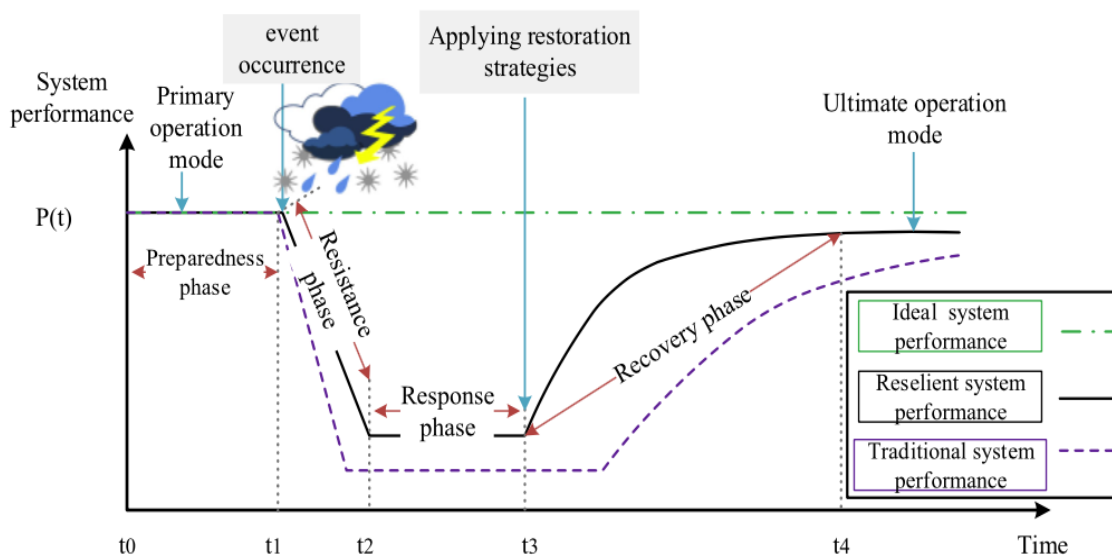


Figure 2.1: The performance levels of a resilient power system in the face of a disruptive event.

The microgrid plays an important role in enhancing these measures in many ways, including its ability to be isolated, ancillary services, and energy reserves. The Grid Modernization initiative implemented by the U.S. Department of Energy has invested in a number of resilience-related projects, including “Industrial Microgrid Analysis and Design for Energy Security and Resiliency”. The project aims to investigate, develop and analyze the risks, costs, and benefits of a microgrid at the UPS World Port and Centennial Hub facilities in Louisville, Kentucky [29]. Several studies have indicated the importance of microgrids in improving the resilience of power systems [32, 33]. The authors in [1] reviewed approaches, methods, and techniques, as well as future trends, to improve the resilience of the power system in the three categories. Their research emphasized the importance of microgrids and DERs in improving the resilience of different aspects of the power system.

### **2.1.1 Resilience-based Planning**

Resilience-oriented planning is an important aspect that lays the foundation for a resilient power system. The microgrid improves resilience-based planning through hardware- and software-based planning by integrating DERs and energy storage units, as well as by operating the distribution system as a multi-microgrid system. Furthermore, the microgrid allows the DERs to operate even when the main grid is out. Therefore, these resources are not subject to disconnection during the main grid fault to provide energy to connected loads and maintain continuity of supply. Investing in the integration of more DER and energy storage units significantly improves the resilience of the power system [34].

Resilience-based planning includes the optimal allocation and sizing of DGs in the distribution system and applies an appropriate control system to form multiple microgrids to accommodate the distribution system for HILP events. In [35],

a stochastic-robust investment planning model was proposed to find the optimal investment plan of microgrid resources to improve the resilience of microgrids against HILP and low-impact, high-probability (LIHP) events. The authors in [36] propose a planning strategy for the optimal location of DERs which divided the distribution system into multi-microgrids based on load density to increase the probability of critical loads being picked up after natural disasters. In [37], a robust sizing method and energy management scheme of multi-energy resource microgrids were proposed to minimize total annual expenses and boost system resilience during an extended grid outage. In terms of software-based planning, the authors in [38] proposed a multi-controller software-defined networking (SDN) architecture based on fog servers in multi-microgrids to improve the security, monitoring, and control of the distribution system. Sedzro *et al.* [39] suggested a methodology for the formation of microgrids in the distribution systems applicable for general power network topologies, including radial and meshed configurations. The authors in [40] provided a quantitative analysis of the resilience of the distribution systems with multiple microgrids and other resources to help the distribution system operators in short-term planning and to justify the control action.

### **2.1.2 Resilience-based Response**

The resilience-based response is the first stage of the resilience-based operation. Preventive and emergency responses are day-ahead and real-time measures, correspondingly, and both are included in resilience-based response [4]. The preventive response includes actions available before the disaster occurs, while the emergency response includes the actions taken in the aftermath of a disaster. The preventive response is a day-ahead plan of the power system to alleviate the impact of HILP events after warning of them. The preventive response aims to prede-

termine the optimal topology of the power system to improve the response while encountering such events [4]. Emergency response, however, aims to pick up the maximum number of critical loads during the events using available spanning and complementary reserves planned the day ahead. The typical solution to improve the resilience-based response is utilizing resilience resources.

Microgrids can be used as local and community resources. The local resource supplies the loads within the microgrid boundary, while the community resource extends the supply to include the loads outside the microgrid boundary. The study in [41] provided an evolution to use the microgrid as a resilient resource in three specific configurations: local resource, community resource, and black start resource. The study concluded that it was feasible to use a microgrid to support operations during severe weather events. In [42], a novel metric analysis framework for control and management was proposed to improve the resilience of network microgrids, including metrics to assess voltage deviation, line loss, performance, and the number of restored loads. Liu *et al.* [43] proposed four resilience indices to measure the impact of extreme events. As a result of this work, a relationship was implemented between the utilization of multiple microgrids and grid resilience employing the Markov model and the Monte Carlo simulation approach. Chen *et al.* [44] proposed a novel approach to form multiple microgrids in the distribution network energized by available DG units after natural disasters. Mixed-integer linear programming was used to maximize the number of energized critical loads while satisfying operational constraints.

### **2.1.3 Resilience-based Restoration**

The main objective of power system restoration is to serve the maximum number of electrical loads at the minimum time of the duration of the power outage after HILP events. Restoring the power system after the main outage involves

three stages: evaluation, system restoration, and load restoration. In the first step, the system status assessment is performed. Then, the available resources are determined. Finally, the locations of the higher-priority loads are identified. DG units enhance grid resilience by improving generation availability (e.g., fuel cells, microturbines, wind turbines, and photovoltaic panels). Furthermore, microgrids are employed to efficiently manage these DGs as well as other resources to improve restoration following natural disasters.

The microgrid is widely recognized as an efficient solution to restore the power system after major events. Several studies have been proposed to restore the power system using the microgrid [45, 46, 47]. In [48], a comprehensive review of service restoration was carried out by forming microgrids in the distribution system that included benefits, challenges, and future trends. The authors in [49] proposed a two-stage plan to restore critical loads in the distribution network by coordinating available microgrids. In the first stage, the post-disaster topology of electrical islands is determined based on active microgrids in the distribution system. In the second stage, an optimization problem based on the generalized Benders decomposition is proposed to maximize the restored critical loads. Khederzadeh *et al.* [50] suggested a method to improve the restoration of service in distribution networks using a spinning tree search strategy after HILP events. A combination of reconfiguration and application of microgrids is proposed to enhance the restoration capability of the distribution system.

## 2.2 The Concept of Microgrid

The microgrid is widely recognized as a promising solution to inject more small-scale renewable energy resources into existing power systems. Furthermore, the microgrid is a crucial factor in boosting the reliability and resilience of the power system through its capabilities and characteristics. The microgrid employs

DERs such as solar photovoltaics (PVs), wind generators, microturbines, and energy storage systems (ESSs) to supply their own loads and support grids as independent entities. The U.S. Department of Energy defines the microgrid as “a group of interconnected loads and distributed energy resources (DERs) within clearly defined electrical boundaries that acts as a single controllable entity relative to the grid and can connect and disconnect from the grid to allow it to operate in both grid-connected or island modes” [51]. The microgrid can improve the operation of the power system in both grid-connected and islanded modes of operation. During grid-connected mode, the microgrid can provide active and reactive power as well as ancillary services to the main grid. While in islanded mode, the microgrid is disconnected from the main grid in an emergency condition to supply the loads connected to it [9].

The concept of microgrids has been extensively reviewed in the literature [52, 53, 54, 55, 56]. In [52], a comprehensive review of the literature related to microgrids and challenges was presented that included the application of DERs, the grid-supporting functionalities of the microgrid, economic aspects, and other related issues. The authors in [53] focused on the architecture, control, and reliability considerations for the microgrid. Furthermore, some studies reviewed other aspects of microgrid, such as control [9, 57, 58, 59, 60], communication [61], protection [62, 63, 64, 65], and energy management [66, 67].

### **2.2.1 Microgrid Architectures and Components**

The microgrid is usually located in a small geographic area as part of the distribution system. Therefore, integrating DERs within the distribution system omits costly transmission power losses, as in the centralized power system paradigm. However, these transformations increase the demand for different architectures and components to run the microgrid efficiently.

At the point of common coupling (PCC), which is the connection point to the main grid, the microgrid can take its own architecture. The microgrid architecture is classified into three types, namely, AC, DC, and hybrid microgrids. The AC microgrid requires minimal modification of the existing distribution system due to existing AC infrastructures. On the contrary, the increasing number of DC loads, as well as the dominant DC energy storage systems and renewable energy resources, impose the need for a DC architecture to reduce the number of power electronics converters, which increases implementation costs and conversion losses [68]. However, the DC microgrid architecture introduces a whole set of challenges associated with its realization in terms of protection and control [69, 70]. As a compromise solution, the hybrid architecture was proposed to increase the efficiency of the microgrid [71]. However, coordination between AC and DC in terms of power flow and sharing remains an active research area [72]. Figure 2.2 shows the architectures of the AC, DC, and hybrid microgrids.

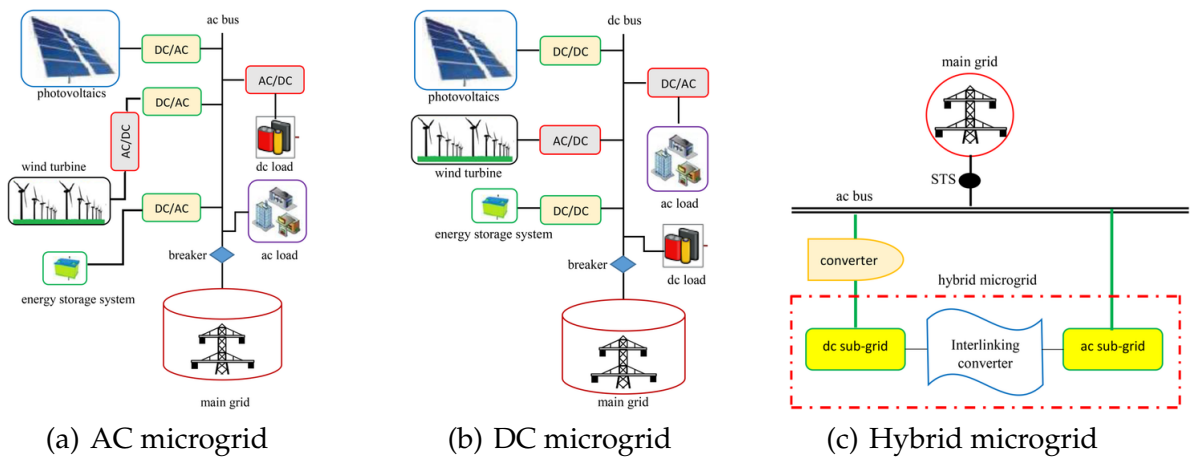


Figure 2.2: Microgrid architectures.

The microgrid consists of DERs, loads, and protection devices among control, communication, and automation systems [52]. DERs are small-scale energy

resources that are distributed within the microgrid's boundary to supply the connected loads. DERs include DGs and ESSs. The combination of these resources reduces the uncertainty of renewable energy resources and improves the continuity of the energy supply. DERs contained within a microgrid must comply with IEEE Standard 1547 [73]. A variety of DG technologies are used in microgrids including PV, wind turbines, fuel cells, biomass, small hydro-turbines, micro-turbines, and diesel generators. ESSs vary in their energy and power densities. High power density ESSs are required in microgrids to improve their stability because of their fast response. High energy density is utilized for energy management [74, 75]. Figure 2.3 represents different ESS technologies and their energy and power densities. Loads in the microgrid are categorized into two types: fixed and flexible (also known as adjustable or responsive). Fixed loads must be satisfied under normal operating conditions, while flexible loads respond to control signals. Flexible loads can be curtailed (i.e., curtailable loads) or deferred (i.e., shiftable loads) in response to economic initiatives or islanding requirements. Flexible loads are the essence of Demand Side Management (DSM) programs and initiatives. DSM is defined by the U.S. Department of Energy as "changes in electric usage by end-use customers from their normal consumption patterns in response to changes in the price of electricity over time, or to incentive payments designed to induce lower electricity use at times of high wholesale market prices or when system reliability is jeopardized" [76]. DSM has several economic, environmental, and reliability benefits. The benefits of DSM include reducing costs, alleviating electrical system emergencies, reducing the number of blackouts, increasing system reliability, and deferring high investments in the capacity of the generation, transmission, and distribution networks [77]. Control, communication, and automation systems among protection devices are required to provide appropriate operation of the microgrid in the grid-connected and islanded modes of operation.

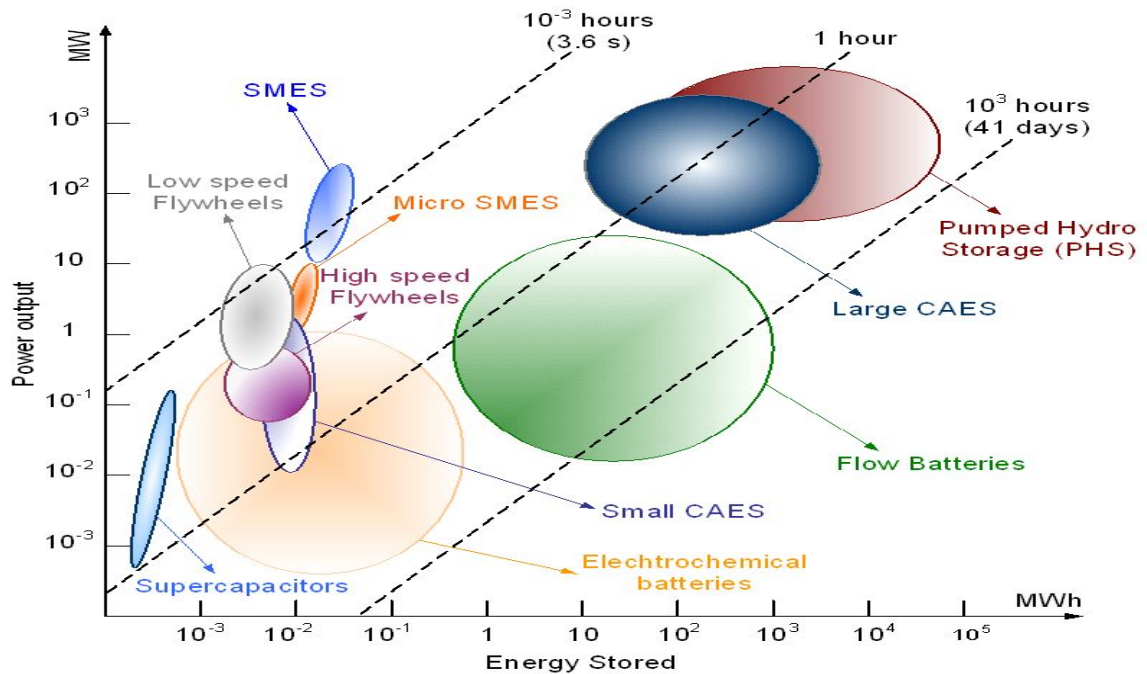


Figure 2.3: Power and energy densities of different energy storage devices.

## 2.2.2 Microgrid Operation

The key benefit of the microgrid resides in its operating capabilities. The microgrid has two modes of operation: grid-connected and islanded. In grid-connected mode, the microgrid supports the main grid by supplying it and ancillary services, while, in islanded mode, the microgrid can be isolated from the main grid and supplies its own loads. The transition from islanded to grid-connected mode requires that all units be synchronized with the main grid. However, the transition from grid-connected to islanded mode requires an islanded detection algorithm to ensure the stability of the isolated microgrid. The typical transitions of the microgrid between modes are shown in Figure 2.4.

When the microgrid is required to connect to the main grid, the voltage at the point of common coupling should be synchronized with the grid voltage in terms of phase, frequency, and amplitude. However, the synchronization al-

gorithm depends on the control strategy of the microgrid in islanded mode [78]. Based on control strategies in islanded mode, various synchronization methods were proposed to ensure a seamless transition to grid-connected mode [79, 80].

In grid-connected mode, the microgrid can absorb or supply the main grid with active and reactive power, and it works as a controllable load or source. The microgrid should respond to the main grid commands signal as a single entity to ensure stable operation of the main grid. Microgrids contribute to the reliability and economic operation of the power system and provide ancillary services to the main grid [81, 82]. Reliability indices such as SAIFI, SAIDI, CAIFI, and CAIDI are evaluated in terms of average interruption frequency and/or duration. These indices are significantly improved by deploying a microgrid in distribution systems [52]. In addition, the microgrid provides a significant improvement in the economic operation of the main grid due to the notable reduction of power losses and its ability to host small-scale renewable resources. Ancillary services are needed to maintain a reliable and secure supply of electricity. Ancillary services are communicated to DGs from the distribution network operator through a Microgrid Central Controller (MGCC) or directly. The ability of DG or ESS to provide these ancillary services depends on the dynamic behavior of the connected DG or ESS. For instance, inertia control requires a fast-dynamic source to react to a disturbance in milliseconds. Some examples of ancillary service provisions include reactive power production and voltage control, frequency control reserves, provision for backup and reserve power, and black start capability [59].

Islanded mode is a challenging mode of operation due to the absence of a stiff grid. Issues such as instability, deteriorated power quality, low inertia, low X/R ratio, and energy management issues limit the effectiveness of islanded microgrids [9]. When islanding is detected, the system controller aims to stabilize the microgrid under islanding by injecting more energy to balance generation with

demand. However, when the energy available in the microgrid is not enough to supply the load, a load-shedding algorithm is triggered to avoid a blackout. The load-shedding algorithm curtails a number of loads until the available generation can provide the rest of the loads [83]. Furthermore, the microgrid control system controls the frequency and voltage after islanded detection through the droop control technique. However, low inertia because of the domination of inverter-based DGs and low  $X/R$  ratio because of the existence of a microgrid in the distribution system lead to difficulties in maintaining stable operation [84]. In addition, the bidirectional power flow in islanded mode and the limited fault current of inverter-based DGs cause complications in the islanded operation of a microgrid [62].

The microgrid can be disconnected from the main grid intentionally (i.e. maintain) or unintentionally (i.e., faults in the main grid). In both cases, the islanded mode should be detected as fast as possible to configure the microgrid for working in such a mode (i.e., voltage and frequency control) before it is subjected to power quality and stability issues. Most islanding detection techniques use power quality indexes to detect the islanded mode. Islanded detection techniques are classified into three categories: passive, active, and communication-based [85]. Passive methods are based on changes in system parameters within a certain tolerance when they exceed changes in normal conditions. These parameters include voltage, frequency, rate of change of voltage (ROCOV) and frequency (ROCOF), voltage phase, THD, selective harmonic (i.e., 3rd, 5th, etc.), and voltage imbalance is typically used [86]. These methods are low-cost and simple to implement. However, passive methods have a non-detection zone (NDZ) when the power mismatch is relatively small and close to zero [87]. Hybrid passive techniques are also considered to avoid the NDZ [88, 89]. In active islanding detection methods, a small disturbance is injected into the utility grid, and based on

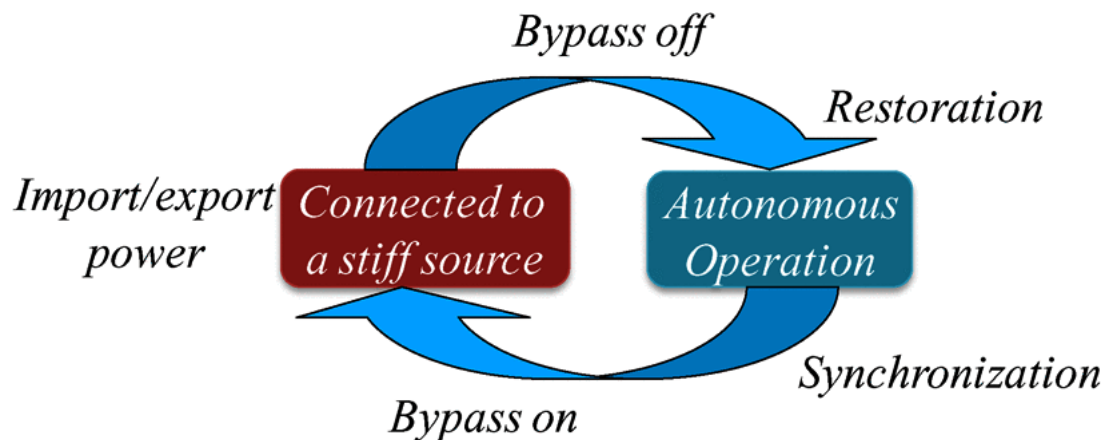


Figure 2.4: Microgrid transition status

its response, the decision to adopt islanded mode is formed [90]. These methods significantly decrease the NDZ; however, they create power quality issues in the microgrid. Communication-based methods are based on communication between the utility grid and DGs. However, communication infrastructure is required for islanding detection methods in the utility grid [86].

### 2.2.3 Microgrid Control

The control system of a microgrid is a key element to ensure appropriate operation in both modes and the transition between them. IEEE defines the microgrid control system as "A system that includes the control functions that define the microgrid as a system that can manage itself, operate autonomously, and connect to and disconnect from the main distribution grid for the exchange of power and the supply of ancillary services; it includes the functions of the microgrid energy management system (MEMS); it is the microgrid controller if implemented in the form of a centralized system." [91]. The microgrid control system consists of software, hardware, or a combination of both that can be implemented in a centralized or distributed structure. In the centralized structure, an MGCC is responsible for supervisory functions and local controllers receive their reference setting from it.

On the other hand, the local controllers are decision-making controllers in a distributed structure. Communication and automation systems are also employed to facilitate the control functions of the microgrid. The most important differences relevant to stability in microgrids compared to bulk power systems are the following: smaller system size, higher penetration of RES, higher uncertainty, lower system inertia, lower X/R ratio of feeders, limited short-circuit capacity, and unbalanced three-phase loading. These inherent differences between microgrids and bulk power systems must be considered when designing the microgrid control system [92]. IEEE Standard P2030.7 (IEEE Standard for the Specification of Microgrid Controllers) specified the core functions of the microgrid control system as follows [93]:

- Functions to manage local resources and loads.
- Control functions for grid-connected mode, including power flow management and supply of ancillary services for the local distribution system, and potentially, the bulk system.
- Control functions for islanded mode including management of local generation, storage, and loads to optimize performance.
- Functions to ensure seamless connection and disconnection from the grid.
- Additional local functions for specific circumstances (such as renewable resource management, load prioritization, and support of grid reliability and automation functions).

The control system of the microgrid has different functions according to the mode of operation. For instance, the voltage and frequency control is maintained by the main grid during the grid-connected mode. However, DERs are responsible for those functionalities during islanding. Based on the function, the time response requirement differs from one to another. In addition, some functions are processed through different time scales. Therefore, a hierarchical control structure

is proposed to provide those functions [84, 10, 9]. However, some challenges such as V & f regulations, accurate load-sharing, power quality issues, DG coordination, and power generation and demand forecasting are associated with microgrid control [94, 9].

#### **2.2.4 Microgrid Protection**

The presence of DERs in the distribution system creates challenges in microgrid protection that are not common in the traditional protection scheme for the distribution network. The microgrid has its own features that require special consideration in the design of the microgrid protection scheme as follows [62]

- Bidirectional Power flow
- The intermittent nature of a renewable-based microgrid
- Fault current level varies based on the mode of operation
- High penetration of inverter-based DERs.

The complication in the microgrid protection scheme occurs in terms of fault current, relay coordination issues, and short-circuit level [63, 95, 62]. Due to bidirectional power flow, traditional protective devices, such as unidirectional over current relays and fuses, are ineffective in providing reliable and safe operation for microgrids. For instance, at a microgrid with high DER penetration, the power can flow in both directions in a bus. Therefore, when a fault occurs in a feeder, unidirectional over-current relays fail to detect reverse fault currents, and DERs continue to feed the fault. In addition, the intermittent nature of renewable energy resources causes fluctuations in power generation. Therefore, the fault current level changes according to the production of renewable resources [96]. Furthermore, the operation mode of the microgrid is altered between the grid-connected and islanded modes. Therefore, a substantial impact on the short-circuit level occurs due to a change in the equivalent impedance. Solutions for

those issues are intensively addressed in the literature, including [97, 98, 99, 100]. Finally, inverter-based DGs have a limited fault current between 1.2 to 2 p.u which leads to undetected faults [97, 99]. Altaf *et al.* [62] summarized these challenges as shown in Figure 2.5.

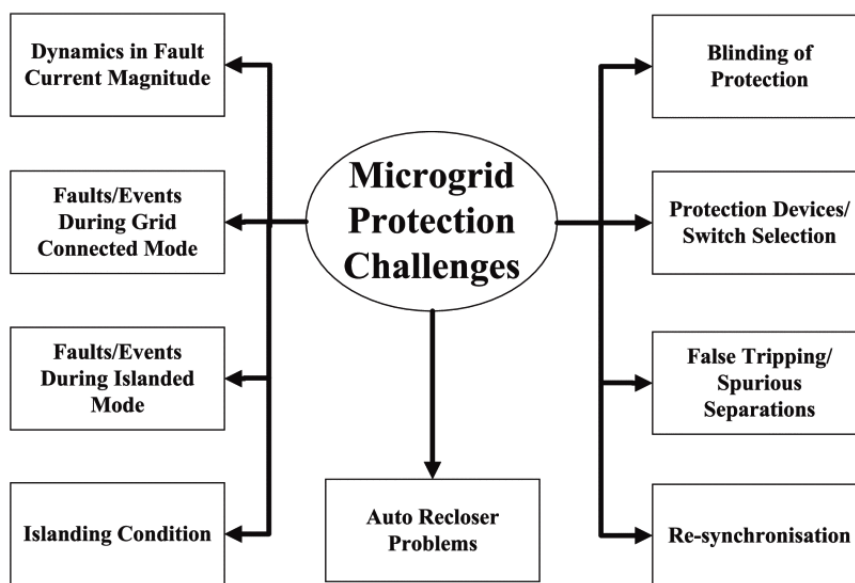


Figure 2.5: Challenges in protection associated with AC microgrids

### 2.2.5 Microgrid Economic Operation

Microgrids offer economic benefits to the power system because of the proximity of generation to load. Moreover, renewable energy generation in the microgrid provides less-expensive energy, especially during peak and congestion hours of the utility grid. Microgrids can also sell the surplus energy and provide ancillary services to the main grid to be paid and credited, thereby lowering the energy cost. The economic evaluation of microgrids has been extensively studied in the literature to explore their merits [60, 101, 102, 103]. These studies include planning, scheduling, and DSM.

Sizing the microgrid is an essential part of planning to optimize the investment of components, operation, and maintenance costs, as well as other aspects of the microgrid's reliability and operation [104, 105, 106]. Microgrid scheduling aims to minimize an objective function subject to a variety of operational constraints, such as energy balance, load management, and DER limitations. The objective function can be used to minimize cost, losses, and CO<sub>2</sub> emissions or maximize profits. A multi-objective function utilizes a variety of objective functions to improve the scheduling problem [107, 108]. The economic scheduling problem is studied in terms of architecture and methodology. The architecture includes centralized [109] and distributed [110, 111] forms, while the methodology may include deterministic [112], heuristic [113, 114], or stochastic [115] methods. Finally, DSM is a promising economic aspect that is working on the load side to engage the consumers in the process. The authors in [116] discussed the demand response in terms of models, infrastructure, and communication, as well as the challenges and future trends. DSM programs encourage consumers to modify their electricity usage and get paid to reduce consumption. To encourage customers to participate in DSM programs, DSM initiatives include [52]

1. Promoting the use of energy-efficient products and equipment
2. Encourage customers to change non-critical electricity use from peak times to evening and early morning hours.
3. Promoting high-efficiency building construction.
4. Promoting energy awareness and education.

### **2.2.6 Microgrid Cybersecurity**

Cybersecurity is an important factor in smart grid operations in general. Recently, the conducted studies on cybersecurity have been intensively reviewed

in literature [117, 118, 119] due to the increasing of cyberattacks in electricity infrastructure. In addition to the vulnerabilities of smart grid applications to cyberattacks that are classified based on the delivery methods, including cyber, communication, physical, and network-based attacks. These attacks include command and code manipulations, Malware and false data injections, electromagnetic and physical damage, and denial of service. According to [118], False Data Injection attacks (FDIA) and Denial-of-Service (DoS) are the most common types of cyberattacks. In FDIA, the data sent from the sensors are manipulated without affecting the code of the controllers. Whereas in DoS, the communication network is flooded with meaningless packets, which leads to inaccessible networks due the excessive traffic.

The cybersecurity methodologies to prevent or mitigate the impact of cyberattacks can be classified into two main categories; preventive and detection approaches. Preventive approaches aim to prevent attacks on the system through an encryption mechanism. However, the effectiveness of the preventive method requires synchronous development with all components of the system which is not practical for large systems and is expensive. In the detection approach, the focus is on recognizing anomaly intrusion and applying mitigation methods to restore the system to its normal state. The detection methods have two categories; model-based and data-driven detection algorithms.

The model-based algorithms detect anomalies in two steps. First, a state estimation algorithm is calculated. Then, the estimated model is compared with actual data from the grid to detect disparities. Weighted least squares estimators were used to produce static-based estimation in [120]. The static-based estimation only considers the current state of the system with no prior knowledge of earlier steps. Dynamic-based state estimation was proposed to include previous states of the system using Kalman filter estimation in [121]. Some other algorithms uti-

lizing model-based detection methods that are estimation-free are reported in the literature such as cooperative vulnerability factor [122] and A voting protocol for Multi-agent system (MAS) [123]. Although the model-based detection approaches are efficient and practical, their performance depends on the accuracy of the system's model.

The other approach for detecting cyberattacks in smart grids is the data-driven detection approach, where the need for a model is eliminated. Such approaches are preferable due to the detection accuracy and flexibility since it only requires measured voltage and current data to be sent [117]. Depending on the accuracy of historical data and the algorithm used, data-driven methods detect the anomaly. A variety of methods are used for data-driven approaches, which are categorized into machine learning and data mining algorithms. In machine learning algorithms, supervised, unsupervised, and reinforcement learning algorithms are used. The supervised machine learning algorithms require data to be labeled in advance and then applied to the training process. Different types of supervised machine learning algorithms are applied for cyberattacks detection, such as linear regression[124], Support Vector Machine (SVM) [125], and Convolution Neural Network (CNN) [126]. Whereas, the unsupervised machine learning algorithms, such as K-mean clustering [127], the data grouped into clusters in which the abnormal behaviors are classified as anomalies. The reinforcement learning was also used for cyberattack detection algorithms in [128]. The second approach in data-driven detection methods is the data mining approach in which large data sets are explored to discover patterns as given in [129].

### **2.3 Hierarchical Control Structure in Islanded AC Microgrid**

A microgrid's control system should maintain the microgrid's stable, reliable, and economic operation in both modes of operation. The desired operation

of a microgrid's control system should ensure [84, 9, 52, 10]:

- Voltage and frequency regulation in both modes of operation.
- An acceptable level of power quality.
- Accurate power-sharing and DG coordination.
- Synchronization with the main grid.
- Seamless transition from grid-connected to islanded mode.
- Power flow control between main grid and microgrid.
- Optimal microgrid operation cost.

The hierarchical control structure used in the conventional power system is proposed to accommodate the above-mentioned control objectives at different time scales. The implementation of hierarchical control allows the interaction between management and control operation of the main grid; therefore, harmonious control of the microgrid within the main grid is improved, as well as their effective integration. The hierarchical control structure is implemented in the microgrid to minimize the operation cost while maximizing efficiency, reliability, and controllability [59]. The hierarchical control structure is classified into three levels: primary, secondary, and tertiary. Those three levels are distinguished by the time scale in which they react and the infrastructure requirements (e.g., communication requirements). All DGs, controllable loads, and ESSs in a microgrid are controlled through different levels of hierarchical structure, as shown in Figure 2.6. Power quality control is included to ensure the high quality of the injected power to the microgrid. The hierarchical control structure is addressed extensively in the literature [130, 10, 131, 84, 57, 9].

### 2.3.1 Voltage and Current Control

DG units in microgrids have a cascaded control loop to control the injected current and voltage. The typical requirements of this level of control are to have: i)

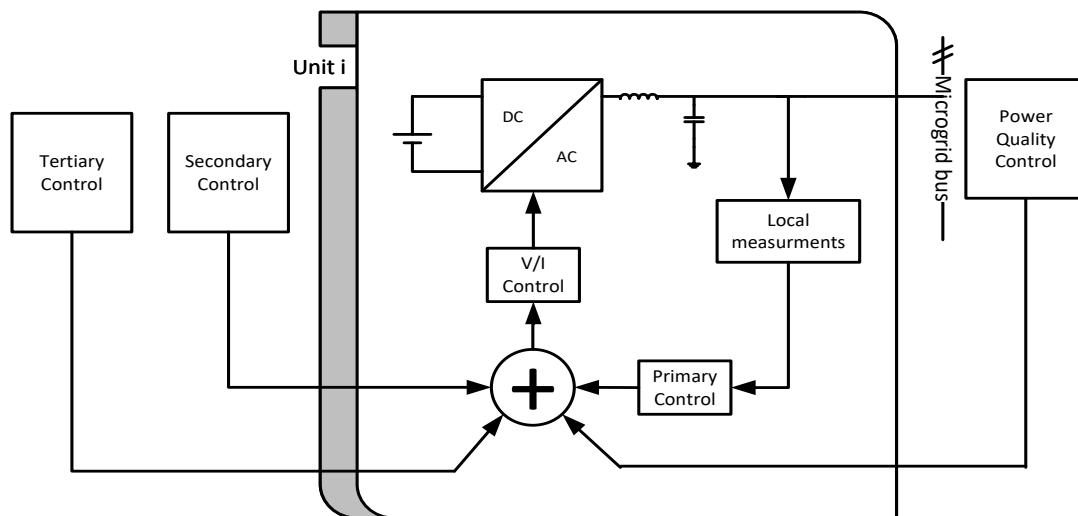


Figure 2.6: Hierarchical control structure.

zero steady-state error; ii) good reference tracking during transients; iii) high bandwidth to ensure fast dynamics; and iv) good low-order harmonic rejection [132]. The inner control loop realizes the instantaneous current control to provide peak-current protection. The current references of the inner control loop are generated from an outer voltage loop with lower bandwidth to ensure dynamic decoupling between the cascaded controllers.

The design methodology of cascaded loop controllers can be classified into three types: i) synchronous reference frame control, ii) stationary reference frame control, and iii) natural frame control [133]. The synchronous reference control uses  $abc \rightarrow dq$  transformation of control variables to control the DC components, which facilitates filtering and control using a proportional-integral (PI) controller. In the stationary reference control, the control variables are transformed into sinusoidal components using  $abc \rightarrow \alpha\beta$  transformation; however, using the PI controller leads to steady-state error, which can be removed by using the proportional resonance (PR) controller instead. In natural frame control, a controller for each phase is implemented; however, the type of phase connection (delta or wye) and

whether there is an isolated neutral need to be considered.

The outer voltage loop receives its reference voltage according to the control strategy of the DG being controlled. In this level of control, the DG can operate in two modes of control: PQ mode and VSI mode [84]. In PQ mode, the reference inputs to the control system of the corresponding DG units are real and reactive power. Those references are obtained from a higher level of hierarchical control where the optimal unit commitment is performed. While in the VSI mode, the references are the desired voltage and frequency of the microgrid to maintain the voltage and frequency within their allowable limits. These two modes are classified based on their output control variables. In PQ mode, the control variables are the active and reactive power injected with a specified voltage and frequency input to feed the microgrid. In VSI mode, the voltage and frequency control variables are based on the measured active and reactive power to form the microgrid.

### **Grid-following DGs**

In grid-connected mode, the frequency and voltage are controlled predominantly by the main grid. Therefore, all DGs in the microgrid operate in PQ modes, and active and reactive power references follow the predetermined values of a higher hierarchy. These values depend on whether the DG consists of dispatchable units (e.g., diesel engine and fuel cell generator) adjusted based on dispatch signals or non-dispatchable units adjusted based on MPPT strategy (e.g., variable speed wind turbine and PV energy system). In PQ mode, the DG inverter is implemented as a current-controlled inverter in which the active and reactive powers are controlled and synchronized using a phase-locked loop (PLL)[134]. The control system of a grid-following DG unit is shown in Figure 2.7

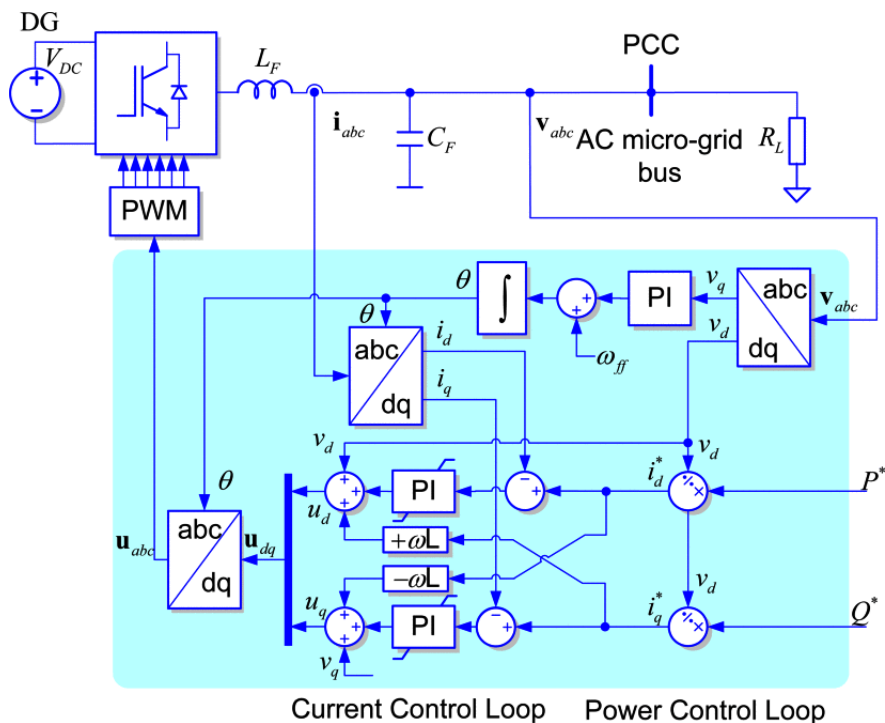


Figure 2.7: Grid-following unit

### Grid-forming DGs

In islanded mode, the microgrid is required to maintain the voltage and frequency within a specific limit. Thus, one or more DGs are assigned to take over the frequency and voltage control by modifying its control strategy to VSI mode. In VSI mode, the DG inverter feeds the microgrid with active and reactive power to keep the voltage and frequency within a predefined tolerance. In VSI mode, the DG inverter acts as a voltage-controlled inverter. The voltage and frequency references are generated by the higher hierarchical level and maintained by injecting active and reactive power into the microgrid. Figure 2.8 shows the control system of a grid-forming DG unit.

Grid-supporting DGs form the third category. These types of DGs are considered when more than one DG unit participates in frequency and voltage regulation. The grid-supporting units can be either a current-controlled-based DG

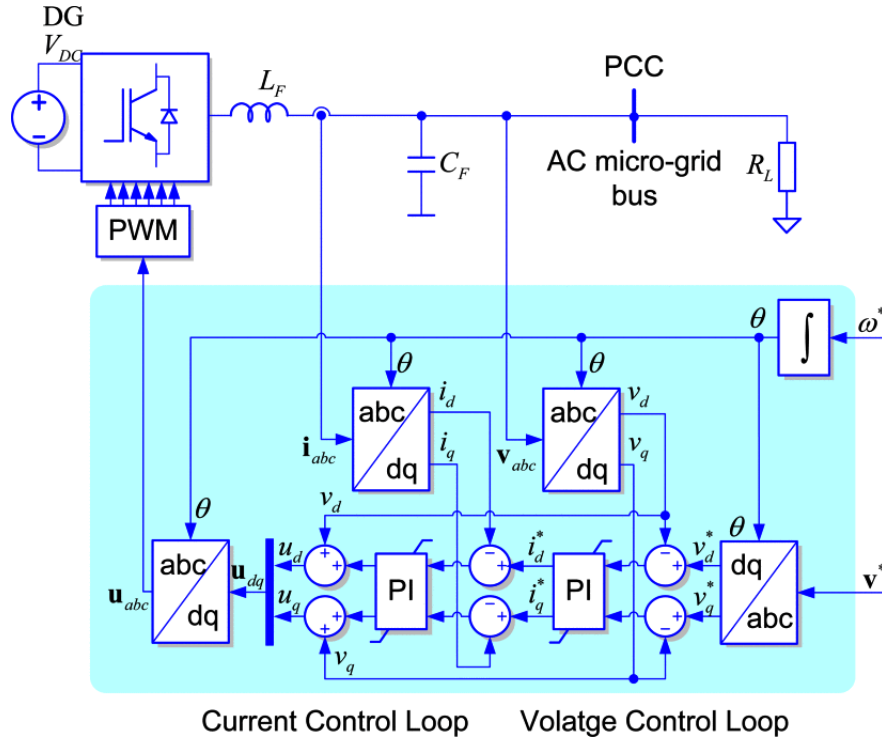


Figure 2.8: Grid-forming unit

to support the frequency or a voltage-controlled-based DG to support the voltage [59]. When a group of grid-supporting DGs is used, a power-sharing between them is considered to avoid overloading.

### 2.3.2 Power Quality Control

It is essential to incorporate power quality in the context of the hierarchical control structure. This is primarily because of the high uncertainty of generation and the lack of inertia in microgrids that causes the system to be extremely oscillatory. Generation is uncertain because of the intermittent nature of renewable energy resources, which is due to varying weather conditions. Therefore, in high-penetration renewable energy microgrids, the system experiences a fast-changing dynamic behavior. This fast dynamic is exacerbated when the inertia is low or zero due to the existence of power electronic converters as the main interface be-

tween DGs and the microgrid, which hides the dynamics of the DG itself behind it. Besides, the dynamic and unbalanced loads lead to other quality-related issues. Hence, power quality control aims to stabilize and ensure the high quality of injected power to the microgrid. Inertia control and harmonic and unbalanced voltage compensation are the main control objectives implemented in this course of control.

In the islanded mode of operation, the inertia of the system is low or even non-existent because of the high penetration of inverter-based DGs. Therefore, when a disturbance occurs in the microgrid, stabilizing the frequency and voltage is difficult and may result in loss of stability and blackout. The inertia control can be implemented within the DG controllers to improve the stability of the microgrid by adding a virtual damping coefficient into the closed-loop control of the DG control system [135, 136]. Inertia control is also achieved by employing the rotating mass of variable-speed wind turbines and sacrificing the MPPT algorithm when the wind speed is below the rated speed. However, at rated wind speed, pitch control of the wind turbines can be activated without affecting the MPPT algorithm [137].

One of the objectives of the DGs is to inject a current with low harmonic distortion. IEEE Std 1547-2018 limited the total rated current distortion (TRD) to 5%, including higher order harmonics as given in Table 2.1 [73]. Current harmonic distortion leads to various problems in the distribution system, such as heating equipment, overloading neutrals, overheating transformers, nuisance tripping of circuit breakers, and over-stressing power factor correction capacitors. Furthermore, these current harmonics lead to voltage harmonic distortion. This leads to power quality degradation in the microgrid [138]. There are various methods used to compensate for harmonics in DG controllers based on controller topology. In DG controllers using the PI control method, the harmonic compensator is designed for

Table 2.1: Maximum odd harmonic current distortion

Odd harmonic order $h$	$h < 11$	$11 \leq h < 17$	$17 \leq h < 23$	$23 \leq h < 35$	$35 \leq h < 50$
#Percentage (%)	4	2	1.5	0.6	0.3

each harmonic order independently (i.e., 5<sup>th</sup>, 7<sup>th</sup>, etc.) Also, controllers based on PR controllers achieve harmonic compensation by cascading several generalized integrators tuned to resonate at the desired frequency [133]. Non-linear controllers with fast dynamics have no issue with low-order harmonics.

Voltage imbalance may exist in the microgrid for various reasons such as nonlinear or unbalanced loads, single-phase generators, or grid faults[139]. The unbalanced voltage causes various undesirable consequences in the microgrid. It has a negative impact on induction motors, power electronic converters, and adjustable speed drives (ASDs). The International Electrotechnical Commission (IEC) limits the acceptable voltage imbalance to less than 2% [140]. The DG's output can compensate for voltage imbalances in the microgrid. One approach is to utilize a shunt inverter with a series inverter; the shunt inverter controls the active and reactive power and the series inverter balances the line current and voltage by injecting a negative-sequence voltage [141]. Another approach as in [142], is based on controlling the DG as a negative sequence conductance to compensate for voltage imbalance in the microgrid.

### 2.3.3 Primary Control Level

Primary control is the lowest level in the hierarchical control structure; hence, it possesses the fastest response. The primary control functions include the stabilization of the voltage and frequency of a microgrid subjected to an islanding event where that microgrid may lose its voltage and frequency stability because of the mismatch between the power generation and demand. In addition, the

primary control ensures accurate power-sharing between all DGs [84, 59]. The power-sharing control is required to ensure proper power-sharing between units participating in voltage and frequency regulation to avoid overloading [14]. The primary control provides the reference points for the voltage and current control loops of DERs.

Communication at this level is unfavorable because of high-bandwidth communication requirements. However, some works consider communication-based control, such as the central control method, master/slave control, and distributed control. In central control methods[143, 144, 145], the MGCC periodically updates the droop control characteristics through communication links that optimize the operation of the microgrid while considering the stability of voltage and frequency. Master/slave controls employ one unit as a master unit to regulate the output voltage and specify the current reference of the rest of the slave units through a high bandwidth communication channel [146, 147]. In distributed control [148], the instantaneous average current sharing is calculated and sent to a current sharing bus, which is considered a current reference for each parallel converter. Another strategy of distributed control utilizes cooperative control to employ a sparse communication network in which the unit is only required to communicate with its neighboring units [149, 150].

Non-communication methods employ droop control characteristics to overcome the high-bandwidth communication requirements. Droop methods mimic the principle of power balance of synchronous generators in the power system, which is to reduce the frequency as the active power increases. Assuming a high inductive grid, the droop equations can be given as

$$\omega_i = \omega_{nom} - K_{p_i}(P_i - P_{ref}) \quad (2.1a)$$

$$V_i = V_{nom} - K_{q_i}(Q_i - Q_{ref}) \quad (2.1b)$$

Where  $\omega_i$  and  $V_i$  are the angular frequency and terminal voltage of  $i^{th}$  unit,  $\omega_{nom}$  and  $V_{nom}$  are the nominal angular frequency and terminal voltage,  $K_{p_i}$  and  $K_{q_i}$  are active and reactive power droop coefficients,  $P_i$  and  $Q_i$  are the measured active and reactive power of  $i^{th}$  unit, and  $P_{ref}$  and  $Q_{ref}$  are the reference active and reactive power, respectively.

The droop coefficients  $K_{p_i}$  and  $K_{q_i}$  identify the power-sharing capabilities of each unit. Furthermore, the time constant of the closed-loop control depends only on the droop control coefficients. The choice of the droop control coefficients also affects the stability of the microgrid. Therefore, stability analysis should be used to choose the appropriate values of the droop coefficients as given in [151, 152, 153]. The authors in [154] proposed a droop control that tunes the time constant without interfering with steady-state power-sharing.

Although the conventional droop control method offers a communication-free framework for the primary control level, challenges are associated with its application to microgrids that impact its effectiveness. These challenges include [14, 155, 9, 131, 156]:

- During islanded mode, the voltage and frequency of the microgrid depend on the load. Therefore, steeper droops provide better load sharing but result in greater frequency and voltage deviations or even instability.
- Conventional droop control assumes that the grid is highly inductive. However, microgrids are normally located in Medium Voltage (MV) or Low Voltage (LV) grids where the lines are mixed impedance or even resistive. Therefore, this assumption is not valid in such grids.
- Unlike frequency, voltage is a local variable because of the voltage drop in the lines with different impedance. Thus, an intrinsic trade-off is initiated between voltage regulation and the sharing of reactive power.

- The conventional droop control method focuses on fundamental power sharing, which is averaged over one cycle. Therefore, harmonic load components cannot be properly shared, leading to harmonic circulating currents and poor power quality.

Several studies in the literature addressed these issues [157, 158, 159]. In [13, 157], the droop control technique was designed for low voltage (LV) grids where the grid is assumed to be resistive. In these techniques, the frequency is controlled through reactive power and the voltage through active power. In a Medium Voltage (MV) microgrid, the resistance of the line is approximately equal to the reactance; hence, a coupling between active and reactive power occurs in controlling voltage and frequency. Therefore, the authors in [160] proposed a V-P-Q droop control method to regulate the PCC voltage with active and reactive power droop coefficients. These droop coefficients are adjusted online through a lookup table based on the PCC voltage level. Some other authors also suggested virtual output impedance methods [158, 161]. In these methods, a virtual inductance is embedded into the closed-loop control system through voltage reference to emulate an inductive behavior. Therefore, the new reference voltage is given as

$$V_{ref}^* = V_{ref} - Z_v(s)i_o \quad (2.2)$$

Where  $V_{ref}$  is the no-load reference voltage,  $Z_v(s)$  is the transfer function of virtual impedance, i.e.,  $Z_v(s) = sL_v$ , and  $i_o$  is the output current.

High-frequency noise due to the differentiation operator can cause instability in the voltage closed-loop control. Therefore, a low-pass filter is used in combination with the virtual inductance [162]. Other authors further developed virtual output impedance methods to realize better reactive and harmonic power-sharing by introducing complex virtual impedance for the fundamental and selected harmonic frequencies [159]. One method employed by [163] and [164] utilized the

virtual frame transformation. In this method, an orthogonal linear rotational transformation matrix is used to calculate "modified" active and reactive powers, which account for the line parameters. The rotational transformation matrix requires the absolute value of the X/R ratio to be implemented. In [165], an adaptive voltage droop scheme was used to compensate for the voltage drop in the line and improve the stability of the system under overload conditions by adding two novel terms to the droop control equations. However, the line parameters R and X are required for the implementation of the controller. Another approach of adaptive droop control was proposed in [166], in which the slope of the voltage drop in the line is tuned to compensate for the effect of the mismatch in the voltage drop across the feeder. Hybrid schemes have also been proposed in the literature [167, 168]. In addition, other techniques such as current sharing [169], angle sharing [170, 171], and voltage integral-based droop control [172] were also considered in the literature to tackle the primary control difficulties.

### 2.3.4 Secondary Control Level

Secondary control restores the voltage and frequency values to their nominal values to compensate for the deviations caused by the primary control. Furthermore, the secondary control is responsible for managing the trade-off between voltage regulation and reactive power-sharing caused by the voltage drop in the microgrid's line with different parameters [9]. The secondary control has a slower time constant to allow the primary control to reach a steady state value to avoid control interaction. To account for the secondary control action, the droop control equations given in (2.1a) and (2.1b) becomes

$$\omega_i = \omega_{nom} - K_{p_i}(P_i - P_{ref}) + \delta\omega_i \quad (2.3a)$$

$$V_i = V_{nom} - K_{q_i}(Q_i - Q_{ref}) + \delta V_i \quad (2.3b)$$

Where  $\delta_{\omega_i}$  and  $\delta_{V_i}$  are the secondary control corrective terms, respectively.

The secondary control architecture is classified according to the communication infrastructure into three main categories: centralized (CSC), decentralized (DESC), and distributed (DISC) [173]. The CSC structure operates in the MGCC to collect data about the system through communication, compute the desired setpoints for all units, and broadcast the setpoints to the corresponding units [174, 175, 176]. The CSC requires high-bandwidth communication and a powerful computational MGCC to perform the secondary control functionalities. The DESC aims to provide secondary control functionalities without utilizing the communication infrastructure [177], [178]. However, such a structure suffers from poor performance, especially in power-sharing, due to the lack of information about the other units. Recently, the state estimation-based approach has been utilized as an alternative for the communication infrastructure [179]. Finally, the DISC is employed as a compromised structure in which the communication link is relaxed and eliminates the need for an MGCC. The structure of DISC is implemented using an average-based approach, in which each unit measures its variables and then transmits them to all other units to calculate the average between them [180, 181]. This type of DISC requires a communication link between all units participating in frequency and voltage control. Another type of DISC is based on a consensus approach in which communication is established between neighboring units described by the connectivity of the graph [182, 183, 184, 185, 186, 187, 188]. In addition, some recent works employed an event-triggered approach to DISC in such a way that the communication link is only established when a defined criterion is initiated [189, 190, 191].

Several recent research projects have focused on trying to solve the poor reactive power-sharing through DISC. In [184], a robust wireless communication algorithm was used to collect information about voltage and frequency errors and

the reactive power of all units based on distributed averaging. PI compensators were utilized to restore the deviations of voltage, frequency, and reactive power-sharing. The authors in [182] proposed a distributed control mechanism based on a consensus protocol in which the trade-off between voltage regulation and reactive power-sharing can be tuned based on the designer's requirements. In [183], A distributed averaging control scheme employing communication and compensation layers utilized a multi-agent system-based (MAS-based) finite-time consensus protocol for voltage restoration and reactive power-sharing. The communication layer collected the global information via a distributed MAS-based finite-time information-sharing protocol, and the compensation layer used a PI controller to compensate for the voltage deviation caused by the Q-V droop. In [191], an event-triggered consensus secondary control was employed with a finite-time control strategy to restore the frequency and voltage of units and provide accurate sharing of reactive power. However, these studies focus on driving the voltage into a common global consensus average while maintaining the reactive power-sharing between units without considering upper or lower bounds for the voltages.

Recently, some work has been done to share the reactive power accurately while bounding the voltage to limits in a consensus manner[17, 18, 19, 20]. [17] implemented two PI controllers in the secondary control level to keep the voltage within a predefined range (a containment-based controller) and maintain precise reactive power-sharing (a consensus-based controller). However, when precise reactive power-sharing cannot be maintained for the given voltage range, settings are required to either enlarge the voltage range of the containment-based controller to keep precise reactive power-sharing or set the error saturation for the consensus-based controller to allow a reactive power-sharing mismatch while keeping the voltage range intact. Additionally, only leader units can access the voltage lower and upper bounds. In [20], two alternative output limitation meth-

ods were used to deal with either the voltage or reactive power-sharing bounds proposed for the consensus-based approach. However, all DGs must be connected to a common critical bus. The authors in [19] employed a model predictive control (MPC) to predict the optimal behavior of DG units in terms of voltage regulation and power-sharing and share it with neighbor units described by the communication graph. The power transfer equations were used to predict the active and reactive power generation in the coupling elements and were combined with droop control equations to predict the optimal behavior of the DG units. The technical constraints contain voltage and power capacity limits. However, the average voltage and frequency value for all units is required, which requires the unit to communicate with all other units to share extensive information. In [18], an optimization function was implemented to minimize the trade-off between voltage regulation and reactive power-sharing subject to the technical constraints of the DGs output, including voltage limits and reactive power capacity. However, the controller requires the line parameters between connected DGs, which is not practical in distribution systems.

### **2.3.5 Tertiary Control Level**

Tertiary control is the highest level in the hierarchical control structure and is located at the host grid level. It coordinates the operation of multiple microgrids that interact with each other to achieve optimal distribution system operation. The tertiary control has a large timescale in the order of minutes [9]. In microgrids, the tertiary control is activated in grid-connected mode since the economic operation is the responsibility of the distribution network operator (DNO). However, some work has been done to integrate economic operation within islanded microgrids [192, 193, 194].

The integration of economic aspects with microgrid operation can be categorized into economic dispatch-based, and optimal power flow-based approaches. In economic dispatch [25, 26, 27], units with different cost coefficients are dispatched based on the lowest price, considering the maximum capacity of the committed units and satisfying power balance equality. On the other hand, optimal power flow considers a variety of objective functions subjected to a range of constraints [21, 22, 23]. Optimal power flow-based techniques are usually performed offline due to the non-convexity of optimal power flow and the need for linear approximation or convex relaxation techniques [24]. Therefore, the economic dispatch approach is more suitable for real-time applications.

Economic dispatch algorithms for islanded microgrids are usually performed on the grid-following units where the reference of active power is determined by these algorithms. Zhiyuan *et al.* [194] proposed a consensus-based economic dispatch algorithm to solve the energy management problem for the islanded microgrid considering the active power with constraints in unit capacity. In [25], an economic dispatch algorithm was presented to dispatch active power in real-time; however, the grid-forming units were not considered. The authors in [27] proposed a real-time economic dispatch-based secondary controller for an islanded microgrid that dispatches the active power in correlation with frequency without considering reactive power generation and voltage control. In [195], a two-layer model was used to provide economic dispatch to the islanded microgrid in a distributed manner where the microgrid was considered as the lower layer while the communication network was the upper layer. In the communication layer, two control laws were derived to ensure supply-demand balance and solve the economic dispatch problem.

## CHAPTER 3 GENERALIZED DROOP CONTROL

### 3.1 Introduction

When the microgrid is isolated from the main grid, the grid-forming units control the frequency and voltage to maintain the microgrid's stability. The hierarchical control structure provides these functionalities through three levels of control. Droop control is used at the primary level to sustain the microgrid's frequency and voltage and maintain the power-sharing between units according to their power rating. Units generate active and reactive powers appropriate for their rating by varying their terminal frequency and voltage. However, the microgrid is implemented in a distribution network where the voltage level is medium. In such a voltage level, the  $X/R$  ratio approaches unity; hence, the frequency and voltage are related to the active and reactive powers through a non-linear relationship of line impedance. Therefore, frequency and voltage must be tuned to supply active or reactive power. Otherwise, instability of frequency and voltage control occurs in the islanded microgrid.

In this chapter, generalized droop control is proposed for the droop control level to maintain the stability of frequency and voltage regardless of the  $X/R$  ratio level. In the generalized droop control, a normalized dependency matrix is derived from identifying the per-unit relationship between the frequency and voltage with active and reactive powers. Then, droop control utilizes the dependency matrix to achieve an accurate relationship between frequency and voltage with active and reactive powers. To implement the dependency matrix, the  $X/R$  ratio is required to calculate the line impedance phase angle. The phasor Measurement Unit (PMU) communicates the grid voltage and current through synchrophasor

communication to calculate the line's active and reactive power consumed. Then, the line parameters are estimated and used to generate the normalized dependency matrix. The results of this chapter are based mainly on [196].

The controller proposed in this chapter implements a per-unit linear relationship between frequency and voltage with active and reactive powers to be used in droop control equations. The features of the proposed controller include

- The frequency and voltage are precisely tuned based on the measured active and reactive powers.
- The X/R ratio is obtained from the line active and reactive power.
- The dependency matrix elements take values from -1 to 1 based on the per-unit relationship between the variables.

The chapter is organized as follows. First, section 3.2 illustrates the main objectives of the primary control level used for the grid-forming unit, and the issue of droop control in a mixed impedance grid is introduced. Then, in Section 3.3, the proposed generalized droop controller is derived and implemented. Then, section 3.4 presents the simulation results and discussion. Finally, Section 3.5 concludes the chapter.

### **3.2 Primary Control in Islanded Microgrid**

During grid-connected mode, frequency and voltage are controlled by the main grid. However, when a fault occurs in the main grid, the microgrid is disconnected and continues to operate in islanded mode, supplying its load. Grid-forming units rapidly take over the frequency and voltage control to ensure a seamless transition. Load shading may require curtailing some loads based on the available power to maintain the frequency and voltage within a stable limit. However, one grid-forming unit may overload during operation based on its capacity. Therefore, a group of grid-forming units is utilized to share the load based

on the droop control technique, in which each unit is allowed to vary its terminal frequency and voltage based on its active and reactive power ratings.

Grid-forming units employ a hierarchical control structure to maintain the frequency and voltage of the microgrid at three sequential levels structured based on different time constants to avoid interaction of control objectives at each level. Figure 3.1 shows the control system of grid-forming units working in parallel. The required active and reactive power is supplied at the primary control level by tuning the frequency and voltage correspondingly. Then, the secondary control restores the voltage and frequency deviations caused by the primary control to their nominal values. The tertiary control level ensures an economical and reliable microgrid operation and includes supervisory control. The control signals of those levels are used to generate the reference values of frequency and voltage, which are processed through voltage and current control loops to ensure an appropriate quality of output quantities and provide current protection to the connected inverter. The inverter receives PWM signals to convert the DC power to AC power and maintains the frequency and voltage based on the reference signals from the controller. Finally, the output is connected to the grid bus through an LC filter to reduce harmonic distortion.

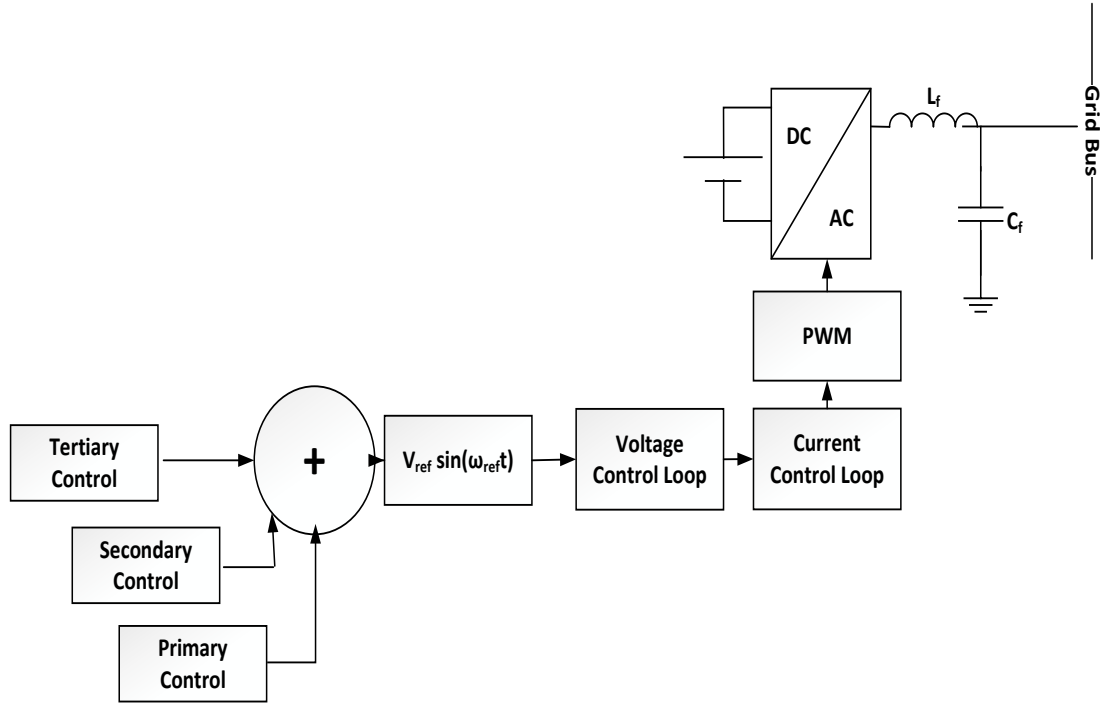


Figure 3.1: The hierarchical control structure of grid-forming units.

### 3.2.1 Droop Control in Mixed Impedance Microgrid

Consider an inverter-based unit connected to a grid bus through a line impedance  $|Z|\angle\theta$  as seen by the inverter as shown in Figure 3.2. The complex power flow is given as

$$S = V_g I^* = \frac{|V_g| |V_s| \angle(\theta - \delta)}{|Z|} - \frac{|V_g|^2 \angle\theta}{|Z|} \quad (3.1)$$

Where  $|V_g|$  and  $|V_s|$  are the magnitude of grid voltage and source voltage, respectively, and  $\delta$  is the power angle.

Based on (3.1), the active and reactive powers flow equations are given as.

$$P = \frac{|V_g| |V_s| \cos(\theta - \delta)}{|Z|} - \frac{|V_g|^2 \cos(\theta)}{|Z|} \quad (3.2a)$$

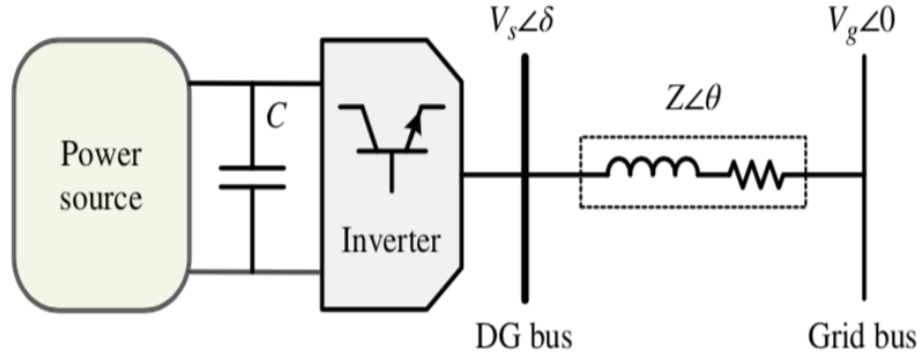


Figure 3.2: Inverter-based unit connected to a grid bus.

$$Q = \frac{|V_g||V_s| \sin(\theta - \delta)}{|Z|} - \frac{|V_g|^2 \sin(\theta)}{|Z|} \quad (3.2b)$$

The interconnection line impedance is transformed to a complex format as  $|Z| \angle \theta = R_l + jX_l = |Z| \cos(\theta) + j|Z| \sin(\theta)$  hence,  $\cos(\theta)$  and  $\sin(\theta)$  are given as

$$\cos(\theta) = R_l / |Z| \quad (3.3a)$$

$$\sin(\theta) = X_l / |Z| \quad (3.3b)$$

Equating (3.2) in (3.3) and assuming the power angle  $\delta$  is small for line impedance analysis, hence,  $\sin \delta \cong \delta$  and  $\cos \delta \approx 1$ . The delivered active and reactive powers are given as

$$P = \frac{|V_g|}{R_l^2 + X_l^2} [R_l(|V_s| - |V_g|) + X_l(|V_s| \delta)] \quad (3.4a)$$

$$Q = \frac{|V_g|}{R_l^2 + X_l^2} [-R_l(|V_s| \delta) + X_l(|V_s| - |V_g|)] \quad (3.4b)$$

(3.4) is given in matrix form as

$$\begin{bmatrix} P \\ Q \end{bmatrix} = \begin{bmatrix} \frac{|V_g||V_s|X_l}{R_l^2 + X_l^2} & \frac{|V_g|R_l}{R_l^2 + X_l^2} \\ -\frac{|V_g||V_s|R_l}{R_l^2 + X_l^2} & \frac{|V_g|X_l}{R_l^2 + X_l^2} \end{bmatrix} \begin{bmatrix} \delta \\ (|V_s| - |V_g|) \end{bmatrix} \quad (3.5)$$

The power angle and the voltage magnitude difference can be found by investing (3.5) as

$$\begin{bmatrix} \delta \\ (|V_s| - |V_g|) \end{bmatrix} = \begin{bmatrix} \frac{X_l}{|V_g||V_s|} & -\frac{R_l}{|V_g||V_s|} \\ \frac{R_l}{|V_g|} & \frac{X_l}{|V_g|} \end{bmatrix} \begin{bmatrix} P \\ Q \end{bmatrix} \quad (3.6)$$

### 3.2.2 Droop Control Equations

In droop control, the power angle  $\delta$  is related to the change of frequency  $\Delta\omega$ , and the voltage magnitude difference ( $|V_s| - |V_g|$ ) is related to the change of voltage  $\Delta V$  given as a function of negative droop coefficients  $K_p$  and  $K_q$  multiplied by measured active and reactive power. The droop coefficients are chosen to relate the maximum change of frequency ( $\Delta\omega_{max}$ ) and voltage ( $\Delta V_{max}$ ) to the rated active ( $P_{max}$ ) and reactive power ( $Q_{max}$ ) of the unit as shown in the following relation.

$$K_p = \Delta\omega_{max} / P_{max} \quad (3.7a)$$

$$K_q = \Delta V_{max} / Q_{max} \quad (3.7b)$$

Therefore, droop control equations are given as

$$\begin{bmatrix} \Delta\omega \\ \Delta V \end{bmatrix} = A \begin{bmatrix} -K_p P \\ -K_q Q \end{bmatrix} \quad (3.8)$$

Where A is a 2x2 dependency matrix,  $A = \begin{bmatrix} a_{11} & a_{12} \\ a_{21} & a_{22} \end{bmatrix}$

The quantities in (3.8) are then used to produce the reference frequency and voltage based on the following:

$$\omega_{ref} = \omega_{nom} + \Delta\omega \quad (3.9a)$$

$$V_{ref} = V_{nom} + \Delta V \quad (3.9b)$$

Matrix A is a dependency matrix that identifies the relationship between the change of frequency and voltage to the drooped active and reactive power.

According to (3.7), elements  $a_{11}$  and  $a_{22}$  are functions of the line reactance ( $X$ ), and the elements  $a_{12}$  and  $a_{21}$  are functions of the line resistance ( $R$ ). In a high voltage grid where  $X/R$ , the resistance is neglected, and the elements of the dependency matrix in equation (3.9) are given as  $a_{11} = a_{22} = 1$  and  $a_{12} = a_{21} = 0$ . In other words, the change of frequency depends on the active power, and the change of voltage is related to the reactive power. While, in a low voltage grid, the grid is resistive, and the relation between the resistance and reactance is given as  $R \gg X$ . Neglecting the line reactance, the dependency matrix elements are given as  $a_{11} = a_{22} = 0$  and  $a_{12} = a_{21} = 1$ . As a result, the change in frequency is related to the reactive power, and the change in voltage is related to the active power. However, at medium voltage, both resistance and reactance are considered, and the changes in frequency and voltage are given as a combination of active and reactive power. Therefore, a mechanism to relate droop control to the equivalent impedance is required, especially because the microgrid is typically located in medium and low voltage grids.

### 3.3 The Proposed Generalized Droop Control

According to (3.9), the elements of dependency matrix  $A$  vary between -1 and 1 through 0 where -1 indicates inversely entirely dependent, 0 infers fully independent, and 1 implies entirely dependent. These elements vary according to the line impedance as shown in (3.7). To include the line impedance effect in the droop control, the dependency matrix should consider a normalized version of the equivalent impedance so that the dependence of changes in frequency and voltage is accurately described based on the equivalent impedance.

### 3.3.1 Derivation of Normalized Dependency Matrix

To identify the normalized dependency matrix, consider the relationship matrix given in (3.7) given as

$$\begin{bmatrix} b_{11} & b_{12} \\ b_{21} & b_{22} \end{bmatrix} = \begin{bmatrix} \frac{X_l}{|V_g||V_s|} & -\frac{R_l}{|V_g||V_s|} \\ \frac{R_l}{|V_g|} & \frac{X_l}{|V_g|} \end{bmatrix} \quad (3.10)$$

From (3.10), one can identify the normalized dependency matrix as follows.

$$\begin{bmatrix} a_{11} & a_{12} \\ a_{21} & a_{22} \end{bmatrix} = \begin{bmatrix} \frac{b_{11}}{|b_{11}|+|b_{12}|} & \frac{b_{12}}{|b_{11}|+|b_{12}|} \\ \frac{b_{21}}{|b_{21}|+|b_{22}|} & \frac{b_{22}}{|b_{21}|+|b_{22}|} \end{bmatrix} = \begin{bmatrix} \frac{X_l}{X_l+R_l} & -\frac{R_l}{X_l+R_l} \\ \frac{R_l}{R_l+X_l} & \frac{X_l}{R_l+X_l} \end{bmatrix} \quad (3.11)$$

As shown in (3.11), the normalized dependency matrix has taken values between -1 and 1. Therefore, when the resistance is neglected, as in a high voltage grid, the frequency and voltage changes are only dependent on active and reactive power correspondingly and vice versa in a low voltage grid when the equivalent reactance is neglected. Additionally, for a medium voltage grid, considering  $R_l = X_l$ , the change of frequency and voltage are dependent on both active and reactive power by 50% each.

### 3.3.2 Identify the Normalized Dependency Matrix Elements

The line resistance and reactance need to be known to identify elements of the normalized dependency matrix. However, these parameters are subject to change due to grid reconfiguration and temperature affecting the line parameter values. Therefore, employing phasor measurement based on synchrophasor communication enables rapid and accurate measurements of the magnitude and phase angle of voltage and current [197].

Considering the system given in Figure 3.2, a phasor measurement unit can be used to communicate the grid voltage and current. In the controlled unit, the

active and reactive power consumed by the line is calculated based on the communicated signals subtracting receiving end power from the power generated by the unit. Per phase line resistance and reactance are found as follows.

$$R_l = \frac{P_{line}}{3I^2} \quad (3.12a)$$

$$X_l = \frac{Q_{line}}{3I^2} \quad (3.12b)$$

The line impedance angle  $\theta$  is related to X/R ratio based on (3.3) as

$$\theta = \tan^{-1} \left( \frac{X_l}{R_l} \right) \quad (3.13)$$

Using (3.13), the phase angle is used to generate the estimated normalized dependency matrix as follows

$$\frac{\sin(\theta)}{\sin(\theta) + \cos(\theta)} = \frac{X_l}{X_l + R_l} \quad (3.14a)$$

$$\frac{\cos(\theta)}{\sin(\theta) + \cos(\theta)} = \frac{R_l}{X_l + R_l} \quad (3.14b)$$

Designating  $K_p$  for frequency and  $K_q$  for voltage, the frequency and voltage deviations are given as

$$\Delta\omega = -a_{11}K_pP + a_{12}K_pQ \quad (3.15a)$$

$$\Delta V = -a_{21}K_qP - a_{22}K_qQ \quad (3.15b)$$

Figure 3.3 shows the proposed generalized droop control for the primary control level. First, the measured P and Q are utilized to identify the equivalent impedance angle based on (3.12). Then, a normalized dependency matrix is generated using (3.10). Finally, the dependency matrix used for generalized droop control is given in (3.8).

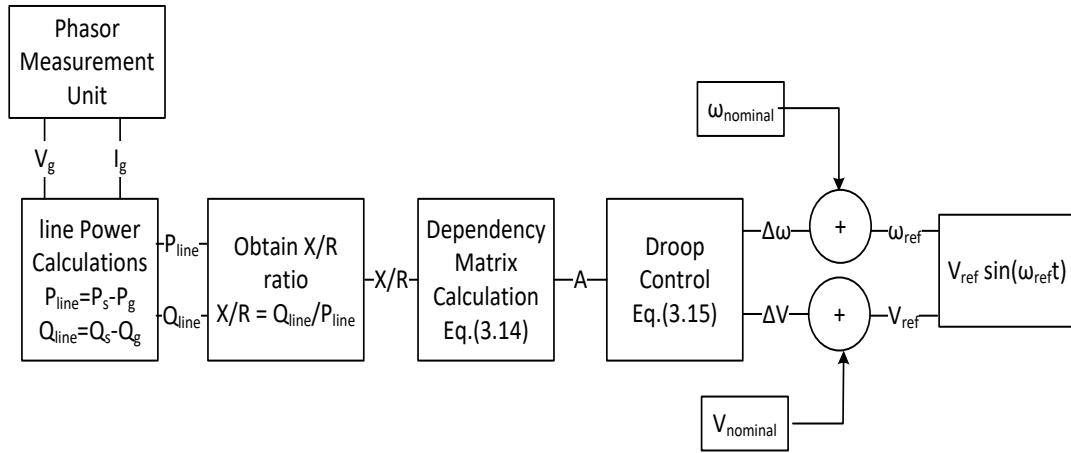


Figure 3.3: The block diagram of the proposed droop controller.

### 3.4 Simulations Results

The proposed droop controller was validated through a test system that included two units supplying a common load through a line impedance, as shown in Figure 3.4. The system and line parameters are shown in Table 3.1 along with the controllers' parameters. In this section, the proposed droop controller was simulated for different load conditions in inductive, mixed impedance, and resistive grids. The frequency and voltage deviations were observed along with the measured active and reactive power. The estimated X/R ratio was compared with actual values, and the corresponding dependency matrix was produced.

At the beginning of the simulation, the active and reactive power loads were as shown in Table 3.1. At  $t = 2s$ , the reactive power load was reduced to  $5kVAR$  while the active power remained the same. The active power was decreased to  $5kW$  at  $t = 4s$ , and the reactive power stayed at  $5kVAR$ . The frequency and voltage deviations given in (3.15) were observed along with the measured active and reactive powers. Additionally, the estimated X/R ratio was measured and compared with its reference value. Finally, the dependency matrix elements shown in

(3.13) were implemented based on the estimated X/R ratio observed during the simulation.

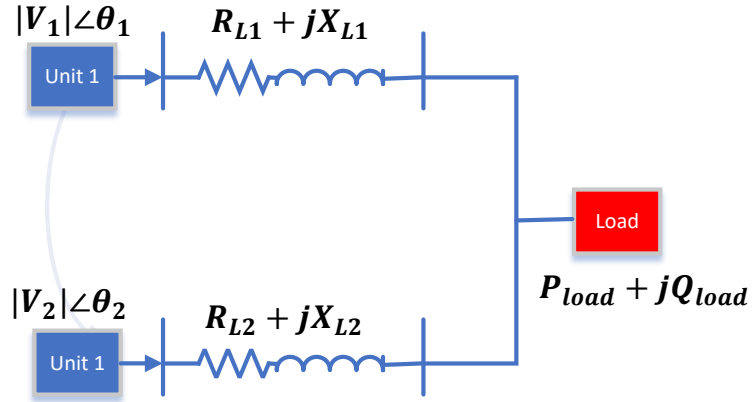


Figure 3.4: Single line diagram of the test system.

Table 3.1: Specifications of the test system

System	parameter	value	parameter	value
	RMS Voltage ( $V_{RMS}$ )	220V	Switching frequency ( $f_{sw}$ )	10KHz
	DC Voltage ( $V_{DC}$ )	700V	Nominal frequency ( $f_{nom}$ )	50Hz
DGs	parameter	DG1	DG2	
	$K_{p_i}$	49 $\mu$ rad/W.sec	188 $\mu$ rad/W.sec	
	$K_{q_i}$	1.3mV/VAR	2.6mV/VAR	
	$R_f$	0.1 $\Omega$	0.1 $\Omega$	
	$L_{f_i}$	1.35mH	1.35mH	
	$C_{f_i}$	50 $\mu$ F	50 $\mu$ F	
Line	Grid Type	$R_{L1} + jL_{L1}$	$R_{L2} + jL_{L2}$	X/R
	Resistive	0.56 + j0.168 $\Omega$	0.56 + j0.168 $\Omega$	0.3
	Mixed	0.56 + j0.56 $\Omega$	0.56 + j0.56 $\Omega$	1
	Inductive	0.56 + j3.92 $\Omega$	0.56 + j3.92 $\Omega$	7
Load	$P_{load} + jQ_{load}$		10KW + j10KVAR	

### 3.4.1 Resistive Grid

In this section, the proposed droop controller was subjected to a resistive grid with an R/X ratio of 0.3. As shown in Figure 3.5, the change of reactive power at  $t = 2s$  was mainly related to the frequency deviation and barely affects the voltage deviation. At  $t = 4s$ , the active power reduction increased the voltage level at a higher rate than the frequency decreased. Note that, the reactive power is inversely related to the frequency as shown in (3.5). Additionally, the estimated X/R ratio was identical to the actual value 0.3, which generated the dependency matrix in Figure 3.5.

### 3.4.2 Mixed Impedance Grid

A similar scenario was applied for a mixed impedance grid with an X/R ratio of 1. Figure 3.6 shows the system behavior under mixed impedance. Since the relationship of voltage and frequency to the active and reactive power was 50% as described in the dependency matrix, the changes in frequency at equal active and reactive power is zero, as shown in (3.15). Both frequency and voltage changed simultaneously according to their droop coefficients when the active and reactive power changed.

### 3.4.3 Inductive Grid

For an inductive grid, the X/R ratio was chosen to be 0.7. Figure 3.7 shows the controller behavior under the inductive grid. Based on the dependency matrix, the frequency was dependent on the active power by 70% and on the active power by 30% and vice versa for the voltage. At  $t = 2s$ , the voltage reacted to the reactive power change more than it reacted to other types of grids. A similar reaction was observed for the frequency with active power change at  $t = 4s$ .

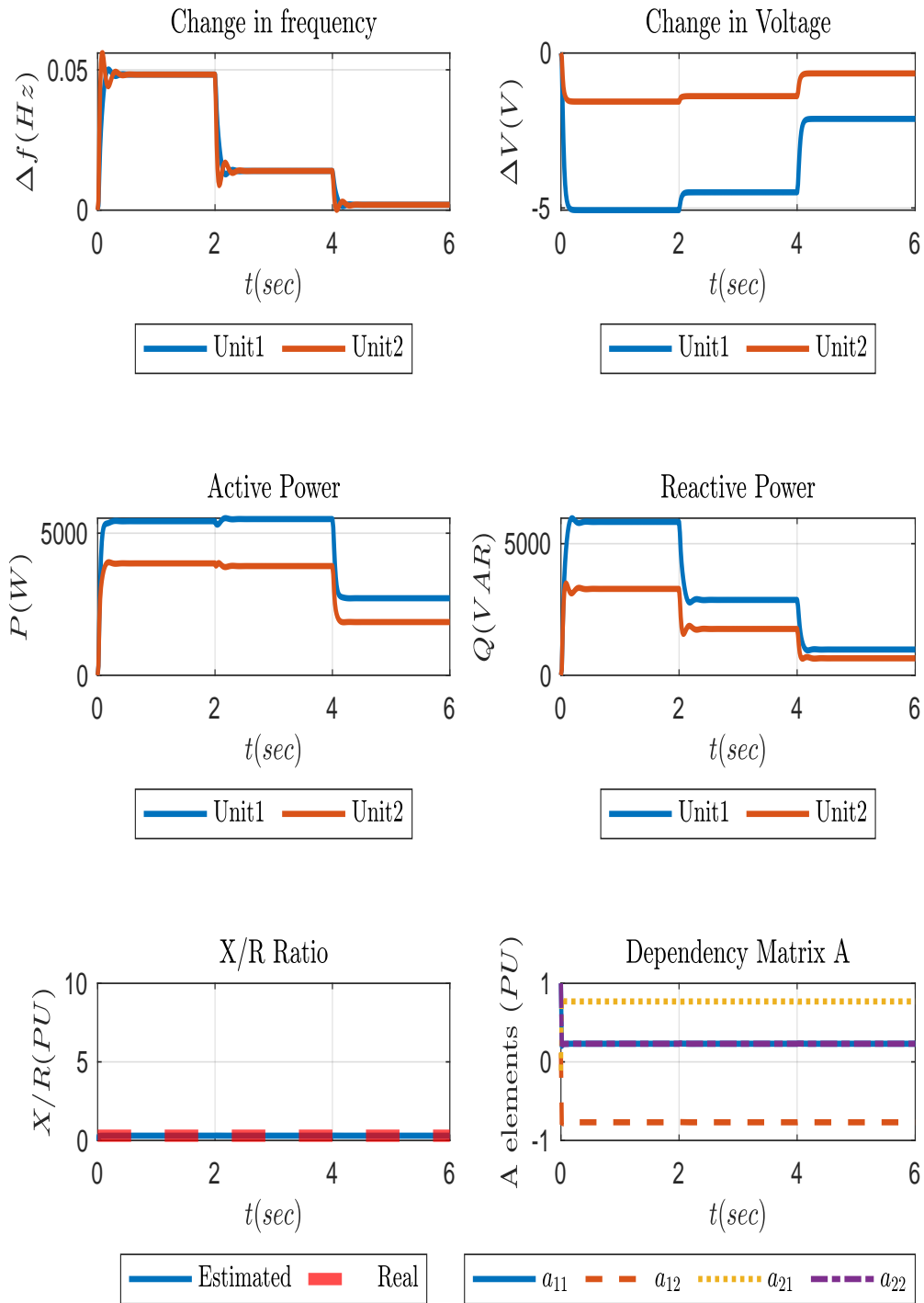


Figure 3.5: System behavior under a resistive grid.

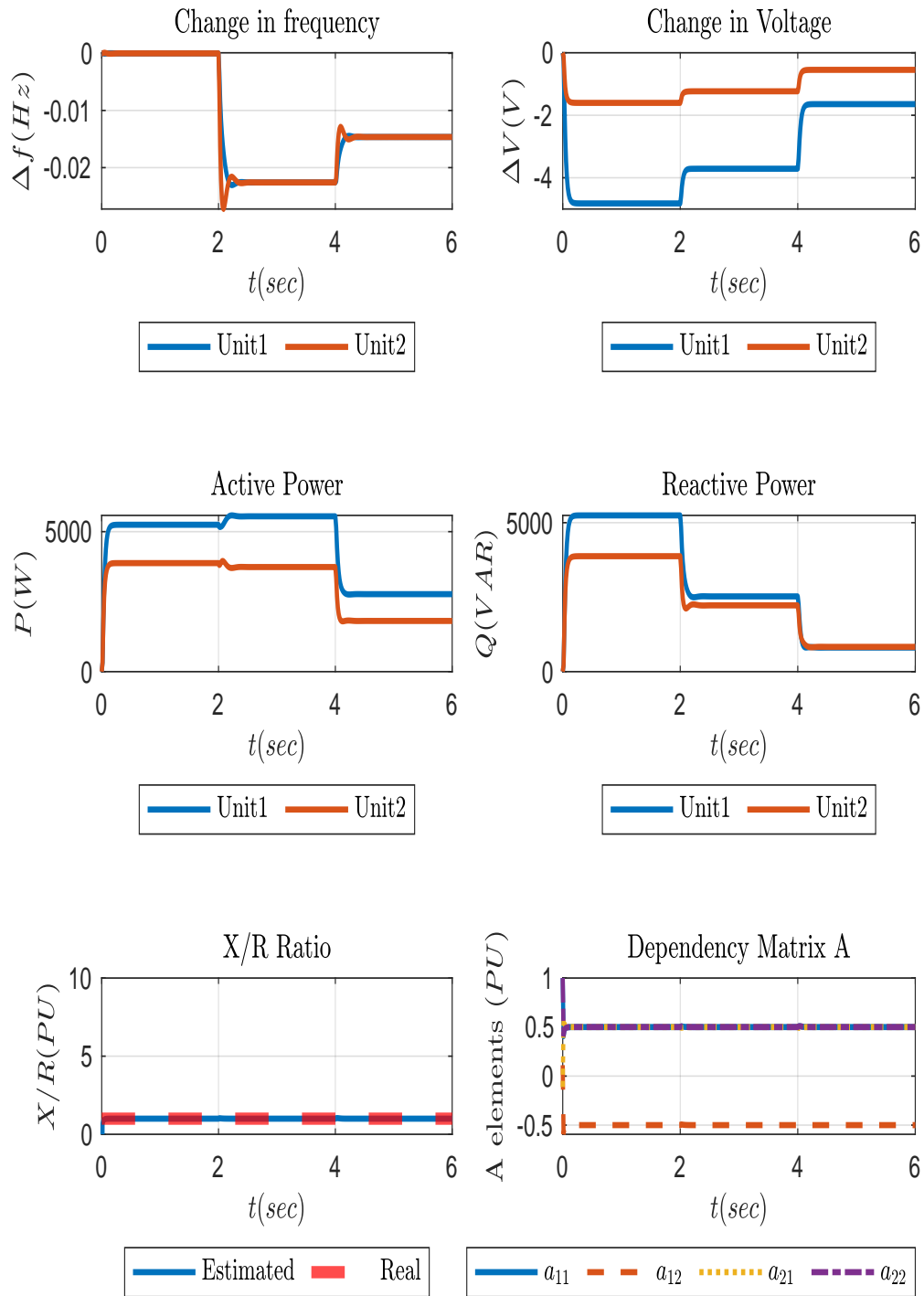


Figure 3.6: System behavior under a mixed impedance grid.

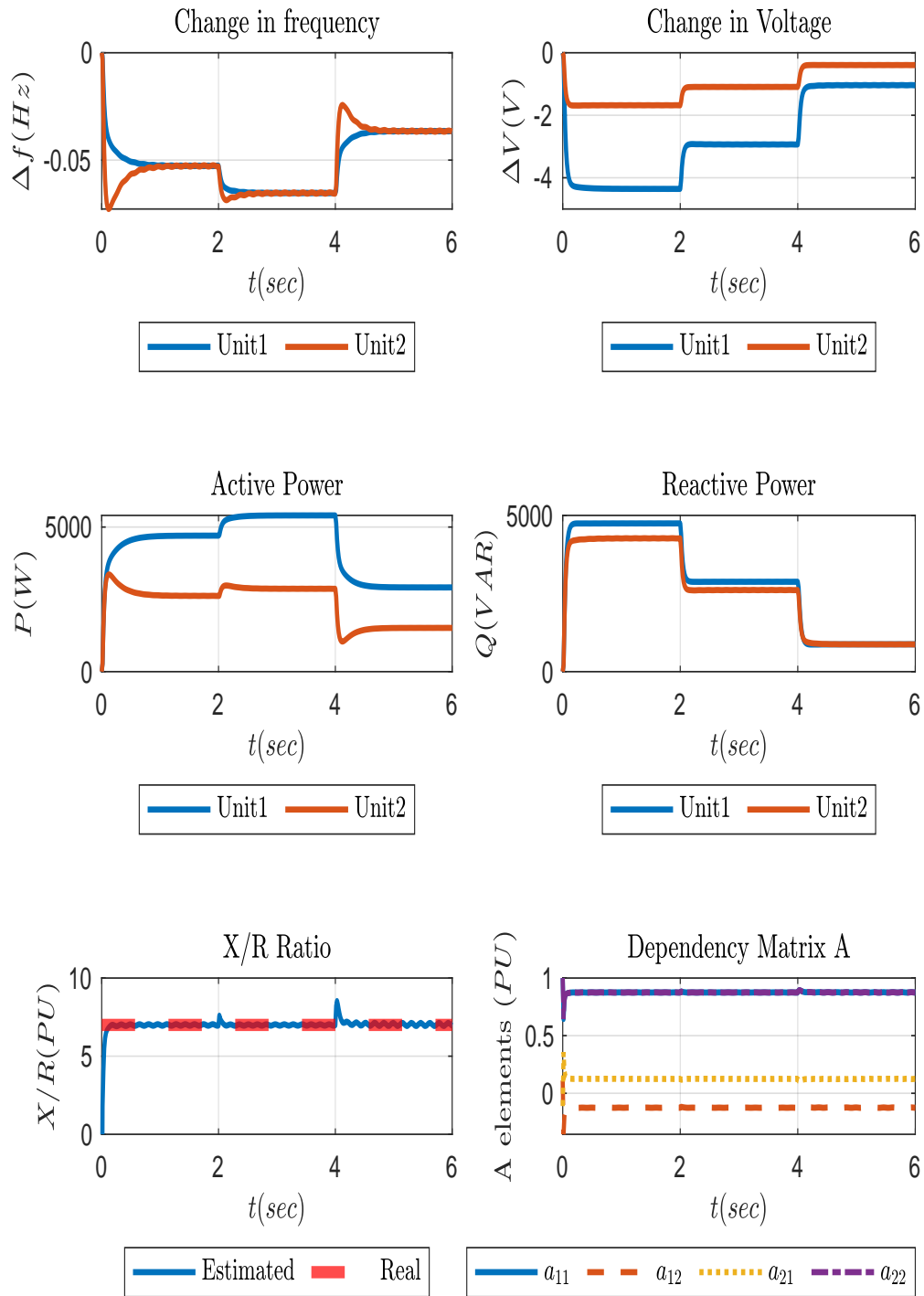


Figure 3.7: System behavior under an inductive grid.

### 3.5 Conclusions

This chapter aims to improve the droop control technique subjected to a mixed impedance grid. In such a grid, the active power variation is a function of both frequency, and voltage as well as the reactive power. Therefore, frequency and voltage need to be tuned accordingly to accurately share power. A normalized dependency matrix was used to explore the per-unit relationship between frequency and voltage with the active and reactive power based on line impedance. To construct the dependency matrix, the X/R ratio was estimated using a phasor measurement unit that communicated the grid voltage and current phasors. The unit calculated the power in the line and then estimated the X/R ratio. Finally, a simulation using MATLAB/SIMULINK was implemented for a test system subjected to inductive, mixed, resistive impedance grids. The simulation results showed superior performance compared to conventional droop control under different grid types.

## CHAPTER 4 CONSENSUS OPTIMIZATION-BASED SECONDARY CONTROL

### 4.1 Introduction

In an islanded microgrid, grid-forming units collaborate to maintain the microgrid's voltage and frequency by utilizing the droop control technique in a hierarchical control structure, including primary, secondary, and tertiary levels. The primary control adjusts the frequency and voltage based on the active and reactive power change to maintain the microgrid's stability and preserve the power-sharing between units utilizing the droop control technique. Secondary control interferes with restoring frequency and voltage to their nominal values. However, traditional droop control applied to an inductive grid with mismatched line parameters experiences a trade-off between reactive power-sharing and voltage regulations. This trade-off is because the higher voltage drop in the lines with higher impedance causes the voltage at each unit's terminal to be measured differently. Therefore, the reactive power deteriorates if the secondary control is to restore the voltages to their nominal value. On the contrary, if the secondary control is to keep equal reactive power-sharing, the voltage is mismatched, and circulating currents flow between units. The secondary control level manages the trade-off between voltage regulation and reactive power-sharing in the inductive grid as an additional function.

Inspired by the fact that the global consensus average of a directed graph is reached when the difference between each unit and its neighbor is zero, a convex optimization function is implemented to minimize the power-sharing difference between each unit and its neighbor, which becomes zero at the optimal solution. Then, internal technical constraints are enforced to keep the frequency at the nom-

inal value and limit the voltages within the range  $\% \pm 5$  of the nominal value. The technique in this chapter allows reactive power-sharing to reach a global consensus average for all units when the voltage limits are not pushed to the boundary. At the voltage boundary, the controller guarantees a minimum difference in reactive power-sharing from the global consensus average. The optimization function is implemented in real-time in a discrete manner such that the optimal solution is obtained before it is applied to the system. This chapter is based on works given in [198, 199].

An analysis is carried out for the reachability of the controller to the global consensus average at the optimal solution. The salient features of the controller proposed in this chapter can be listed as follows:

- The controller is implemented to seek the global consensus average of power-sharing (Regulator consensus); therefore, there is no need for a leader unit to capture a reference value.
- Only information about power-sharing is communicated between units, which reduces the communication intensity in the communication network.
- At the voltage limit, the reactive power-sharing autonomously starts to diverge optimally without modifying the controller settings.

This chapter is organized as follows. In Section 4.2, the role of the grid-forming unit in the secondary control of islanded microgrid is identified in the context of the hierarchical control structure, in addition to the issue of poor reactive power-sharing. Section 4.3 presents an analysis to verify the optimality and consensus reachability for an unconstrained convex optimization function. Then, section 4.4 presents the proposed optimization-based consensus secondary controller's implementation where the optimization function is derived, and the constraints are defined for the islanded microgrid. The simulation results of the con-

troller's performance and behavior in islanded microgrids are presented in Section 4.5. Finally, Section 4.6 provides conclusions for the proposed controller.

## 4.2 Secondary Control in Islanded Microgrid

During islanded mode, grid-forming units collaborate to regulate the frequency and voltage of the microgrid. The hierarchical control structure is employed to perform these functionalities through primary and secondary control, assuming that the grid is inductive based on the following

$$\omega_i = \omega_{nom} - K_{p_i} P_i + \delta\omega_i \quad (4.1a)$$

$$V_i = V_{nom} - K_{q_i} Q_i + \delta V_i \quad (4.1b)$$

Where  $\omega_i$  and  $V_i$  are the angular frequency and terminal voltage of  $i^{th}$  unit,  $\omega_{nom}$  and  $V_{nom}$  are the nominal angular frequency and terminal voltage,  $K_{p_i}$  and  $K_{q_i}$  are active and reactive power droop coefficients,  $P_i$  and  $Q_i$  are measured active and reactive power of  $i^{th}$  unit, and  $\delta\omega_i$  and  $\delta V_i$  are the secondary control corrective terms, respectively.

A grid-forming unit employing the hierarchical control structure is shown in Figure 4.1. The local controller receives the reference voltage amplitude and frequency from the primary control level and commands the connected unit to follow its reference by generating the modulation index to pulse width modulation. Primary control produces reference voltage and frequency by mimicking the synchronous machine's behavior in the inductive grid, where the change in frequency is related to the change of the active power, and the change in voltage is associated with the change of the reactive power. The secondary control aims to restore the terminal voltage and frequency to their nominal values by generating the error terms  $\delta\omega_i$  and  $\delta V_i$  to the primary control on a slower timescale. The timescales of these levels of control are detached to avoid interaction between the control levels.

In addition to restoring terminal voltage and frequency, secondary control ensures proper power-sharing between units. Therefore, three philosophies are introduced in the literature to deliver those functionalities, namely, Decentralized Secondary Control (DESC), Centralized Secondary Control (CSC), and Distributed Secondary Control (DISC) [173]. These philosophies are classified based on communication link implementation. In DESC, the communication layer is omitted; however, in CSC and DISC, the communication is established between the unit and MGCC or neighbor units, respectively.

Decentralized secondary control restores the terminal voltage and frequency solely based on local measurements. However, power-sharing is poor due to the voltage drop in the lines. Centralized secondary control is dependent on the Microgrid Control Center (MGCC) to obtain appropriate voltage and frequency reference values for secondary control. However, intensive communication is required between the MGCC and the grid-forming units. Furthermore, a computation burden can limit the extendibility of the microgrid. Distributed secondary control is based on cooperation between all grid-forming units to reach proper reference values, ensuring proper restoration and power-sharing between units. In distributed secondary control, the plug-and-play feature is preserved since disconnection and connection of units do not require a centralized controller to change its setting. The distributed secondary control, which is based on the averaging technique, utilizes a peer-to-peer communication mechanism to reach average frequency and voltage errors, as well as average reactive power-sharing. Another type of distributed control uses consensus-based communication to reach proper values restoration and power-sharing between units through communication with neighboring units.

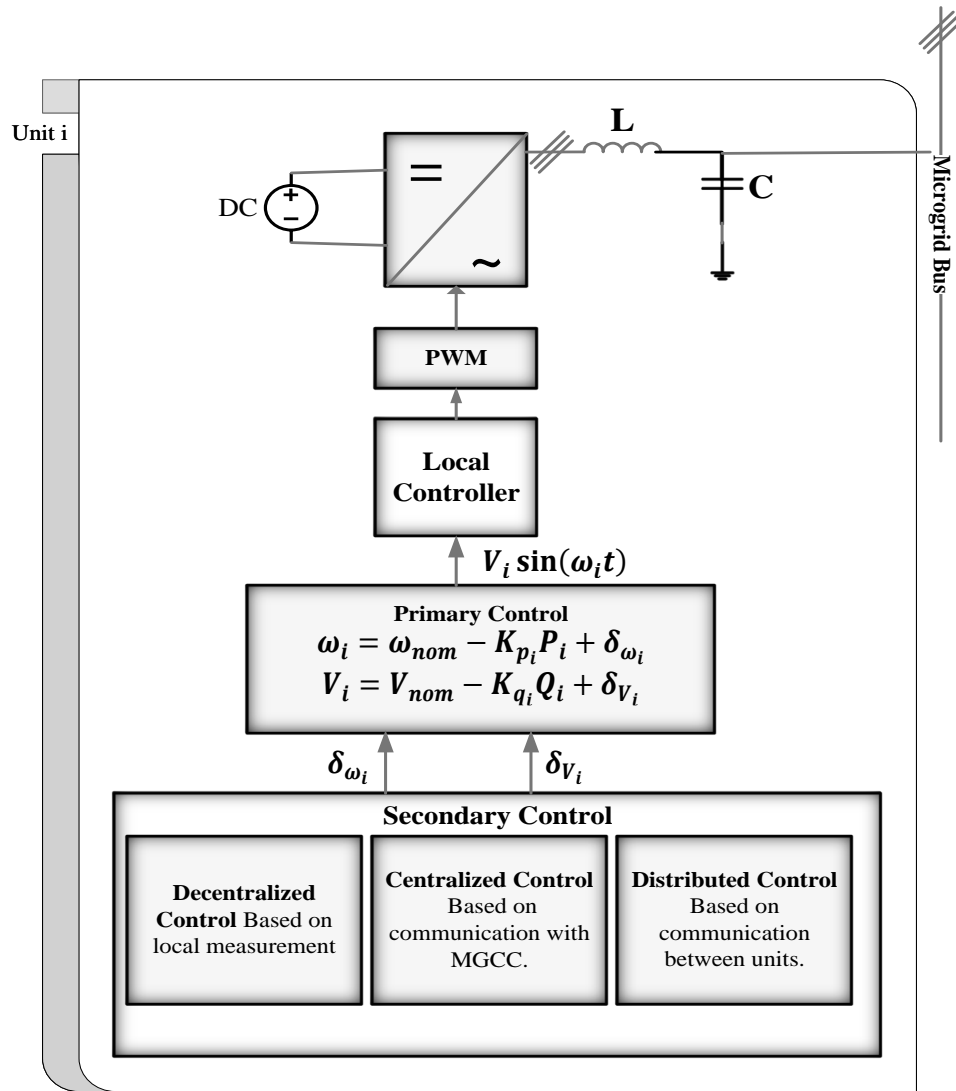


Figure 4.1: Grid-forming unit in the hierarchical control structure.

#### 4.2.1 Reactive power-sharing

The droop coefficients identify the amount of power-sharing for each unit based on its rated power, as shown in the following

$$K_{p_i} = \Delta\omega_{max} / P_i^{max} \quad (4.2a)$$

$$K_{q_i} = \Delta V_{max} / Q_i^{max} \quad (4.2b)$$

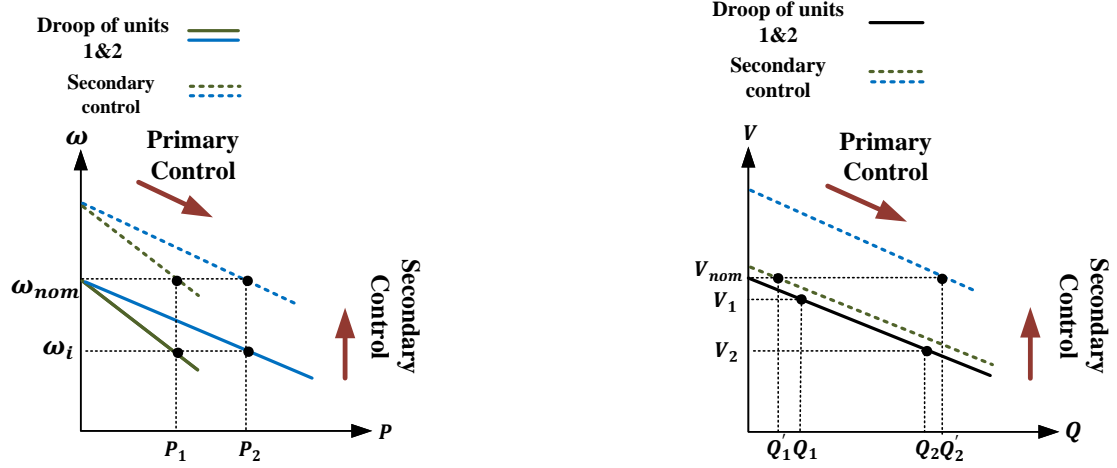
Where  $\Delta\omega_{max}$  and  $\Delta V_{max}$  are the maximum allowable changes in angular frequency and terminal voltage, and  $P_i^{max}$  and  $Q_i^{max}$  are active and reactive rated power of each unit, respectively.

The load is adequately shared when all units compensate for the same amount of  $K_{p_i}P_i$  and  $K_{q_i}Q_i$ . The condition under which power-sharing is satisfied is given as follows

$$K_{p_1}P_1 = K_{p_2}P_2 = \dots = K_{p_i}P_i = \Delta\omega_{max} \quad (4.3a)$$

$$K_{q_1}Q_1 = K_{q_2}Q_2 = \dots = K_{q_i}Q_i = \Delta V_{max} \quad (4.3b)$$

The system's frequency is a global variable; therefore, the active power-sharing between units is satisfied at the primary level. However, the terminal voltage of each unit is affected by the line impedance; hence, a different voltage is observed in each unit. Secondary control is used to enhance the sharing of reactive power between units in addition to its functionality to restore the frequency and voltage to their nominal values. Figure 4.2 shows the droop characteristics of two grid-forming units, including frequency and voltage as a function of active and reactive power, respectively, as treated at primary and secondary levels. For  $P - \omega$  droop characteristics, two units with different droop coefficients converge onto a common steady-state angular frequency  $\omega_i$  with active power ( $P_1$  and  $P_2$ ) shared between them based on their primary level's droop coefficient values. Then, the secondary control level restores the frequency to its nominal value  $\omega_{nom}$ , without affecting the active power-sharing. However, the  $Q - V$  droop characteristic shows that two units with similar droop coefficients converge onto different voltages at the primary level corresponding to the reactive power  $Q_1$  and  $Q_2$ . As a result, the voltages converge onto a common nominal voltage at the secondary control level, while the reactive power-sharing ( $Q'_1$  and  $Q'_2$ ) is exacerbated.



(a)  $P - \omega$  droop with similar droop coefficients

(b)  $Q - V$  droop with equal droop coefficients.

Figure 4.2: Droop characteristics of two grid-forming units

#### 4.2.2 Sensitivity Analysis

It is essential to study the effect of a change per unit of line parameter mismatch on the change per unit of reactive power mismatch. Considering a system composed of two units sharing a load through a line impedance as given in Figure 4.3, the reactive power generated by each unit is given as

$$Q_i = \frac{V_{pcc}(V_i - V_{pcc})}{X_{L_i}} \quad (4.4)$$

The reactive power-sharing mismatch is given as a function of the line impedance mismatch as follows

$$\Delta Q = \left| \left( \frac{V_{pcc}(V_1 - V_{pcc})}{X_{L1}} \right) - \left( \frac{V_{pcc}(V_2 - V_{pcc})}{X_{L2}} \right) \right| \quad (4.5)$$

Assuming the line 1 impedance ( $X_{L1}$ ) and line 2 impedance ( $X_{L2}$ ) vary from 100% to 200% of their per-unit values, which are assumed to be  $0.0389 pu$ . The amount of reactive power mismatch in  $pu$  is observed in Figure 4.4. The reactive power mismatch is kept at zero when the lines are equivalent. However, the reactive power mismatch increases as the line impedance mismatch increases.

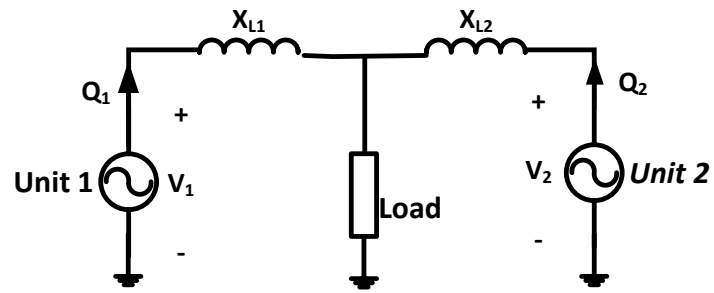


Figure 4.3: Two units are supplying a common load.

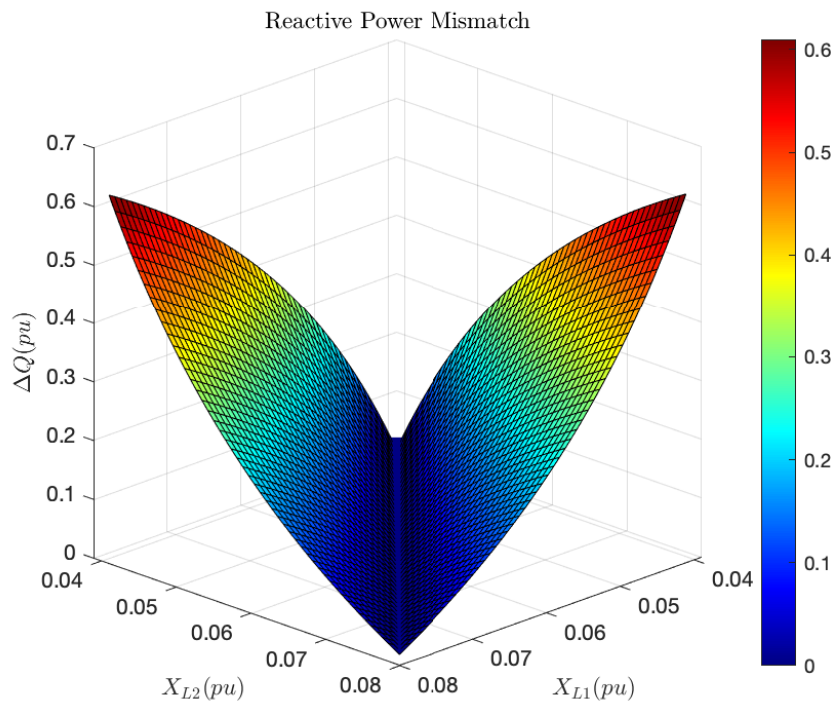


Figure 4.4: Sensitivity analysis of the line impedance mismatch to the reactive power mismatch.

### 4.3 Analysis of Optimization-Based Control for Uniform Power-Sharing between Units

In this section, an analysis of the reachability of the global consensus average given as  $1/N \sum_{i=1}^N x_i$  is derived for a system described by the directed graph shown in Figure. 4.5 for units seeking the minimum difference between its output and its neighbor. The graph given in this analysis is balanced and strongly connected, as explained in Appendix A.

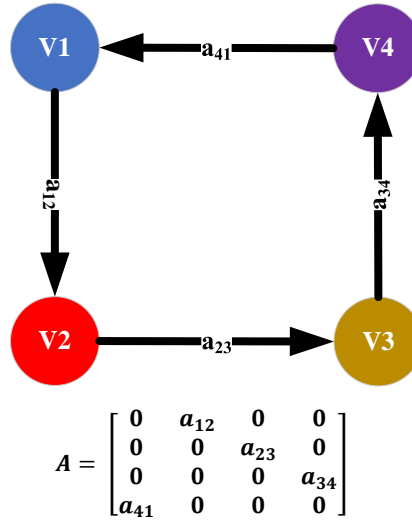


Figure 4.5: An example of constructing an adjacency matrix for four nodes.

Consider  $N$  units connected according to a topology described by a directed graph (digraph)  $\mathcal{G}$ . Let the state variable  $x$  be the reactive power-sharing between units. Each unit has access to only its state  $x_i$  and its neighbor  $x_j$ . Using the droop control equation given in (4.1b) without the secondary control correction term, one can obtain the representation of the state space of the system by defining the state as  $x_i = K_{q_i} Q_i = V_{nom} - V_i$  and differentiating the state equation with respect to time as.

$$\dot{x}_i = -\dot{V}_i = u_i \quad (4.6)$$

Define a cost function that aims to minimize the difference in power-sharing between unit  $i$  and unit  $j$  as follows

$$\min_{x_i} \sum_{i=1}^N f(x_i, t) \quad (4.7)$$

**Assumption 1.** *There exists a continuous  $x_i^*(t)$  that minimizes the team cost function given in (4.7)*

**Assumption 2.** Function  $f(x_i, t)$  is twice differentiable with respect to  $x_i$ , with invertible Hessian  $H(x_i, t)$ ,  $\forall x_i, t$ .

**Lemma 1.** let  $f(x)$  be a continuous differentiable convex function. The function  $f(x)$  is minimized at  $x^*$  if and only if  $\nabla f(x) = 0$  [200].

**Lemma 2.** let  $f(x)$  be a convex function, and assumption 2 holds, then Hessian is a positive definite function. Hence, the direction of Newton's step is in a descending direction unless  $\nabla f(x) = 0$ .

By applying the Newton step for solving the optimization function, the control input  $u_i$  is derived as

$$u_i = -H^{-1}(x_i, t) \left( \tau \nabla f(x_i, t) + \frac{\partial}{\partial t} \nabla f(x_i, t) \right) \quad (4.8)$$

**Theorem 1.** Given that the cost function  $f(x_i, t)$  satisfies the assumptions 1 and 2, using (4.8) in (4.6),  $x_i(t)$  converges to an optimal value  $x_i^*(t)$ , the minimizer of (4.7) i.e.  $\lim_{t \rightarrow \infty} x_i(t) \rightarrow x_i^*(t)$ .

*Proof.* Define a positive-definite Lyapunov function candidate  $W = \frac{1}{2} \nabla f(x_i, t)^T \nabla f(x_i, t)$ . The derivative of  $W$  along  $x_i$  is  $\dot{W} = \nabla f(x_i, t)^T H(x_i, t) \dot{x}_i + \nabla f(x_i, t)^T \frac{\partial}{\partial t} \nabla f(x_i, t)$ . Equating (4.8) in (4.6) we obtain  $\dot{W} = -\tau \nabla f(x_i, t)^T \nabla f(x_i, t)$ . Therefore,  $\dot{W} < 0$  for  $\nabla f(x_i) \neq 0$ , which guarantees that  $\nabla f(x_i)$  asymptotically converges to zero as  $t \rightarrow \infty$ . Then, under assumption 1 and using the lemma 1 and 2,  $x_i(t)$  converges to  $x_i^*(t)$  and  $f(x_i, t)$  will be minimized [201].  $\square$

Consensus is achieved for the system given in Figure 4.5, when all units share the same amount of power, satisfying the following equality defined for a unit  $i$  at optimal solution.

$$x_i^* = 1/N \sum_{i=1}^N x_i^* \quad (4.9)$$

**Remark 1.** The unconstrained problem in (4.7) tries to demand all units to follow a global consensus average of power-sharing  $x_i$ . When power-sharing  $x_i$  is subjected to internal constraints that prevent  $x_i$  from reaching a global consensus average, the objective function will keep the difference from the global consensus average at a minimum.

#### 4.4 Proposed Optimization-based Consensus Control

The secondary control terms  $\delta_{\omega_i}$  and  $\delta_{V_i}$  in (4.1a) and 4.1b constitute the functionalities of the secondary control. Those terms are dispatched based on an optimization problem. The

controller aims to minimize reactive power-sharing mismatch and keep active power-sharing equal between units at nominal frequency. Due to the inherited trade-off between voltage regulation and reactive power-sharing, the voltage is restricted within a limit, that is,  $\pm 5\%$  of the nominal voltage. In the following sections, the optimization problem's derivation is performed, which contains an objective function to minimize the reactive power-sharing mismatch between units subjected to constraints to obtain equal active power-sharing, restore frequency at a nominal value, and keep the voltage within a predefined limit.

#### 4.4.1 Objective Function

The secondary controller's objective function is to minimize the power-sharing mismatch between units in a consensus manner where each unit communicates its power-sharing with its neighbor to reach a global consensus average. Expressing the active and reactive power-sharing of unit  $i$  given in (4.3a) and (4.3b) as  $x_{\omega_i}$  and  $x_{v_i}$  respectfully, a quadratic optimization function is defined to minimize the mismatch between  $x_{\omega_i}$  and  $x_{v_i}$  with their neighbor  $x_{\omega_j}$  and  $x_{v_j}$  described by the connected directed graph as

$$\min_{x_{\omega_i}, x_{v_i}} ||x_{\omega_i} - x_{\omega_j}||^2 + ||x_{v_i} - x_{v_j}||^2 \quad (4.10)$$

The objective function given in (4.10) satisfies assumptions 1 & 2; therefore, theorem 1 is valid. The active and reactive power-sharing can be represented in terms of the voltage secondary control correction term as

$$x_{\omega_i} = \omega_{nom} - \omega_i + \delta_{\omega_i} \quad (4.11a)$$

$$x_{v_i} = V_{nom} - V_i + \delta_{v_i} \quad (4.11b)$$

Therefore, the objective function in (4.10) can be written in terms of active and reactive power-sharing as

$$\min_{x_{\omega_i}, x_{v_i}} ||(\omega_{nom} - \omega_i + \delta_{\omega_i}) - x_{\omega_j}||^2 + ||(V_{nom} - V_i + \delta_{v_i}) - x_{v_j}||^2 \quad (4.12)$$

#### 4.4.2 Nominal Frequency Constraint

The angular frequency of unit  $i$  ( $\omega_i$ ) should track the nominal angular frequency i.e.,  $\omega_i = \omega_{nom}$ . By imposing a convex constraint on the value of  $\delta_{\omega_i}$ , tracking  $\omega_{nom}$  is guaranteed. The constraint on  $\delta_{\omega_i}$  can be obtained from 4.11a as

$$\delta_{\omega_i} = K_{pi} P_i \quad (4.13)$$

#### 4.4.3 Terminal Voltage constraint

A constraint on the voltage magnitude is imposed to maintain the voltage within a specified range i.e.,  $\pm 5\%$  of its nominal value. As a result, reactive power is minimized, while the voltage magnitude is kept within the given limit. By defining the minimum and maximum voltage limits  $V_{min}$  and  $V_{max}$ , respectively, the inequality constraint that keeps the voltage  $V_i$  between those values is given as

$$V_{min} \leq V_{nom} - K_{qi}Q_i + \delta_{V_i} \leq V_{max} \quad (4.14)$$

The term  $K_{qi}Q_i$  is obtained by local measurements. Note that the variables  $V_{min}$  and  $V_{max}$  are tunable parameters chosen based on the system operator requirements.

#### 4.4.4 Minimization Algorithm

The optimization function is used to minimize the difference in active and reactive power-sharing between grid-forming units while keeping the angular frequency at its nominal value, and terminal voltage within its accepted tolerance. The optimization function generates optimal values of secondary control correction terms in (4.1a) and (4.1b) satisfying the following objectives:

- (i) The differences in active and reactive power-sharing are minimized based on the objective function given in (4.12).
- (ii) The angular frequency of each unit  $\omega_i$  is restored to its nominal value as in (4.13).
- (iii) The terminal voltage at each unit  $V_i$  is within its tolerance as in (4.14).

The overall optimization problem is provided as

$$\begin{aligned} & \text{minimize} \quad \|(\omega_{nom} - \omega_i + \delta_{\omega_i}) - x_{\omega_j}\|^2 + \|(V_{nom} - V_i + \delta_{v_i}) - x_{v_j}\|^2 \\ & \text{subject to} \quad \delta_{\omega_i} = K_{pi}P_i \\ & \quad \quad \quad V_{min} \leq V_{nom} - K_{qi}Q_i + \delta_{V_i} \leq V_{max} \end{aligned} \quad (4.15)$$

The proposed secondary control is shown in Figure 4.6. The controller obtains the power-sharing data from its neighbor unit  $j$  through low bandwidth communication and measures its terminal voltage and frequency and its corresponding active and reactive powers. Those data are processed in a convex optimization function to obtain the minimum active and reactive power-sharing between units while keeping the constraints satisfied. The output of the secondary control represents the optimal voltage and frequency error terms that feed into the primary control. The

error terms are optimal in terms of minimizing the difference in active and reactive power-sharing. The optimization function minimizes a quadratic objective function over convex equality and inequality constraints. Therefore, the minimum value obtained is guaranteed to be the optimal global solution for the convex set [200].

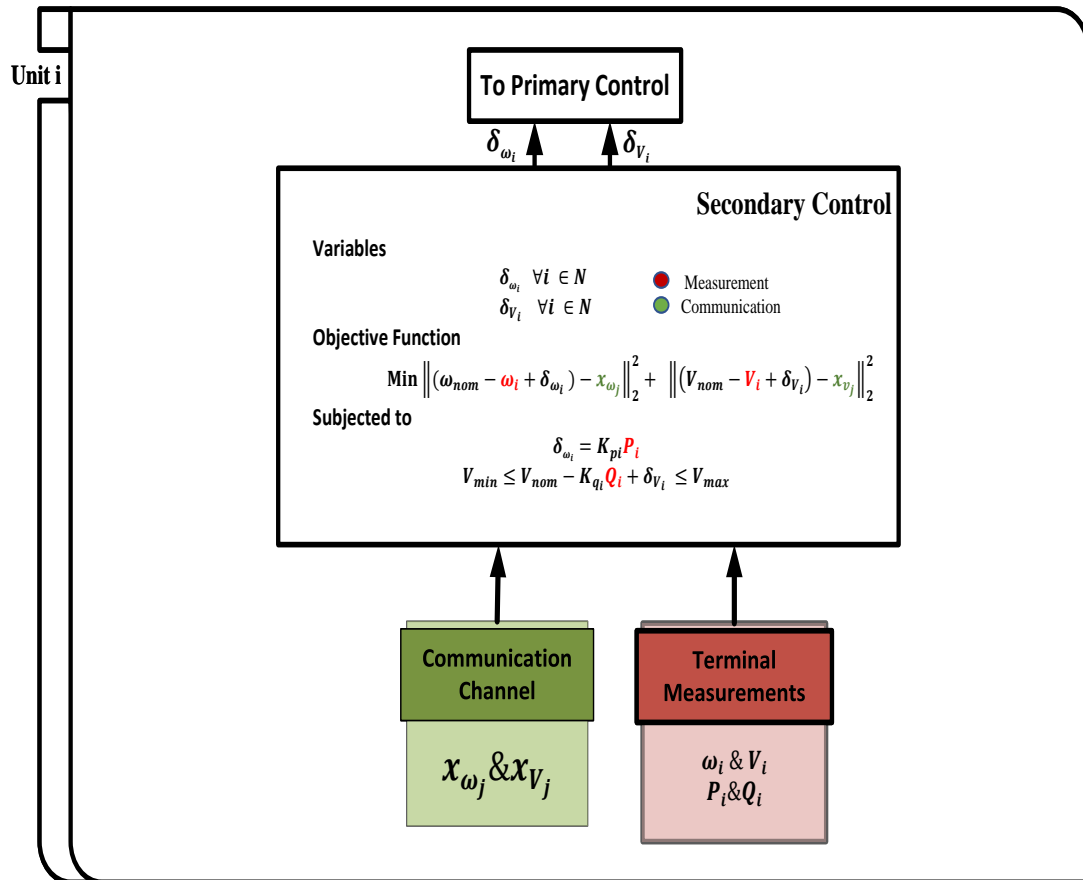


Figure 4.6: Optimization-based consensus secondary control.

#### 4.5 Simulation Results

The proposed controller was validated on a test system given in Figure 4.7 which represents the test model of a microgrid with four DG units and two loads. The line parameters of line 2 were different from lines 1&3 to show the trade-off between voltage regulation and reactive power-sharing under line parameters mismatch. All units had the same reactive power-sharing

droop coefficients such that any reactive power mismatch was solely caused by the line parameters effect. Table 4.1 shows the system specification of the DG units, lines, and loads. The optimization function was implemented in CVX/CVXGEN to generate fast custom optimization solver suitable for real-time applications [202]. An overview of CVX/CVXGEN is given in Appendix B.

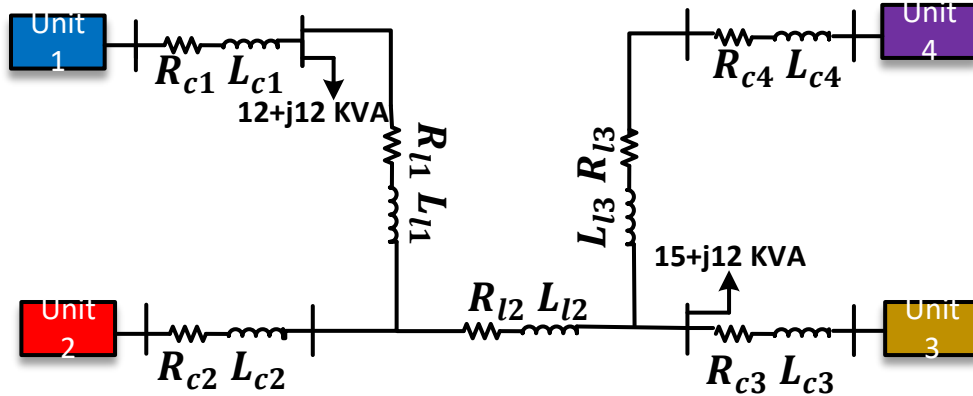


Figure 4.7: Single-line diagram of the microgrid test system .

Two communication network topologies were used to validate the optimization-based secondary controller; consensus-based and centralized-based topologies. In consensus-based topology, each unit communicates its power-sharing with its neighbor as given in Figure 4.8a. The configuration is called a directed graph, where arrows indicate the data flow from one unit to another. While centralized-based topology employs a central processor to collect the power-sharing from all units, calculate the average, and transmit the average power-sharing to all units as shown in Figure 4.8b. The two-way data transmission stream increases the communication links required in the network. It also could be done in a distributed manner by implementing a two-way communication link between all units in such a way that each unit received the power-sharing data from all units and calculated the average in its own local controller.

#### 4.5.1 Control Objective

The proposed controller was simulated for different control objectives with consensus-based communication topology given in Figure 4.8a to validate the ability of the controller to reach

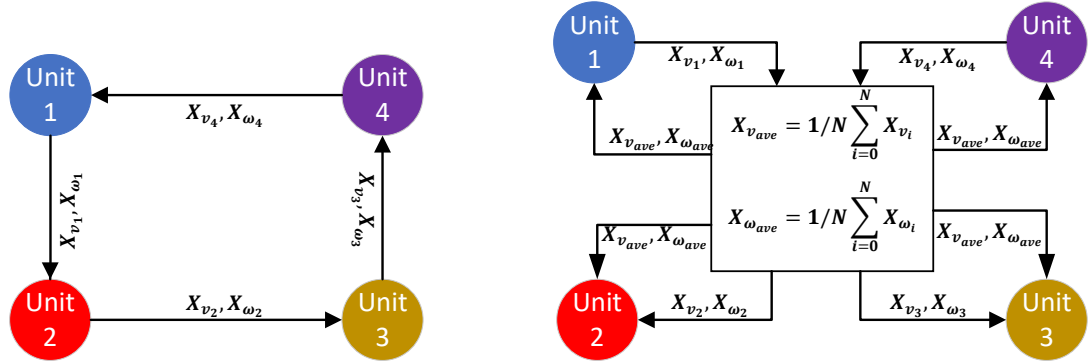
Table 4.1: Specifications of the test system

System	Parameter	Value	Parameter	Value
	$V_{RMS}$	220V	$f_{sw}$	10KHz
	$V_{DC}$	700V	$f_{nom}$	50Hz
DGs	Parameter	DG 1&2	DG 3&4	Unit
	$K_{p_i}$	49	125	$\mu rad/W.sec$
	$K_{q_i}$	2	2	$mV/VAR$
	$R_{f_i}$	0.1	0.1	$\Omega$
	$L_{f_i}$	1.35	1.35	$mH$
	$C_{f_i}$	50	50	$\mu F$
	$R_{c_i}$	30	30	$m\Omega$
	$L_{c_i}$	0.35	0.35	$mH$
Lines	Parameter	Value		Unit
	$Z_{l1}$	$0.23 + j0.318$		$m\Omega$
	$Z_{l2}$	$0.35 + j1.847$		$m\Omega$
	$Z_{l3}$	$0.23 + j0.318$		$m\Omega$
Loads	$P_{load1} + jQ_{load1}$	$36 + j36$		KVA
	$P_{load2} + jQ_{load2}$	$45 + j36$		KVA

the global consensus average as explained in Section 4.3 where the states are the power-sharing variables  $K_{p_i}P_i$  and  $K_{q_i}Q_i$  and the input variables are the frequency and voltage correction terms  $\delta\omega_i$  and  $\delta v_i$ . The following sections show the system variables for three different cases, including unconstrained, and constrained for voltage regulation, and reactive power-sharing.

#### Unconstrained Problem

In the first simulation, the unconstrained problem was considered, in which the controller seeks minimum power-sharing between units without frequency and voltage constraints to validate the ability of the controller to reach a global consensus average of power-sharing. The frequency and voltage constraints were removed to confirm that the global consensus average of



(a) Consensus-based communication topology. (b) Centralized-based communication topology.

Figure 4.8: Communication topology employed for the optimization-based secondary controller.

power-sharing is reached as proven analytically in Section 4.3. In Figure 4.9, the active and reactive power-sharing reached the global consensus average using the input control signals generated from the optimization solver. The control signals were given as frequency and voltage correction terms. The frequency and voltage variables were out of limits because there were no constraints imposed on their values. Consequently, the active and reactive powers were only shared based on their droop control coefficients. Note that the control signals for active power-sharing for all units were zeros when there were no constraints on the frequency values, which indicates the global consensus average for active power can be reached without an effort from the secondary control. However, the voltage correction terms of the unconstrained problem had various values attempting to unify the reactive power-sharing between units, which implies the voltages at each unit are measured differently due to the voltage drop in the lines.

### Constrained Problem for Voltage Regulation

The second simulation studied the effect of the trade-off between the reactive power-sharing and the voltage regulation as explained in Section 4.2. The objective function seeks the minimum power-sharing difference between units subjected to equality constraints, where the frequency and voltage are constrained to follow their nominal values. The simulation setting represents the case where the voltages of the units are strict about following the reference values while the reactive power-sharing is allowed to mismatch based on the line impedance and reactive power

droop coefficients. Thus, units may share reactive power beyond their reactive power capacity. Figure 4.10 shows that the active power-sharing reached the global consensus average while the reactive power-sharing failed due to the strict voltage constraints. Unit 3 contributed more reactive power than any other unit, although all units had similar reactive power droop coefficients. This implies the measured voltage at unit 3 had the lowest value among other units due to the higher voltage drop in the line. The frequency and voltage were kept at their nominal values. This is the case where the constraints drive the states to fail in reaching the global consensus average discussed in Remark 1. However, this case may fit some microgrid operators, who require strict voltage regulations and allow the reactive power-sharing to deviate optimally.

### **Constrained Problem for Reactive power-sharing**

Finally, to manage the trade-off between voltage regulation and reactive power-sharing in acceptable behavior, a constraint was imposed on the terminal voltage in such a way the voltage limits were relaxed and allowed to vary within  $\% \pm 5$  of its nominal value. Therefore, all units could reach the global consensus average of reactive power-sharing within these allowable voltage limits. The optimization problem in this simulation is given in Figure 4.6. As shown in Figure 4.11, all units behaved similarly to the previous section for active power and frequency values. However, because of the relaxed constraint imposed on the voltage, the reactive power for all units reached the global consensus average while the voltages were kept within the predefined range. The input signal correction terms for the voltages were generated so that all units kept the voltage limit unviolated while the global consensus average was reached. Note that unit 3 reactive power was reduced significantly while unit 2 increased its reactive power to reach a consensus with other units. This case managed the trade-off between voltage regulation and reactive power-sharing in such a way that the voltage limits were not violated. However, voltages were allowed to vary within the given limits to keep units aligned with the global consensus average of reactive power-sharing.

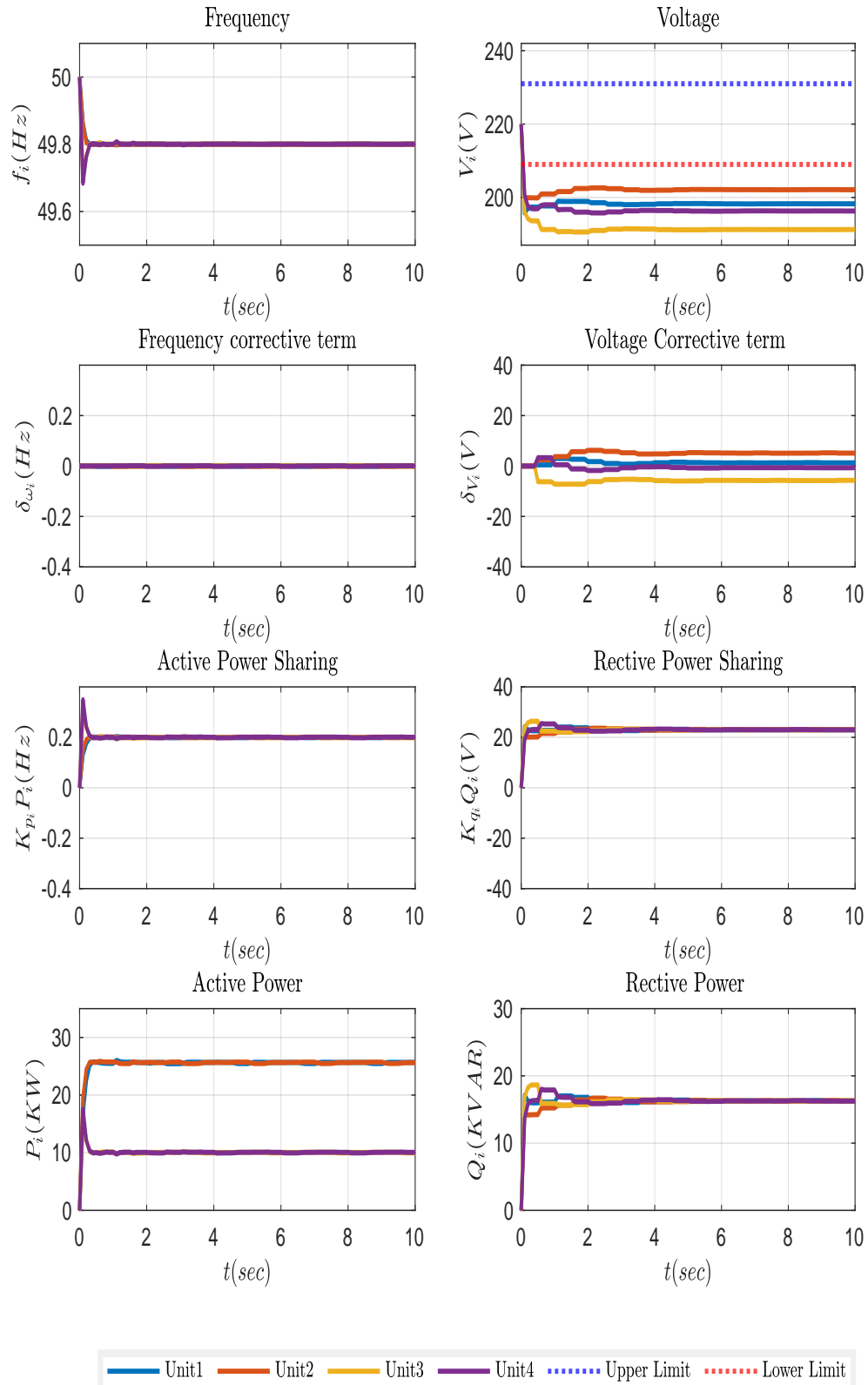


Figure 4.9: System variables for the unconstrained problem.

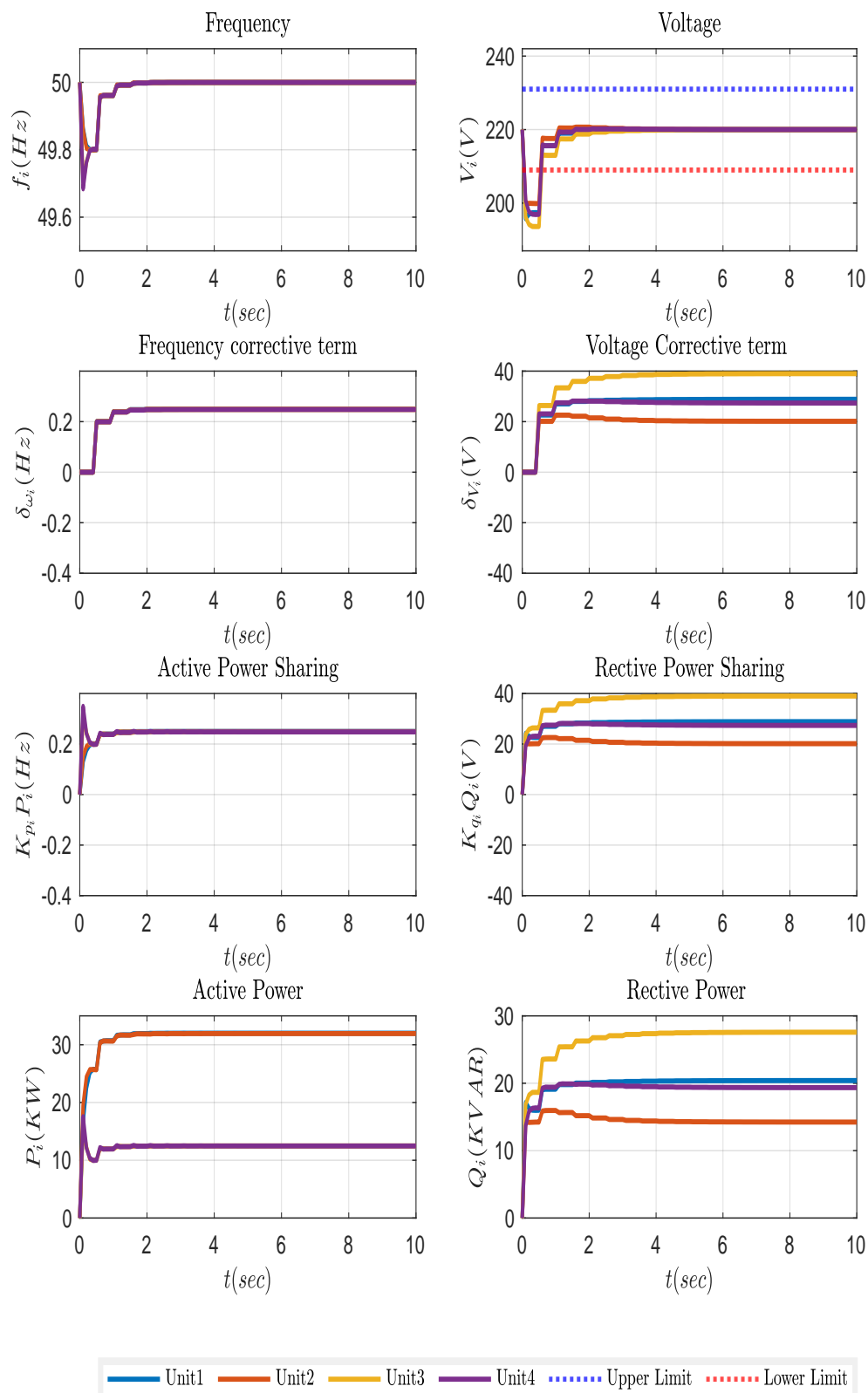


Figure 4.10: System variables for constrained problem for voltage regulation.

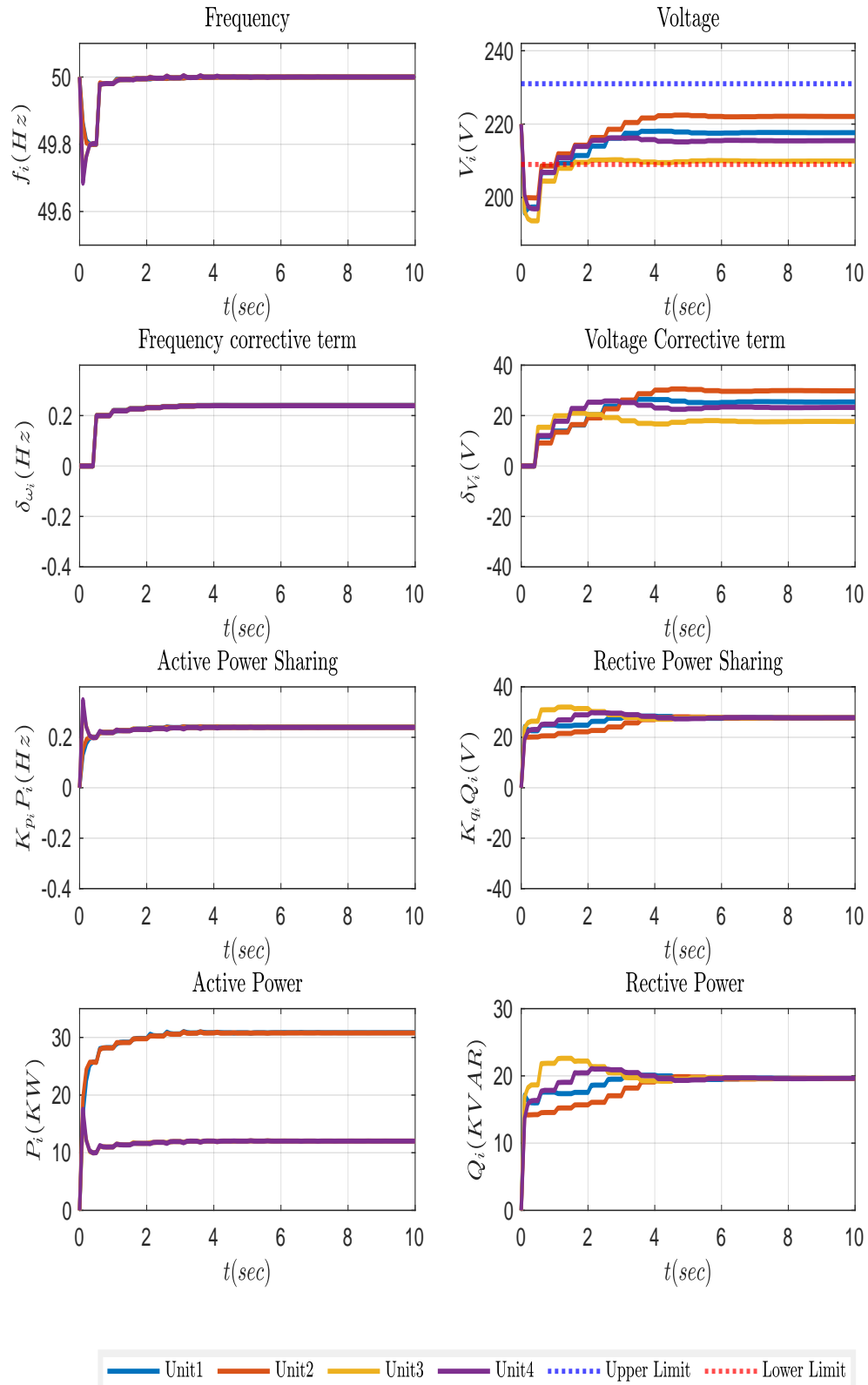
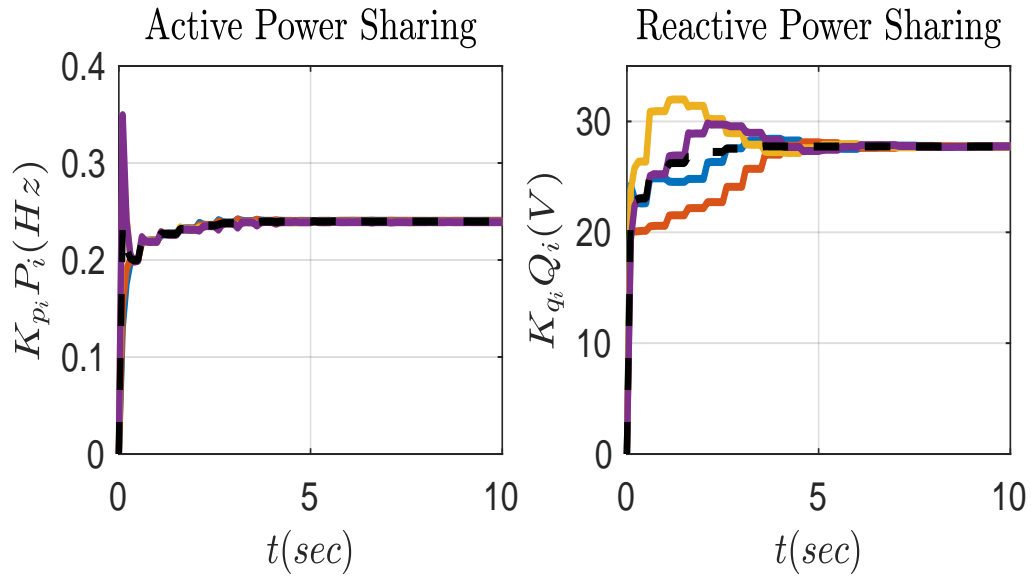


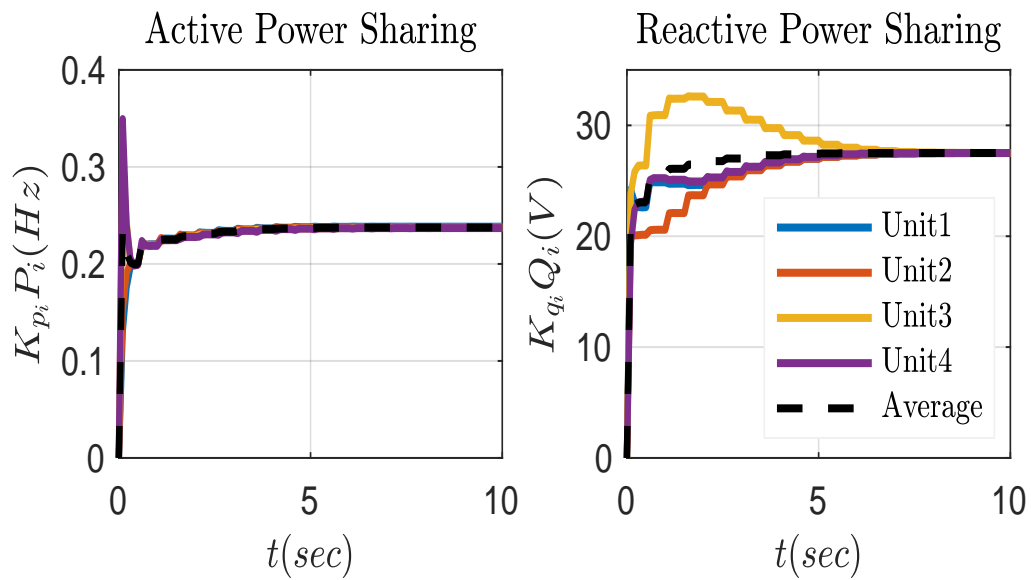
Figure 4.11: System variables for constrained problem for reactive power-sharing.

#### 4.5.2 Communication Channel Comparison

In this section, a comparison between consensus-based and centralized-based communication topology, as described in Figure. 4.8, has been performed on the proposed optimization-based secondary controller. In consensus-based communications, units broadcast their power-sharing values to their corresponding neighbor in one direction, forming a directed graph shown in Figure 4.8a, therefore, the communication link is minimum. On the other hand, centralized-based communication collects information about power-sharing from all units, calculates the global average value then, and then forwards the global average value to all units forming a two-way communication channel between the centralized processor and all grid-forming units in the system as shown in Figure 4.8b. This can also be done in a distributed manner, as explained at the beginning of this section. The objective function used for this simulation was constrained to reactive power-sharing given in the previous section. Figure 4.12a shows the active and reactive power-sharing along with their average values obtained by the consensus-based communication layer, while Figure 4.12b shows an application of a centralized-based communication layer. The active power-sharing was identical for both communication layers. However, the reactive power-sharing took about  $6sec$  to reach the average values for both topologies. Note that the reactive power-sharing with consensus-based communication topology oscillated more closely around the global average before they converged as compared with the centralized-based communication system.



(a) Consensus-based communication topology.



(b) Centralized-based communication topology.

Figure 4.12: Active and reactive power-sharing generated from the optimization-based secondary controller with different communication topologies.

### 4.5.3 Controller Behavior Under Line Parameters Mismatch

To observe the controller behavior under different line parameters mismatch, line 2 in Figure 4.7 was subjected to different values. The line parameters values for line 2, which are given in Table 4.1 were halved at the beginning of the simulation. At  $t = 10s$ , the line parameters of line 2 were restored to their given value. Then, line 2 parameters were multiplied by a factor of 4 at  $t = 20s$ .

Figure. 4.13 shows the frequencies, voltages, active and reactive powers of all units. For active powers, there was no interaction between the frequency regulation and the active power-sharing; hence the frequencies were restored probably without affecting the active power-sharing. Notice that as line parameters were increased, the active powers were increased to compensate for line losses. However, reactive power-sharing had an interfering effect between reactive power-sharing and voltage regulation. At the start of the simulation, the reactive powers were shared equally between the units, and the voltage was kept within limits. When  $Z_{l2}$  increased, the voltage differences increased while the reactive power-sharing was kept at the global consensus average. At  $t = 20s$  where  $Z_{l2}$  is increased four times, the upper and lower voltage limits were reached; therefore, there was not enough capacity for the controller to reach the global consensus average for all units and unit 2 reactive power-sharing deviated from other units. However, due to the convexity nature of the controller equations, the minimum deviation from the global consensus average was guaranteed.

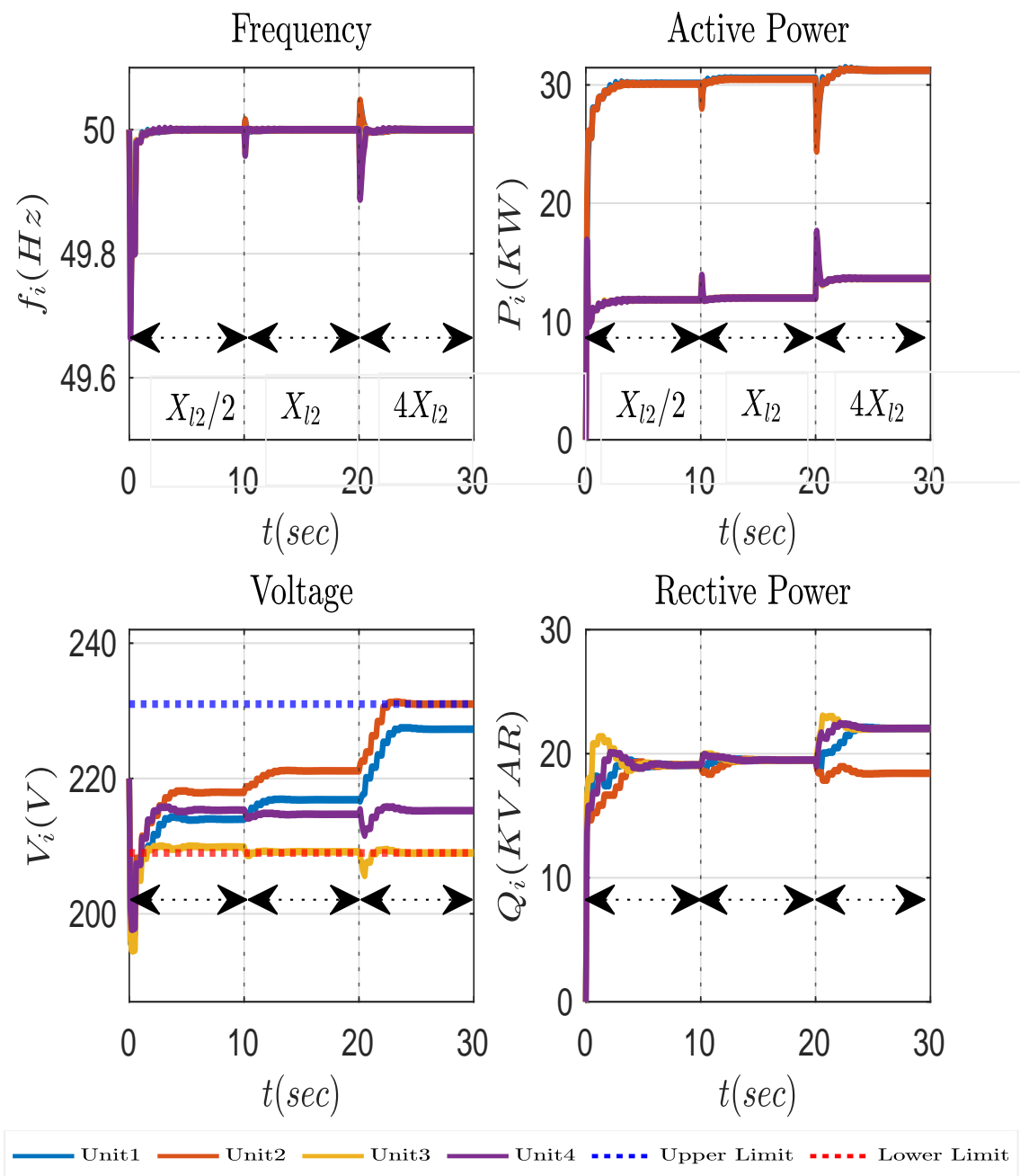


Figure 4.13: The controller behavior under different line parameter values.

#### 4.5.4 Resilience-based Cybersecurity

Smart grid applications are vulnerable to cyberattacks targeting the control systems of microgrids through different levels. As discussed in section 2.2.6, the detection algorithms are used

to detect cyberattacks and apply corrective measures to maintain the system's operation. These measures aim to isolate parts of the system that are under cyberattack. To boost the robustness of the proposed controller against such attacks, the connectivity graph should preserve the balanced and strongly connected properties. Therefore, undirected edges are used to preserve those properties when a unit or a communication link is disconnected from the system, as shown in Figure 4.14. Such a communication paradigm adds redundancy to the communication links between units so that each unit in the system is reachable by any other unit through multiple paths. Two cases were considered to validate the proposed controller's resilience to cyberattacks. In the first case, the False Data Injection Attack (FDIA) was detected in the communication link. While the second case considered the FDIA detected in the unit.

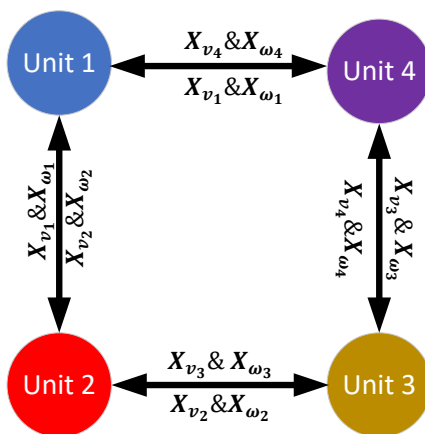


Figure 4.14: Undirected graph connectivity for the proposed controller.

### Disconnection of a Communication Link

In this section, FDIA was assumed to be detected at the communication link between units 3&4 at  $t = 5\text{sec}$ . Therefore, the communication link was disconnected to avoid false data, as shown in Figure 4.15. In Figure 4.16, the system variables are shown for disconnection of the communication link between units 3 & 4 at  $t = 5\text{sec}$ . The disconnection did not affect the system variables because the property of a balanced and strongly connected graph was still preserved using an undirected graph for the communication layer. Therefore, units 3&4 indirectly communicated with each other through units 1 & 2.

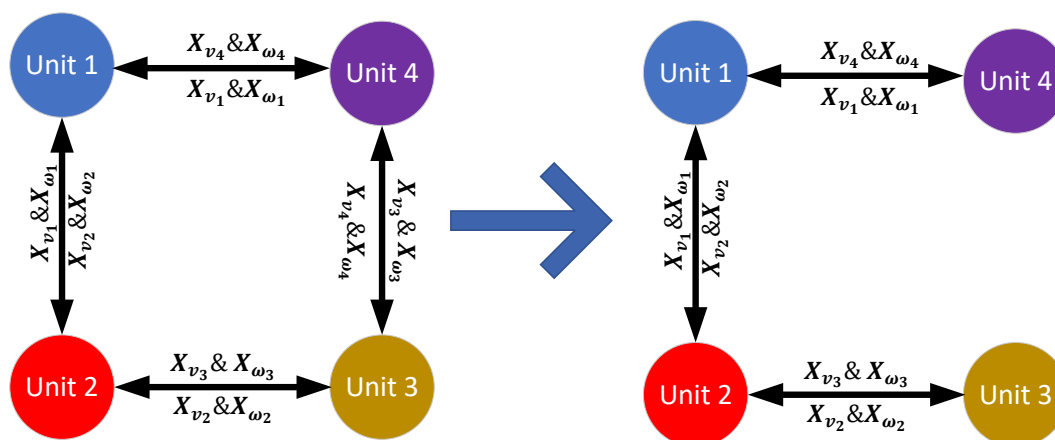


Figure 4.15: System variables for disconnection of the communication link between units 3 & 4.

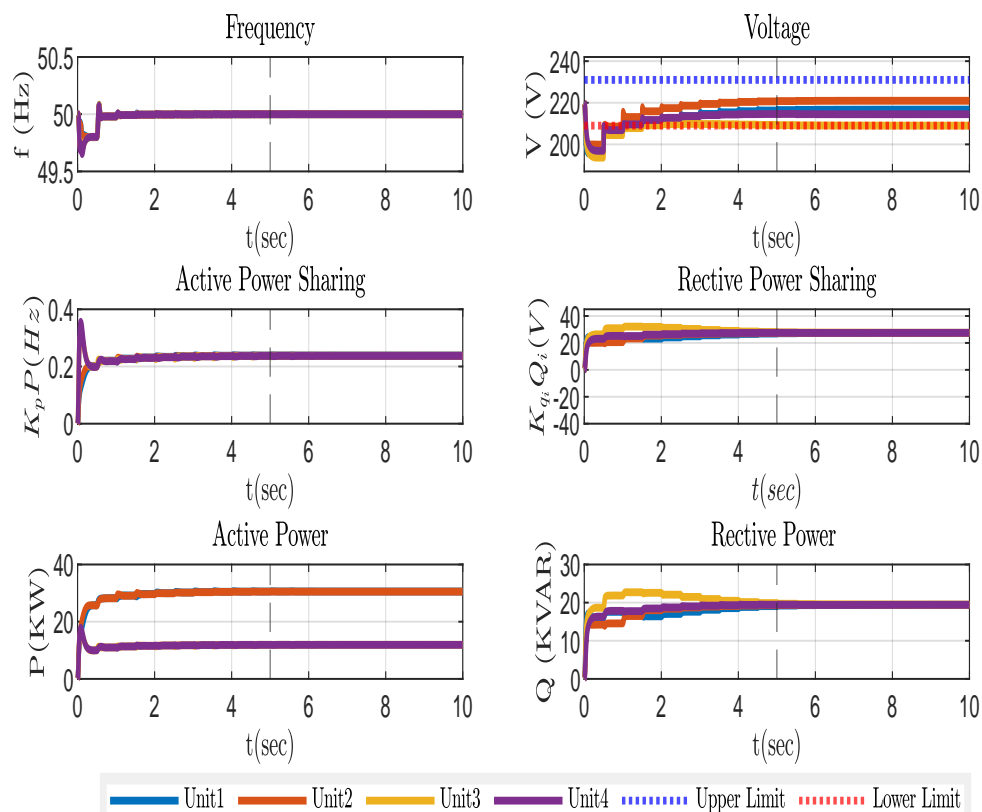


Figure 4.16: System variables for disconnection of the communication link between units 3 & 4.

### Disconnection of a Unit

This section focuses on the detection of FDIA at the unit's controller. Unit 3 was disconnected from the system at  $t = 5\text{sec}$ . Figure 4.17 shows the system's connectivity after unit 3 was disconnected. Figure 4.18 shows the system variables for disconnection of unit 3 as given at  $t = 5\text{sec}$ . The system could keep power sharing between the remaining units at a global consensus average while keeping the frequency and voltage within their limits.

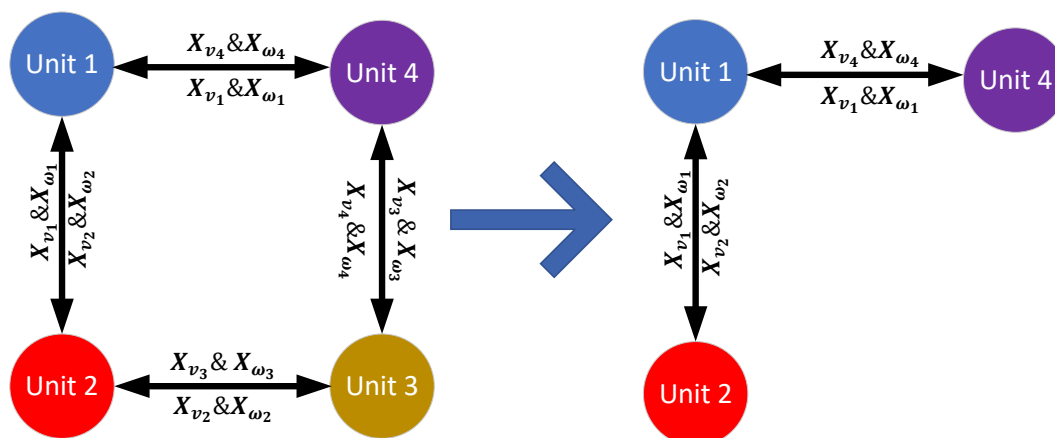


Figure 4.17: System variables for disconnection of the communication link between units 3 & 4.

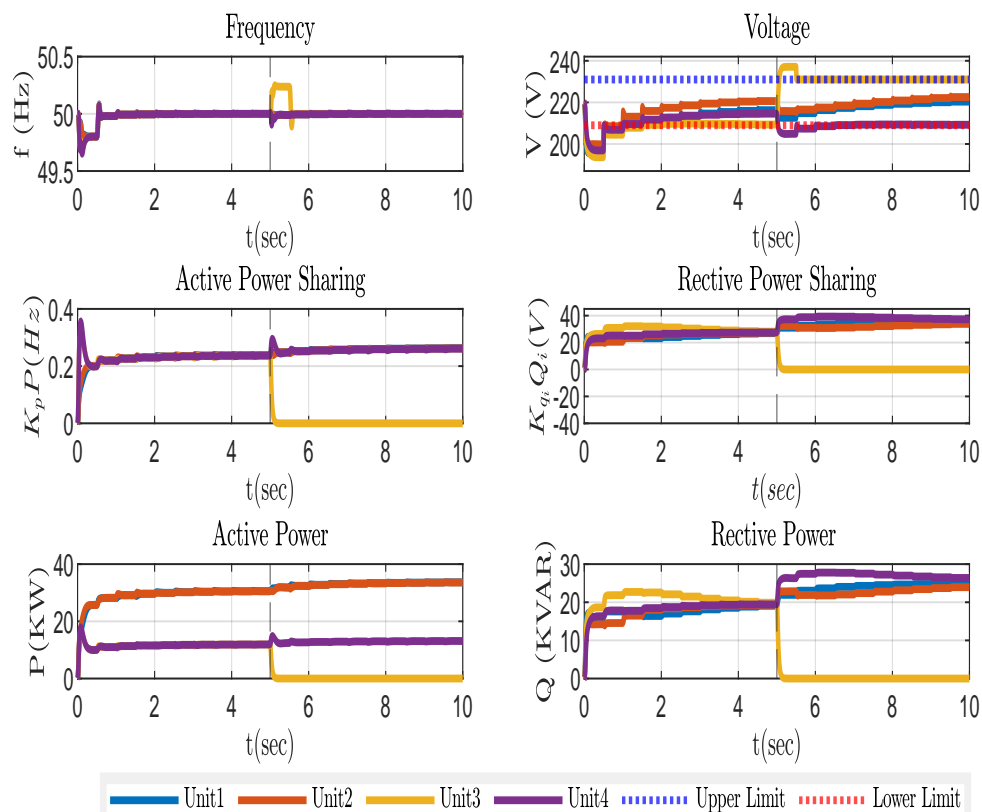


Figure 4.18: System variables for disconnection of unit 3.

## 4.6 Conclusions

This chapter applied an optimization-based consensus controller to the secondary control of islanded microgrids. The controller's function was to maintain the global consensus average of active and reactive power-sharing while restoring the frequency to its nominal value and keeping the voltages within the allowable limit of (i.e.,  $\pm 5\%$ ). A real-time quadratic convex optimization function was implemented by CVX/CVXGEN and embedded in a simulation model using MATLAB/SIMULINK. The controller's performance and behavior were validated through simulations for different control objectives. In addition, consensus-based and centralized-based communication models were compared for the proposed controller. The proposed controller efficiently kept the voltage and frequency levels within allowable limits and the power-sharing difference at a minimum mismatch. Moreover, the controller's behavior under different line parameter values was studied. The simulation showed that the reactive power-sharing started to mismatch optimally when the voltage limits were reached, and there was not enough capacity for the controller to keep the reactive power-sharing in global consensus average values.

## CHAPTER 5 ECONOMIC DISPATCH-BASED SECONDARY CONTROL

### 5.1 Introduction

In microgrids, the economic considerations are usually taken at the tertiary control level, which is managed by the distribution network operator (DNO). Economic dispatch and optimal power flow are standard algorithms implemented at this level. In such algorithms, the time constant takes several minutes to hours. Therefore, the loads and renewable energy production are required to be estimated. The estimation-based methods introduce uncertainty to the optimization function that degrades the optimal solution.

In this chapter, the economic dispatch algorithm is implemented within the secondary control level for an islanded microgrid. The proposed secondary control levels aim to dispatch active power based on fuel cost, restore the frequency and voltage to their nominal values, and manage the reactive power-sharing. A real-time optimization function is employed to solve the economic dispatch problem and manage the reactive power generation in relation to frequency and voltage, respectively. The proposed controller assumes the grid is inductive; hence, the active power only depends on the frequency and reactive power on the voltage. A coupling inductance is used to realize this assumption. The frequency and voltage are kept at nominal values to avoid circulating currents, while the generated active and reactive powers are subjected to maximum power capacity constraints. The controller proposed in this chapter is based on work given in [203].

The proposed controller integrates the economic dispatch algorithm into the secondary control of grid-forming units in an islanded microgrid. The features of the proposed controller can be summarized as follows:

- The active power is generated based on an economic dispatch algorithm subjected to maximum active power capacity and nominal frequency constraints.
- The reactive power is managed so that the reactive powers are maintained below their maximum capacity and the voltages are maintained at their nominal values.
- The algorithm is performed in real-time on a timescale 0.5 sec such that the required powers are based on measurements to avoid prediction errors caused by the estimation of loads and renewable energy generation quantities.

This chapter is organized as follows. First, section 5.2 introduces the hierarchical control structure of grid-forming units in islanded mode. Then, in Section 5.3, the optimization function of the proposed controller is derived and explained. Next, in Section 5.4, the simulation results are presented and compared with the decentralized secondary controller. Finally, Section 5.5 provides conclusions and future work for the proposed controller.

## 5.2 Tertiary Control in islanded Microgrid

The hierarchical control structure equations employing the droop control method that controls the grid-forming units in islanded mode are given as follows.

$$\omega_i = \omega_{nom} - K_{p_i}(P_i - P_{ref_i}) + \delta\omega_i \quad (5.1a)$$

$$V_i = V_{nom} - K_{q_i}(Q_i - Q_{ref_i}) + \delta V_i \quad (5.1b)$$

Where  $\omega_i$  and  $V_i$  are the angular frequency and terminal voltage of  $i^{th}$  unit,  $\omega_{nom}$  and  $V_{nom}$  are the nominal angular frequency and terminal voltage,  $K_{p_i}$  and  $K_{q_i}$  are active and reactive power droop coefficients,  $P_i$  and  $Q_i$  are measured active and reactive power of  $i^{th}$  unit,  $P_{ref}$  and  $Q_{ref}$  are the reference values of active and reactive power commanded by tertiary control level, and  $\delta\omega_i$  and  $\delta V_i$  are the secondary control corrective terms, respectively.

The overall control system of the grid-forming units is shown in Figure 5.1. The droop control equations set the voltage and frequency reference values by measuring the active and reactive power and receiving the primary, secondary, and tertiary command signals. Then, the voltage and frequency reference values are processed through the internal control loops of the grid-forming units. The active and reactive powers  $P_{ref_i}$  and  $Q_{ref_i}$  of the tertiary control level are responsible for the economic operation of the islanded microgrid. These economic aspects are regarded as optimal power flow or economic dispatch problems.

### 5.2.1 Optimal Power Flow

In optimal power flow, we are interested in the minimum or maximum feasible set of the objective function that satisfies the equality and inequality constraints. The objective function can be used to minimize fuel cost, line losses, voltage deviation, CO2 emissions, or maximize profit and penetration of renewable energy. The optimization problem can be in the form of a single objective or a multi-objective. The multi-objective function is solved by either Pareto or scalarization methods. In the Pareto method, the line between the two optimal solutions of multi-objective

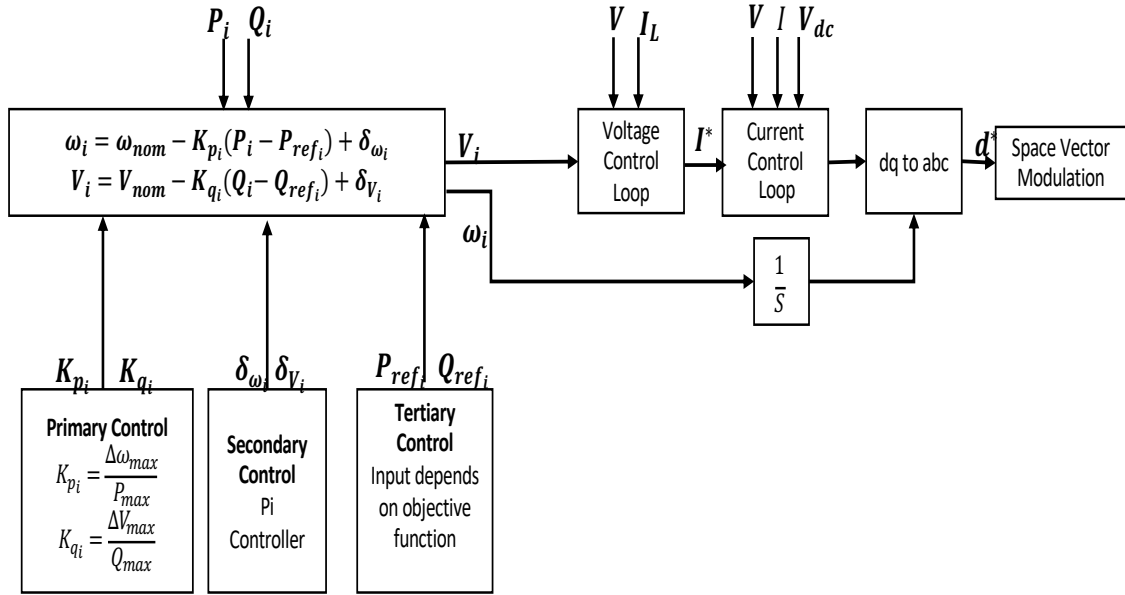


Figure 5.1: Hierarchical control structure.

optimization is called the Pareto line. Any point on this line is an optimal solution in such a way that moves to the optimal point of one variable affects the other. In the Scalarization method, the objective functions are prioritized in the sense that the optimal solution of one of the objectives is more favorable than the other. The fuel cost function can be given as

$$C(P_{ref_i}) = \sum_{i=0}^N a_i P_{ref_i}^2 + b_i P_{ref_i} + c_i \quad (5.2)$$

Where  $a_i$ ,  $b_i$ , and  $c_i$  are the generation cost parameters of  $i$ th DG unit.

To consider the operation limits while optimizing the objective function, constraints are subjected to the optimization problem. These constraints are either hard constraints that must be satisfied or soft constraints that are allowed to deviate from a tolerance based on a penalty factor in the objective function. Some examples of constraints applied to OPF are listed in Table 5.1. The optimal power flow considers each system bus, including the generation, load, and slack buses.

To perform a convex optimization, the objective function and constraints must be convex or affine functions. Therefore, linearization or convex relaxation is required. Linearization of non-convex constraints is based on assumptions on the grid such that the constraints become convex,

Table 5.1: Examples of constraints applied to OPE

Constraint	Equation	Description
Power flow constraints	$P_i =  V_i  \sum_{k=1}^n  V_k  (G_{ik} \cos(\theta_i - \theta_k) + B_{ik} \sin(\theta_i - \theta_k))$ $Q_i =  V_i  \sum_{k=1}^n  V_k  (G_{ik} \sin(\theta_i - \theta_k) - B_{ik} \cos(\theta_i - \theta_k))$	Ensures power flow equations are satisfied
Power balance constraints	$\sum_{i=1}^N S_{ref_i} = \sum_{i=1}^N S_{i,k}^{line} + \sum_{j=1}^N S_j^{load}$	Ensures the conservative principle is satisfied
Thermal capacity constraints	$f_{ik}(V_i, V_k) \leq I_{i,k}^{max}$	Ensures resistive losses in the line within an acceptable range
Active power generation capacity constraints	$P_{ref_i}^{min} \leq P_{ref_i} \leq P_{ref_i}^{max}$	Limits of the active power generation
Reactive power generation capacity constraints	$Q_{ref_i}^{max} \leq Q_{ref_i} \leq Q_{ref_i}^{max}$	Limits of the reactive power generation
Voltage magnitude limit constraints	$(V_i^{min})^2 \leq  V_i ^2 \leq (V_i^{max})^2$	Ensures voltages at buses are within a given range

such as DC-OPF and linearization around the no-load voltage profile. The DC-OPF, for instance, includes four assumptions that hold for the transmission system as follows

1. The line is lossless, and the shunt elements are neglected
2. The angle between buses is small such that  $\sin(\theta_i - \theta_j) \approx (\theta_i - \theta_j)$
3. The voltage magnitude at each bus is 1pu.
4. The reactive power flow is neglected.

However, the convex relaxations enclose the non-convex feasible spaces associated with the power flow equations in a larger space, such as Semidefinite Programming (SDP) and Second Order Cone Programming (SOCP). The advantage of solving OPF problems by a convex relaxation is the ability to certify a solution as being globally optimal: if an optimal solution of a relaxation satisfies an easily checkable condition.

The overall optimization problem aims to minimize the generation cost through generated active ( $P_{ref_i}$ ) and reactive ( $Q_{ref_i}$ ) powers in generation buses by solving the following optimization function.

$$\min \sum_{i=0}^N C(P_{ref_i}) \quad (5.3a)$$

$$P_i = |V_i| \sum_{k=1}^n |V_k| (G_{ik} \cos(\theta_i - \theta_k) + B_{ik} \sin(\theta_i - \theta_k)) \quad (5.3b)$$

$$Q_i = |V_i| \sum_{k=1}^n |V_k| (G_{ik} \sin(\theta_i - \theta_k) - B_{ik} \cos(\theta_i - \theta_k)) \quad (5.3c)$$

$$\sum_{i=1}^N P_{ref_i} = \sum_{i=1}^N P_{i,k}^{line} + \sum_{j=1}^N P_j^{load} \quad (5.3d)$$

$$\sum_{i=1}^N Q_{ref_i} = \sum_{i=1}^N Q_{i,k}^{line} + \sum_{j=1}^N Q_j^{load} \quad (5.3e)$$

$$f_{ik}(V_i, V_k) \leq I_{i,k}^{max} \quad (5.3f)$$

$$P_{ref_i}^{min} \leq P_{ref_i} \leq P_{ref_i}^{max} \quad (5.3g)$$

$$Q_{ref_i}^{max} \leq Q_{ref_i} \leq Q_{ref_i}^{min} \quad (5.3h)$$

$$(V_i^{min})^2 \leq |V_i|^2 \leq (V_i^{max})^2 \quad (5.3i)$$

### 5.2.2 Economic Dispatch

Economic dispatch uses an optimization function to set an optimal reference power for each unit that controls voltage and frequency. The economic dispatch solution is specified through variables  $P_{ref_i}$  and  $Q_{ref_i}$  in the droop control equations given in (5.1a) and (5.1b). The optimization function minimizes a cost function subjected to power balance and unit capacity constraints. Unlike the OPF, the economic dispatch considers only generation units. Considering a quadratic global cost function that minimizes the generation cost of each unit as given in (5.2). The optimization function pursues the minimum cost of generation while keeping the constraints on the power balance and the unit's capacity satisfied.

$$\min \sum_{i=0}^N C(P_{ref_i}) \quad (5.4a)$$

$$\underline{P}_i \leq P_{ref_i} \leq \bar{P}_i \quad (5.4b)$$

$$\sum_{i=0}^N P_{ref_i} = P_{load} \quad (5.4c)$$

Where  $C(P_{ref_i})$  represents the generation cost function,  $\underline{P}_i$  and  $\bar{P}_i$  represent the minimum and maximum of the rated capacity of the  $i$ th DG unit, respectively.

In the economic dispatch algorithm, renewable energy resources such as PV and wind energy systems that utilize MPPT are considered negative loads, adding to the load demands connected to the microgrid. Furthermore, given that the tertiary control level has a time scale in order of minutes, the loads and renewable energy generation quantities require estimation, which introduces prediction errors to the optimization function that degrade the efficiency of the economic dispatch of the microgrid.

### 5.3 Proposed Economic Dispatch-based Secondary Control

The proposed economic dispatch-based controller uses a centralized real-time optimization function to provide cost minimization, reactive power-sharing management, and frequency and voltage restorations at the secondary control level. The proposed controller utilizes the droop control equations that control the grid-forming units to maintain the frequency and voltage of the microgrid. The droop control equations in (5.1a) and (5.1b) are adopted without considering the secondary control corrective terms as

$$\omega_i = \omega_{nom} - K_{p_i}(P_i - P_{ref_i}) \quad (5.5a)$$

$$V_i = V_{nom} - K_{q_i}(Q_i - Q_{ref_i}) \quad (5.5b)$$

The variables  $P_{ref_i}$  and  $Q_{ref_i}$  are proposed to provide the economic dispatch-based secondary control signals through an optimization function that minimizes the generation cost subject to the constraints of secondary control functionalities. The controller attempts to control the measured active and reactive power ( $P_i$  and  $Q_i$ ) through variables  $P_{ref_i}$  and  $Q_{ref_i}$  as

$$P_i = 1/K_{p_i}(\omega_{nom} - \omega_i) + P_{ref_i} \quad (5.6a)$$

$$Q_i = 1/K_{q_i}(V_{nom} - V_i) + Q_{ref_i} \quad (5.6b)$$

In (5.6a) and (5.6b), the microgrid is assumed to be inductive, where the frequency is controlled by the active power and the voltage by the reactive power.

### 5.3.1 Cost Minimization

In the microgrid, different generation technologies are used for grid-forming units. Therefore, the generation cost may differ from one unit to another. A quadratic cost function is used to express the cost of generation as

$$C(P_i) = a_i P_i^2 + b_i P_i + c_i \quad (5.7)$$

Where  $a_i$ ,  $b_i$ , and  $c_i$  are generation cost coefficients associated with the generation cost of unit  $i$ .

Therefore, the objective function aims to minimize the generation cost given in (5.7). Equating (5.6a) in (5.6b), the cost function in terms of generated active power is given as

$$C(P_i) = a_i(1/K_{p_i}(\Delta\omega_i) + P_{ref_i})^2 + b_i(1/K_{p_i}(\Delta\omega_i) + P_{ref_i}) + c_i \quad (5.8)$$

### 5.3.2 Active and Reactive power management

In a grid-forming unit control system, power-sharing is required to ensure that the ratings of the units are not exceeded, and each unit shares power based on its ratings. However, the frequency and voltage regulations must be considered in the droop control equations as given in (5.5a) and (5.5b). Therefore, maintaining equal power-sharing at nominal frequency and voltage values is the desired behavior. However, the reactive power is shared not only based on reactive power droop coefficients but also based on the measured voltage at the terminal of each unit. As a result, a trade-off occurs between voltage regulation and reactive power-sharing. Hence, the proposed controller sets an upper limit for the active and reactive power generation to ensure that

the unit's ratings are not exceeded. Other constraints are imposed on the voltage and frequency to restore their nominal values and hence avoid circulating currents. The active and reactive power constraints are given as

$$1/K_{p_i}(\omega_{nom} - \omega_i) + P_{ref_i} \leq \bar{P}_i \quad (5.9a)$$

$$1/K_{q_i}(V_{nom} - V_i) + Q_{ref_i} \leq \bar{Q}_i \quad (5.9b)$$

### 5.3.3 Frequency and Voltage restorations

In secondary control of the microgrid, it is desired to keep the frequency and voltage in all grid-forming units at the same values to avoid circulating currents. Therefore, according to (5.5a) and (5.5b), the frequency and voltage of all units follow the nominal value when the measured active and reactive power are equal to their reference values. However, the active power is subjected to economic dispatch to minimize the cost of active power generation. Therefore, the power balance constraint requires that the sum of measured active powers be equal to the sum of active output powers.

$$\sum_{i=0}^N P_m = \sum_{i=0}^N P_i \quad (5.10)$$

Equating (5.6a) in (5.10) as

$$\sum_{i=0}^N P_{m_i} = \sum_{i=0}^N (1/K_{p_i}(\omega_{nom} - \omega_i) + P_{ref_i}) \quad (5.11)$$

Given that frequency is a global variable and the variable  $\omega_i$  is the same at all units, the constraint that keeps the change of frequency at zero can be given as

$$\sum_{i=0}^N P_{m_i} = \sum_{i=0}^N P_{ref_i} \quad (5.12)$$

For reactive power, it is sufficient to keep the measured reactive power equal to the reactive output power in each unit to restore the voltages in all units to their nominal values. When the rated output reactive power is reached, the voltage is allowed to be decreased to keep the reactive output power below the rated values as given in (5.9b). The constraint that governs reactive power management is given as

$$Q_{m_i} = Q_{ref_i} \quad (5.13)$$

The proposed economic dispatch-based controller requires a centralized processor to generate the optimal solution for the secondary controller. The data of the measured active and reactive

power, as well as the measured frequency and voltages, are collected in the centralized processor, which generates the optimal solution for reference values of active and reactive power. Then, these results are sent to all grid-forming units that participate in frequency and voltage control in islanded mode. Figure 5.2 shows the proposed controller architecture in which the economic dispatch-based controller is implemented at the secondary control level and sends its signals to the primary control level. The overall optimization problem is given as

$$\begin{aligned}
& \text{minimize} && a_i(1/K_{p_i}(\omega_{nom} - \omega_i) + P_{ref_i})^2 + b_i(1/K_{p_i}(\omega_{nom} - \omega_i) + P_{ref_i}) + c_i \\
& \text{subject to} && 1/K_{p_i}(\omega_{nom} - \omega_i) + P_{ref_i} \leq \bar{P}_i \\
& && 1/K_{q_i}(V_{nom} - V_i) + Q_{ref_i} \leq \bar{Q}_i \\
& && \sum_{i=0}^N P_{m_i} = \sum_{i=0}^N P_{ref_i} \\
& && Q_{m_i} = Q_{ref_i}
\end{aligned} \tag{5.14}$$

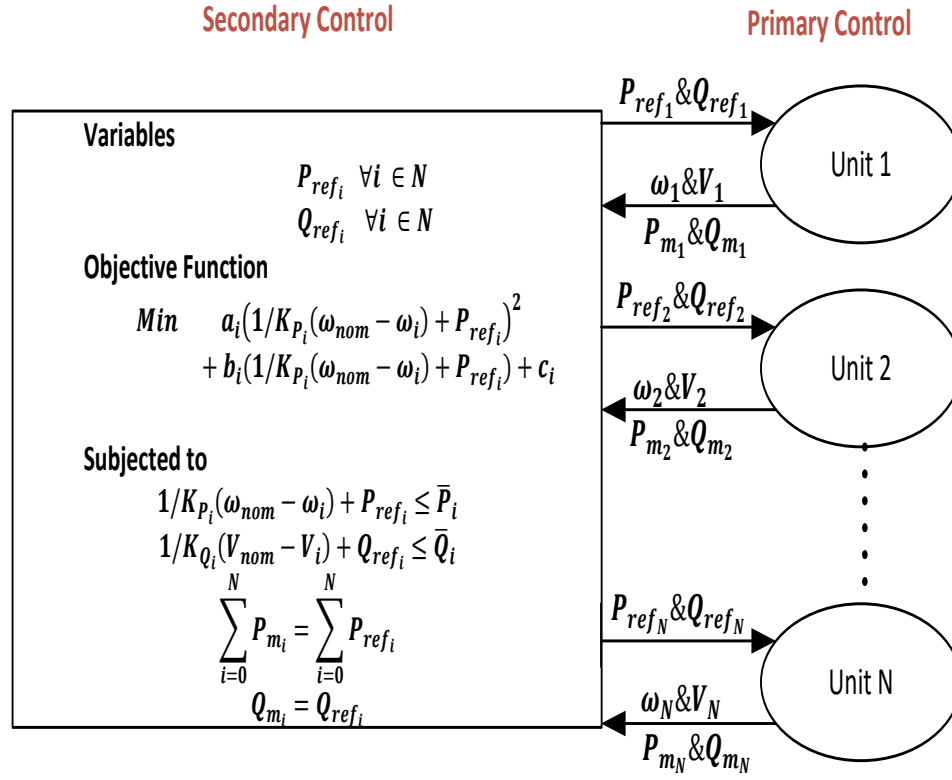


Figure 5.2: Economic dispatch-based secondary controller

#### 5.4 Simulation Results

The proposed secondary controller was validated through simulation for a microgrid test system shown in Figure 5.3. All units sent the measured quantities to the central controller and received the reference values of active and reactive powers in (5.5). The secondary control functionalities of the proposed controller, including economic dispatch, reactive power management, and frequency and voltage restoration, were considered in the control signal  $P_{ref_i}$  &  $Q_{ref_i}$ . The system parameters are listed in Table 5.2. The active and reactive power droop coefficients were chosen to be identical for all units to observe the controller's behavior based solely on the proposed optimization function. The cost of generation is given in Table 5.2, where the cost is ranked in ascending order such that unit 1 is the cheapest and unit 4 is the most expensive in terms of

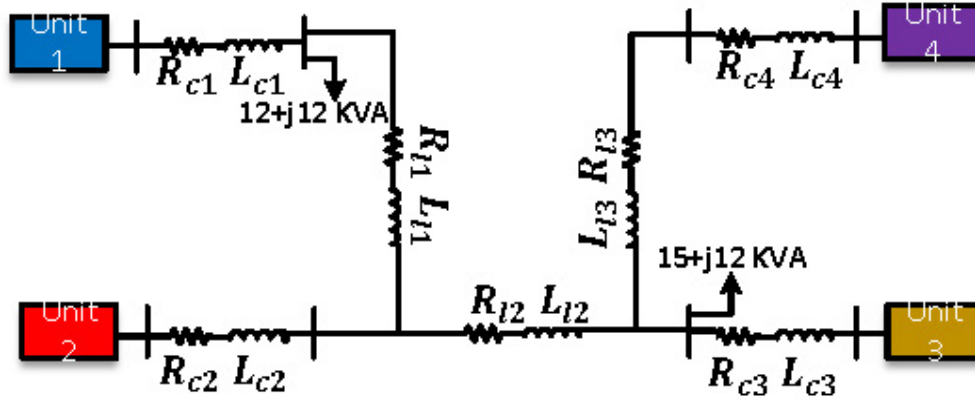


Figure 5.3: Single-line diagram of the microgrid test system.

generation cost.

#### 5.4.1 Performance of Controller

The behavior of the economic dispatch-based secondary controller was validated for the system given in Figure 5.3. In addition, the system was subjected to the load given in Table 5.2. The secondary control optimization function was implemented in a real-time centralized solver with a time step of  $0.5\text{sec}$  generated by CVX/CVXGEN code generator explained in Appendix B [202].

Figure 5.4 shows all unit variables, including frequency, voltage, active, and reactive powers. For active power, the controller effectively dispatched the active power based on the generation cost, while the frequency was kept at a nominal value for all units. For reactive power, the voltages were maintained at nominal values, and the reactive power generations were below the reactive power ratings.

Table 5.2: Specifications of the test system

<b>System</b>	<b>Parameter</b>	<b>Value</b>	<b>Parameter</b>	<b>Value</b>
	$V_{RMS}$	220V	$f_{sw}$	10KHz
	$V_{DC}$	700V	$f_{nom}$	50Hz
<b>DGs</b>	<b>Parameter</b>	<b>DG 1&amp;2</b>	<b>DG 3&amp;4</b>	<b>Unit</b>
	$\bar{P}_i$	50	50	KW
	$\bar{Q}_i$	20	20	KVAR
	$K_{p_i}$	49	49	$\mu rad/W.sec$
	$K_{q_i}$	2	2	$mV/VAR$
	$R_{c_i}$	30	30	$m\Omega$
	$L_{c_i}$	0.35	0.35	$mH$
<b>Lines</b>	<b>Parameter</b>	<b>Value</b>		<b>Unit</b>
	$Z_{l1}$	0.23 + j0.318		$m\Omega$
	$Z_{l2}$	0.35 + j1.847		$m\Omega$
	$Z_{l3}$	0.23 + j0.318		$m\Omega$
<b>Loads</b>	<b>Parameters</b>	<b>Value</b>		<b>Unit</b>
	$P_{load1} + jQ_{load1}$	36 + 36		KVA
	$P_{load2} + jQ_{load2}$	45 + 36		KVA
<b>Cost coefficients</b>	<b>DGs</b>	<b><math>a_i</math></b>	<b><math>b_i</math></b>	<b><math>c_i</math></b>
	<b>DG 1</b>	0.002	15	0
	<b>DG 2</b>	0.003	20	0
	<b>DG 3</b>	0.004	25	0
	<b>DG 4</b>	0.005	30	0
	<b>Unit</b>	$\$/MW^2hr$	$\$/MWhr$	$\$/hr$

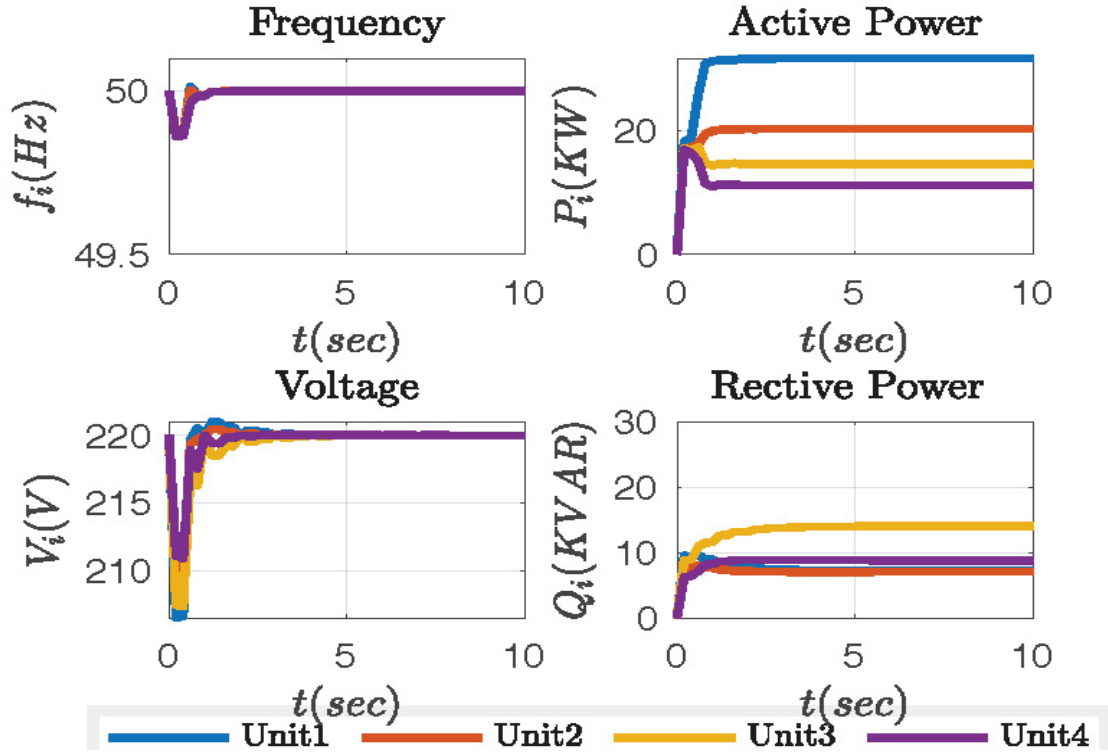


Figure 5.4: Economic dispatch-based secondary control.

#### 5.4.2 Comparison with decentralized secondary control

To verify the generation cost reduction of the proposed controller, the economic dispatch-based secondary controller was compared to a decentralized secondary controller. The objective of the decentralized secondary controller is to restore the frequency to its nominal values regardless of the active power management. In the decentralized controller, the droop control equations, given in (5.1), were employed. The secondary control corrections terms  $\delta\omega_i$  and  $\delta V_i$  were used to compensate for the frequency and voltage deviations in the unit's terminal.

In Figure 5.5, the variables of the system are shown for decentralized secondary control. The active power was only dispatched based on the droop control coefficient. The active power was shared equally between units because all units have similar active droop coefficients. Figure 5.6 shows the cost of generation of both controllers. The economic dispatch-based secondary controller effectively reduces the cost by %7.

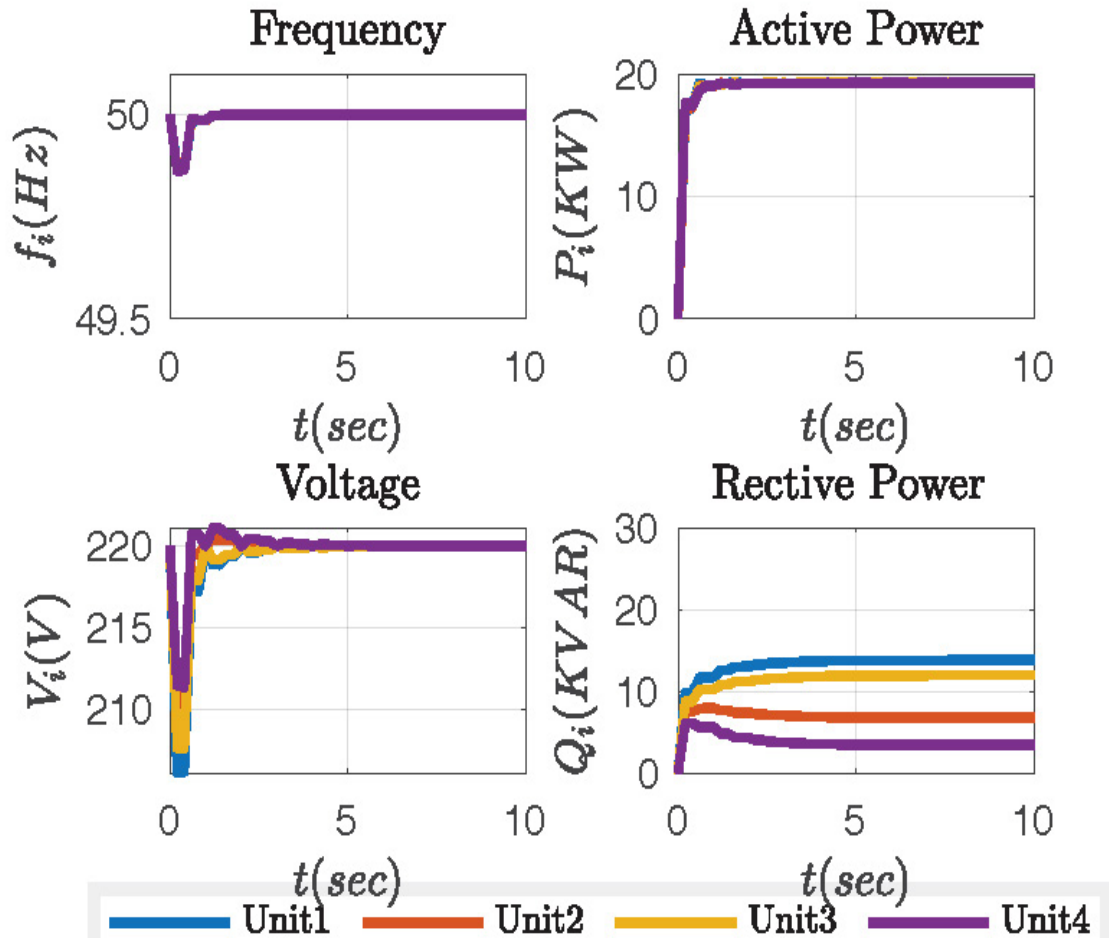


Figure 5.5: Decentralized secondary controller.

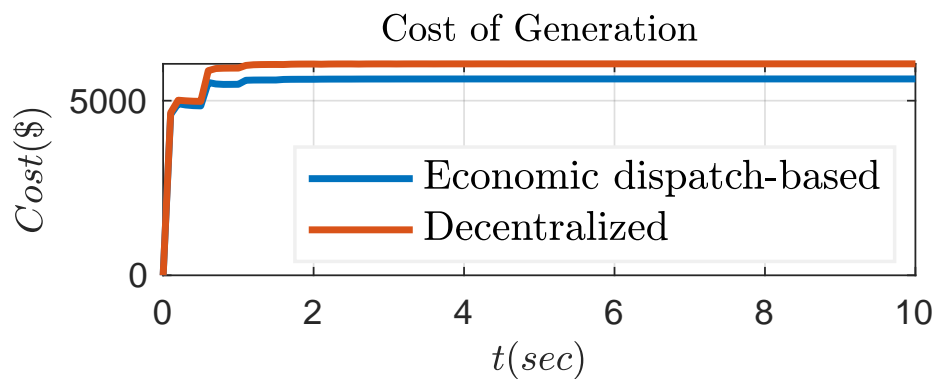


Figure 5.6: Comparison with the decentralized secondary controller.

## 5.5 Conclusions

This chapter employed the secondary control level of grid-forming units to provide frequency and voltage restorations, reactive power management, and economic dispatch. An optimization function was derived for providing these functionalities and implemented in a real-time solver on a timescale of 0.5 sec to avoid interaction with the primary control level and allow the controller to solve the optimization problem. The proposed controller was simulated using MATLAB/SIMULINK and compared to a decentralized secondary control with the objective of restoring the frequency and voltage of grid-forming units to their nominal values. In addition, the controller effectively dispatched the active power of units based on their cost. As a result, the cost of generation was reduced by 7%.

## CHAPTER 6 SCALABILITY VALIDATION ON CIGRE NORTH AMERICA MICROGRID BENCHMARK SYSTEM

### 6.1 Introduction

In this chapter, the scalability of the proposed controllers is validated in the CIGRE North American LV distribution network benchmark. The CIGRE benchmark was modified to be presented as an islanded microgrid by disconnecting it from the main grid and integrating DG units within its defined boundaries.

This chapter is structured as follows. Section 6.2 introduces the North America LV CIGRE distribution network benchmark with corresponding modifications to simulate the islanded microgrid. The generalized droop control was applied to the primary control of the CIGRE benchmark in section 6.3. In section 6.4, the secondary control of the islanded microgrid was implemented by the optimization-based consensus secondary controller and results are shown for two cases. Section 6.5 shows the economic operation of the islanded microgrid by applying the economic dispatch-based secondary controller. Finally, Section 6.6 summarizes this chapter.

### 6.2 CIGRE North America LV Distribution System

CIGRE Task Force (TF) C6.04.02 sets a baseline for testing the integration of DER and Smart Grid technology [204] to promote the analysis of the integration of DER at high voltage, medium voltage, and low voltage levels for the specifications of European and North American power systems. The benchmark provides a platform for analyzing, designing, and validating methods for the integration of renewable and distributed energy resource networks. These methods cover various domains, including operation and control, planning and design, power quality, protection, and stability.

CIGRE MV and LV distribution system benchmarks are widely used for microgrid applications due to their diversity of available specifications. In this dissertation, the North American LV commercial distribution benchmark was modified to serve as an islanded microgrid. The North America commercial benchmark is a 12-bus system located in a low-voltage distribution system. The  $X / R$  ratio is approximately 0.11, which makes it a practical candidate for validation of the generalized droop control proposed in Chapter 3. However, for the application of secondary controllers proposed in Chapters 4 and 5, a coupling impedance was used to increase the inductivity of

the system. A value of  $30 + j1m\Omega$  was placed at the terminal of each grid-forming unit to increase the X/R ratio to approximately 10. Furthermore, the line parameters mismatch between lines is generally low, which is suitable for case 2 of the optimization-based consensus secondary control in Chapter 4, where the voltage is kept at nominal values while the reactive power-sharing is minimized. Given that the CIGRE benchmark is based on real-life applications, the cost minimization algorithm proposed in Chapter 5 is a useful economic application for it.

The commercial feeder of the North America LV distribution network benchmark was slightly modified to present an islanded microgrid with a defined boundary. The PCC was placed at the distribution transformer where the islanded operation was initiated by switching off the PCC switch. Additionally, four grid-forming units were randomly installed in the system to operate the microgrid during disconnect from the main grid. Figure 6.1 shows the modified single-line diagram of the commercial feeder of the North America LV distribution network benchmark. Grid-forming units are located on buses 5,7,9 and 10. The system data is given in Table 6.1 where the data are derived from the CIGRE benchmark data as given in Appendix C.

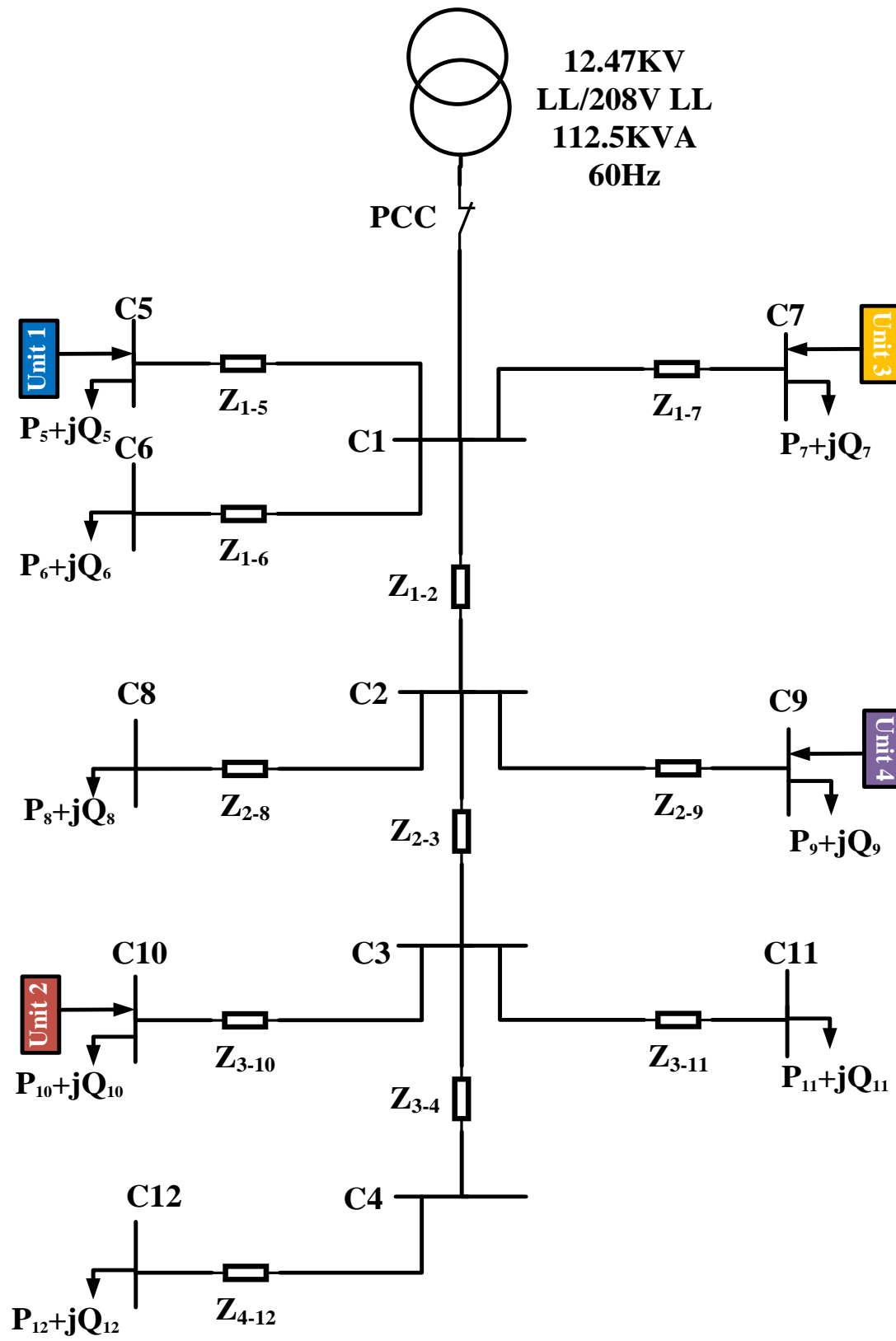


Figure 6.1: The modified commercial feeder of LV North America distribution system benchmark.

Table 6.1: The modified commercial feeder parameters

<b>DGs</b>	<b>Parameters</b>	<b>Value</b>	$K_{p_i}$	$K_{q_i}$
	Unit 1	$120 + j60 \text{ KVA}$	$2.6\mu\Omega\text{rad}/\text{Ws}$	$0.23\text{mV}/\text{VAR}$
	Unit 2	$120 + j60 \text{ KVA}$	$2.6\mu\Omega\text{rad}/\text{Ws}$	$0.23\text{mV}/\text{VAR}$
	Unit 3	$120 + j60 \text{ KVA}$	$2.6\mu\Omega\text{rad}/\text{Ws}$	$0.23\text{mV}/\text{VAR}$
	Unit 4	$120 + j60 \text{ KVA}$	$2.6\mu\Omega\text{rad}/\text{Ws}$	$0.23\text{mV}/\text{VAR}$
<b>Lines</b>	<b>Parameters</b>	<b>Value</b>	<b>Unit</b>	
	$Z_{1-2}$	$2.5583 + j2.1$	$m\Omega$	
	$Z_{1-5}$	$27.3 + j2.58$	$m\Omega$	
	$Z_{1-6}$	$27.3 + j2.58$	$m\Omega$	
	$Z_{1-7}$	$27.3 + j2.58$	$m\Omega$	
	$Z_{2-3}$	$8.57 + j2.34$	$m\Omega$	
	$Z_{2-8}$	$27.3 + j2.58$	$m\Omega$	
	$Z_{2-9}$	$18.56 + j1.75$	$m\Omega$	
	$Z_{3-4}$	$5.83 + j1.59$	$m\Omega$	
	$Z_{3-10}$	$18.56 + j1.76$	$m\Omega$	
	$Z_{3-11}$	$18.56 + j1.76$	$m\Omega$	
	$Z_{4-12}$	$8.73 + j0.83$	$m\Omega$	
<b>Loads</b>	<b>Parameters</b>	<b>Value</b>	<b>Unit</b>	
	$P_5 + jQ_5$	$9.09 + j4.4$	KVA	
	$P_6 + jQ_6$	$12.15 + j5.88$	KVA	
	$P_7 + jQ_7$	$14.365 + j8.9$	KVA	
	$P_8 + jQ_8$	$12.15 + j5.88$	KVA	
	$P_9 + jQ_9$	$16.05 + j5.27$	KVA	
	$P_{10} + jQ_{10}$	$9.59 + j3.15$	KVA	
	$P_{11} + jQ_{11}$	$16.05 + j5.27$	KVA	
	$P_{12} + jQ_{12}$	$9.09 + j4.4$	KVA	

### 6.3 Generalized Droop Control

In Chapter 3, the generalized droop control was validated for a four-bus system where three cases are simulated resistive, mixed-impedance, and inductive grid. In this section, the generalized droop control is applied to the CIGRE benchmark to ensure the scalability of the proposed controller. The CIGRE benchmark for commercial feeders was located on the LV distribution network, where the  $X/R$  ratio is significantly small. The calculated value of the  $X/R$  ratio according to the locations of the units in Figure 6.1 is 0.11 on average where the grid was assumed to be resistive.

Figure 6.2 shows the changes in frequency and voltages, active and reactive power, the estimated and calculated  $X/R$  ratio, and the elements of the dependency matrix for the generalized droop controller applied for the primary control of grid-forming units. At  $t = 2\text{sec}$  the load on bus C9 with  $16.05 + j5.27\text{KVA}$  was disconnected. Then, the load on bus C12 with  $9.09 + j4.4\text{KVA}$  was disconnected at  $t = 4\text{sec}$ .

Given that the grid was resistive, the voltage changes more for a greater change in active power, as can be seen for the disconnection of the load on bus C9. The system was stabilized by applying the generalized droop control and could estimate the  $X/R$  ratio to use it in the dependency matrix. In the dependency matrix, the absolute values of elements  $a_{12}$  and  $a_{21}$  were almost 0.9, and 0.1 for  $a_{11}$  and  $a_{22}$ , indicating the dependence of frequency on reactive power and voltage on active power. This behavior is typical for a resistive grid. Note that the change in frequency was positive due to the linear relationship between frequency and reactive power given in (3.15a) and a higher value of  $a_{12}$  as compared to  $a_{11}$ .

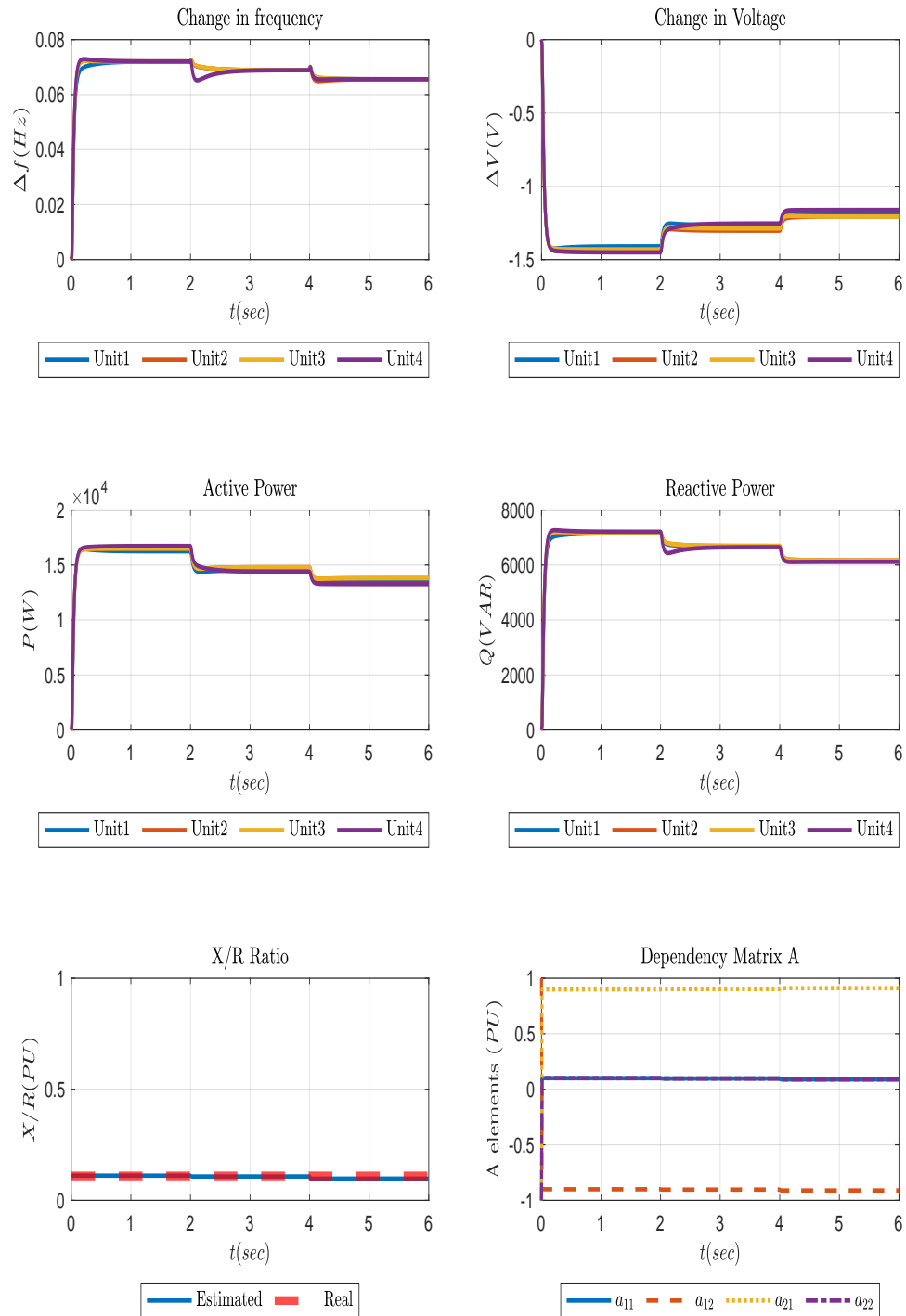


Figure 6.2: The unit variables with generalized droop control applied to the CIGRE LV benchmark.

#### 6.4 Optimization-Based Consensus Secondary Control

The optimization-based consensus secondary controller proposed in Chapter 4 was applied to the secondary control of grid-forming units. A coupling impedance of  $30 + j1m\Omega$  was applied to each unit's terminal to increase the  $X/R$  ratio to approximately 10 since the proposed controller was designed for an inductive grid. The proposed controller was applied for two cases in terms of the control objective. The first case was constrained for voltage regulation where the voltage was kept at a nominal level, i.e., 120V, while the reactive power mismatch was minimized. In the other case, the reactive power mismatch was minimized as long the voltage was kept within a predefined limit, i.e.,  $\pm 5\%$ . However, the controller aimed to reduce differences in reactive power-sharing in highly mismatched line impedance systems. In the CIGRE benchmark, the line impedance mismatch is minimal; therefore, the optimization function given in case 2, where the objective function was restricted for voltage regulation, is more suitable for the commercial feeder of the LV CIGRE benchmark.

Figure 6.3 shows the variables of grid-forming units for the proposed controller with a control objective to keep the voltage at a nominal value while minimizing the reactive power-sharing mismatch. This was achieved during the experiment. Note that, due to the minimal mismatch between the impedance of the lines, the reactive power-sharing mismatch was minimized as explained in Section 4.2.

In Figure 6.4, the grid-forming unit variables of the optimization-based consensus controller are shown for the control objective to keep the voltage within  $\pm 5\%$  of nominal value while minimizing the reactive power-sharing mismatch between units. Although the voltage constraint was not reached, the voltages were mismatched to allow unified reactive power-sharing among units.

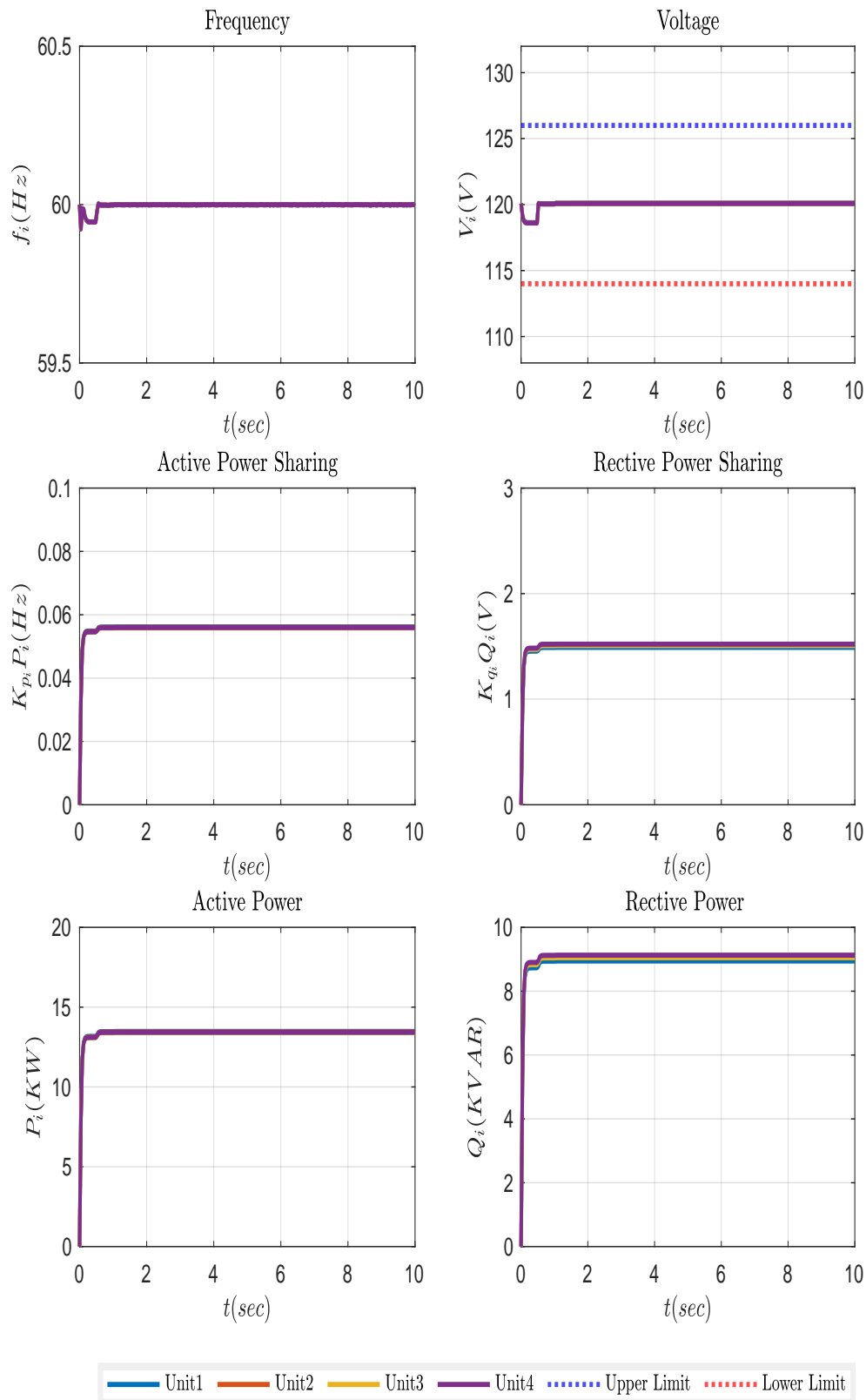


Figure 6.3: Constrained for voltage regulation

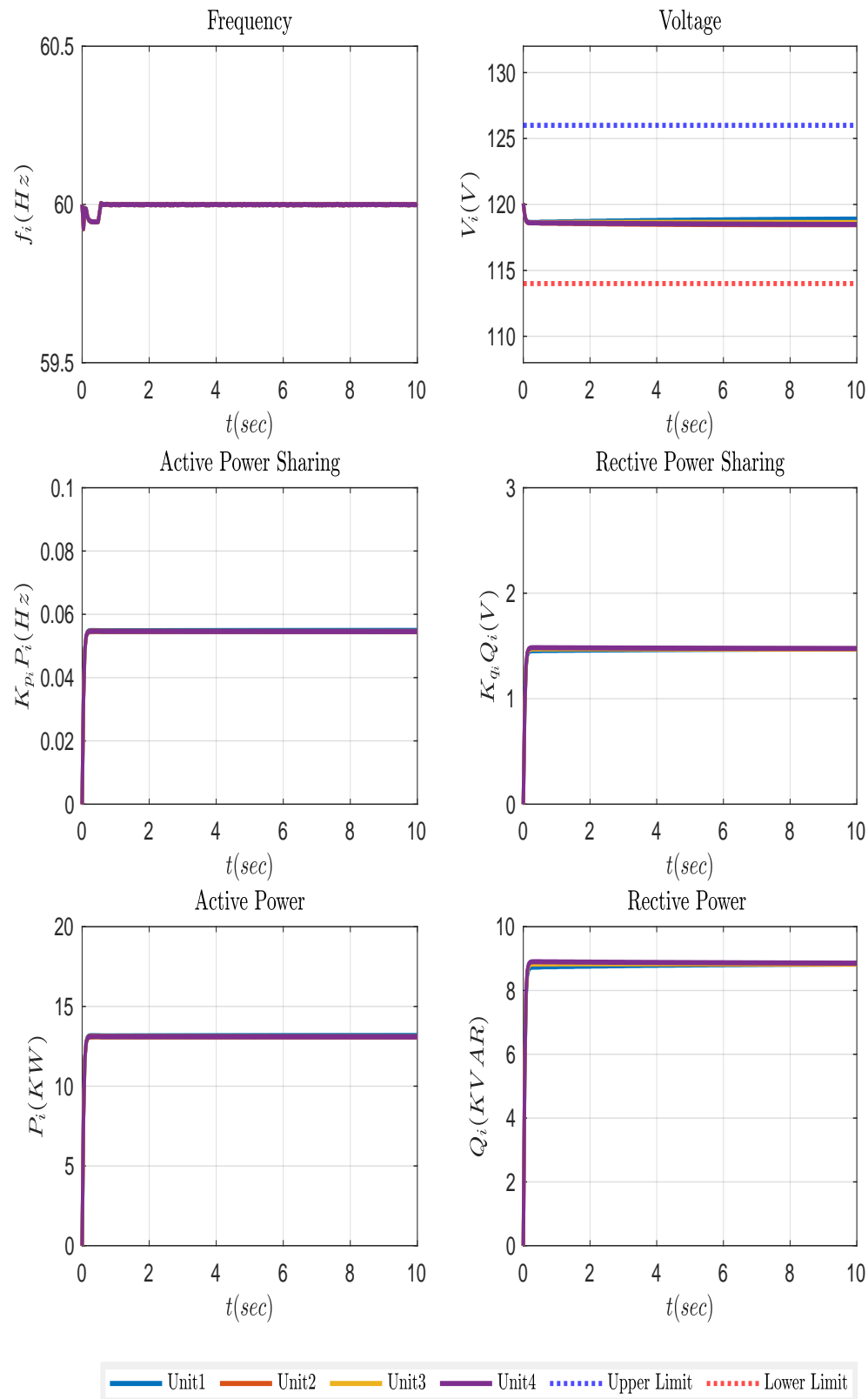


Figure 6.4: Constrained for reactive power-sharing

## 6.5 Economic Dispatch Secondary Control

The secondary controller based on economic dispatch in Chapter 5 is capable of reducing the cost of generation by 7%. The proposed controller was applied to the NA CIGRE benchmark with similar cost coefficients given in Table 5.2.

Figure 6.5 shows the variables of the grid-forming units with the economic dispatch-based secondary controller. Units dispatch active power based on their cost of generation. The frequency and voltage were kept at nominal values. In contrast, Figure 6.6 shows the variables when a decentralized secondary control was used to restore only the frequency and voltage of the units. The active power was dispatched based on the droop control coefficients without considering the cost of generation. In Figure 6.7, a comparison between the generation costs of the two controllers is shown. The secondary controller based on economic dispatch reduced the cost of generation by approximately 13%.

### 6.5.1 The effect of conductivity on economic dispatch.

The proposed economic dispatch-based secondary controller was implemented based on the assumption that the grid was inductive where the active power was dispatched by controlling the frequency and reactive power by controlling the voltage. According to (3.5), even with an inductive grid ( $X \gg R$ ), there is a voltage component in active power and a frequency in reactive power. However, as the inductivity of the grid increases, these components fade. Therefore, the economic operation is improved as the inductivity of the grid increases because the active power is further decoupled from the voltage, which has the objective of managing the reactive power. Additionally, the above phenomena explain the reactive power mismatch in Figure 6.5. In (3.6), the voltage was constrained at a nominal value while the active power changed based on economic dispatch. Therefore, to keep the voltage constant, the reactive power changes in the opposite direction of active power.

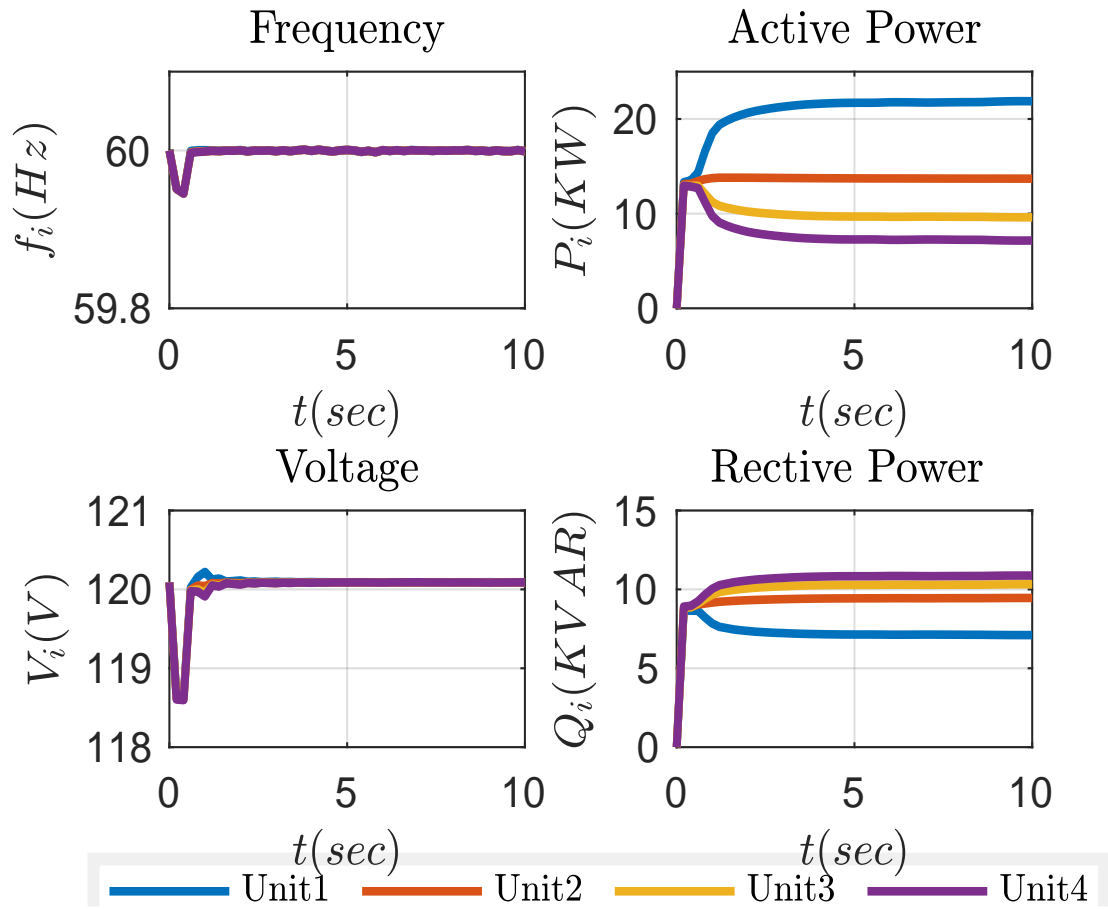


Figure 6.5: System behavior with the economic dispatch-based secondary controller.

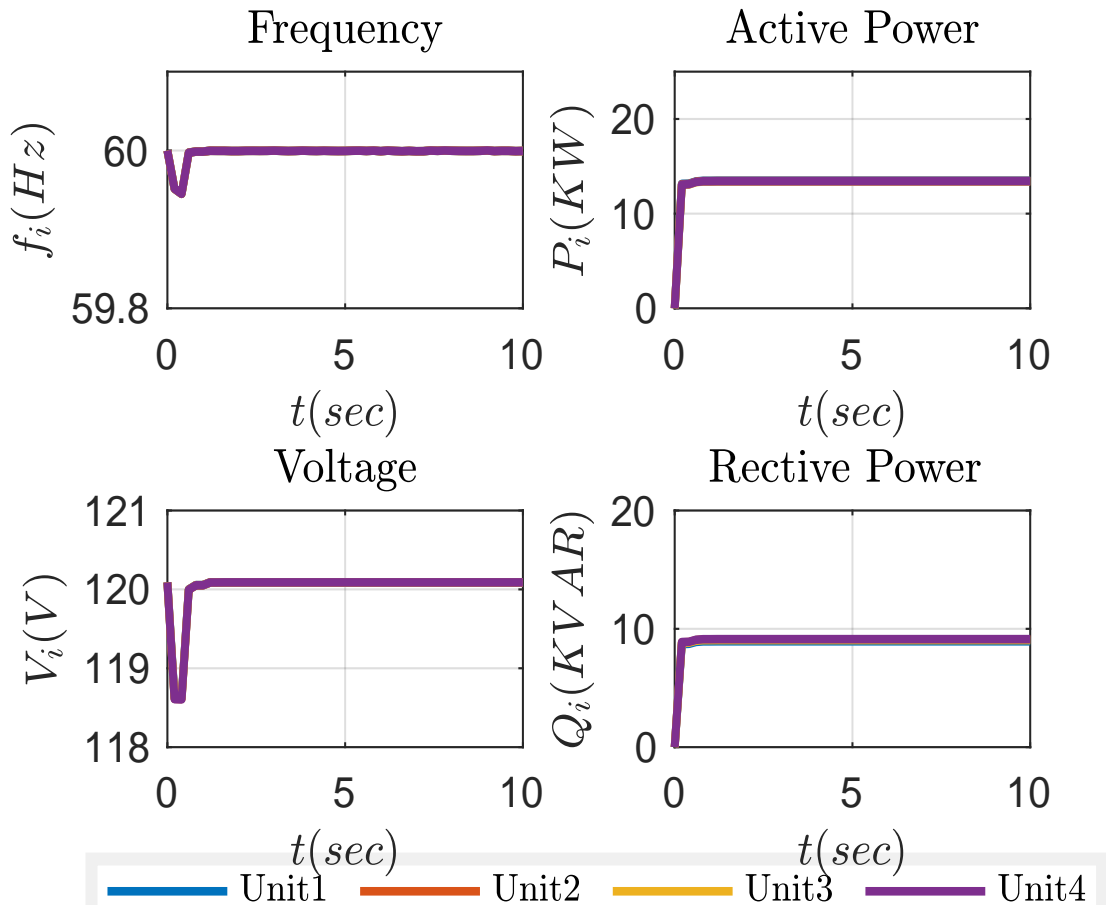


Figure 6.6: System behavior with the decentralized secondary controller.

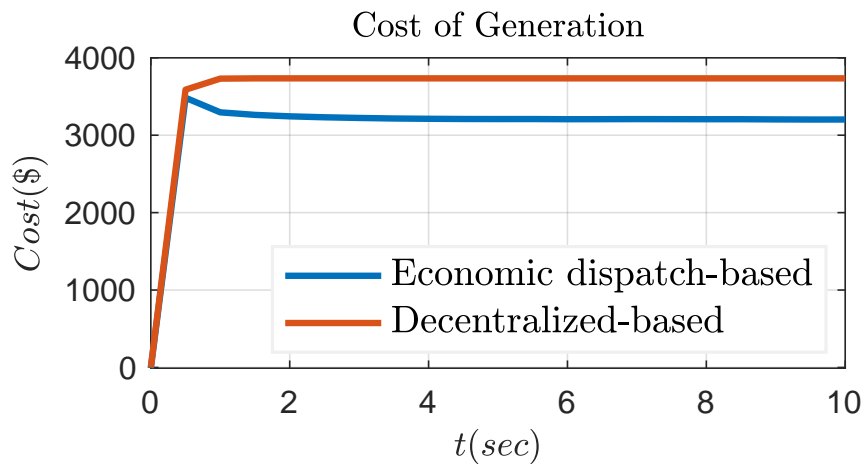


Figure 6.7: Cost of generation comparison.

## 6.6 Conclusions

The North America LV CIGRE distribution network benchmark was used to validate the scalability of the proposed controllers. It was modified to emulate an islanded microgrid by integrating grid-forming units and disconnecting it from the main grid. For the primary control, the generalized droop control was applied to show the effectiveness of the controller in maintaining the stability of frequency and voltage control under the CIGRE benchmark, which is a resistive grid with an  $X/R$  ratio of approximately 0.11. In addition, the optimization-based consensus secondary controller was applied, including two control objectives constrained to voltage regulation and reactive power-sharing. Finally, the economic dispatch-based secondary controller was applied to the CIGRE benchmark. The proposed controller improved the cost of generation by 13%. The effect of the inductivity of the grid for economic dispatch-based controllers is also discussed.

## CHAPTER 7 CONCLUSIONS

This dissertation aimed to enhance the resilience of power systems by improving the island operation of microgrids. These enhancements addressed three known issues found in the frequency and voltage control of islanded microgrids as applied by grid-forming units employing a hierarchical control structure. The issues discussed in this dissertation included the non-linear relationship between frequency and voltage with active and reactive power in a mixed impedance grid, the trade-off between voltage regulation and reactive power-sharing in an inductive grid with highly mismatched line impedance, and prediction errors in economic dispatch caused by estimation of load and renewable energy generation. The proposed controller for the primary control level was capable of maintaining the stability of the frequency and voltage control in resistive, mixed-impedance, and inductive grids. Furthermore, the optimization-based consensus secondary controller was able to maintain equal sharing of reactive power within predefined voltage limits to allow units to share reactive power based on their ratings and avoid circulating currents. Finally, the economic operation was improved for grid-forming units by utilizing the economic dispatch-based controller at the secondary control level, eliminating the need for an estimation algorithm for load and renewable energy generation. Solving these issues helps the power system improve resilience-based operation in the form of response to and recovery from HILP events.

This chapter is structured as follows. In Section 7.1, the dissertation is summarized along with the key contributions of this research. Section 7.2 discusses the recommendation and extensions that could improve the work proposed in this dissertation.

### **7.1 Summery and Contributions**

In Chapter 1, the significance of research on improving the islanded operation of microgrids in the context of improving the overall resilience of the power system was discussed. Furthermore, the control challenges associated with an islanded microgrid employing a hierarchical control structure were reviewed in light of recent literature. It was pointed out that there is a need for stable and economical operation of frequency and voltage control of grid-forming units employing a hierarchical control structure in an islanded microgrid. The organization of this dissertation was also outlined in this chapter.

Chapter 2 reviewed the literature on three topics related to this research. In the first part, the role of microgrids in improving the resilience of power systems was discussed in three regards: resilience-based planning, response, and restoration. The second part reviewed the concept of the microgrid and recent works on its operation, control, protection, and economic aspects. In the third part of this chapter, the literature on the hierarchical control structure of islanded microgrids was explored, along with associated issues.

A generalized droop controller to improve the stability of frequency and voltage control in a mixed impedance grid was discussed in Chapter 3. The primary control level was explained along with the issue of instability of frequency and voltage control in a mixed impedance grid. The proposed generalized droop controller was designed and simulated in this chapter. In addition, a discussion of the dependency matrix elements was presented.

In Chapter 4, The issue of the trade-off between voltage regulation and reactive power-sharing in an inductive grid was introduced, along with a discussion about the secondary control level of a hierarchical control structure. Furthermore, the optimization-based consensus secondary controller was proposed to overcome this issue with minimal communication links between units. Simulation results to verify the effectiveness of the proposed controller were presented.

The economic operation of frequency and voltage control in an islanded microgrid was introduced in Chapter 5. The optimal power flow and economic dispatch algorithms were discussed, along with the need to use an estimation algorithm to predict the loads and renewable energy generation quantities. The proposed economic dispatch-based secondary controller was implemented in real-time to eliminate the prediction caused by the estimation-based optimization algorithms. The effectiveness of the proposed controller in the simulation was validated in this chapter.

Chapter 6 validated the scalability of the proposed controllers in the commercial feeder of the North American CIGRE LV distribution network. The CIGRE benchmark was modified to incorporate grid-forming units with the microgrid boundary defined by placing the PCC between the feeder and the main grid. The generalized droop controller was applied to the CIGRE benchmark, and the results of the simulation were shown. Additionally, the optimization-based controller was applied with two control objectives, including constraints for voltage regulation and reactive power-sharing. Finally, the economic operation of the CIGRE model for applying the economic dispatch-based secondary controller was shown.

### 7.1.1 Key Contributions

This dissertation focuses on improving the islanded operation of microgrids with a hierarchical control structure. The key contributions of the presented work include three aspects of an islanded microgrid.

At the primary control level, the proposed generalized droop control could maintain the stability of the frequency and voltage control for resistive, mixed-impedance, and inductive grids. The key features of the proposed controller are as follows.

- The frequency and voltage were tuned precisely based on the measured active and reactive power.
- The X/R ratio was obtained from the active and reactive power consumed in the lines.
- The dependency matrix elements took values from -1 to 1 based on the per-unit relationship between the variables.

At the secondary control level, the optimization-based consensus secondary controller aims to manage the trade-off between voltage regulations and reactive power-sharing in an inductive grid with highly mismatched line impedance. The contribution of the proposed controller can be listed as follows:

- An analysis was carried out for the controller to reach the global consensus average at the optimal solution using the Lyapunov theory.
- The controller was fully distributed because it was implemented to seek the global consensus average of power-sharing (regulator consensus); therefore, there was no need for a leader unit to capture a reference value.
- Only information about power-sharing was communicated between units, which reduced the communication intensity in the communication network.
- At the voltage limit, the reactive power-sharing autonomously started to diverge optimally without the need for modification of the controller settings.

Another controller was proposed for the secondary control level to improve the economic operation of the islanded microgrid. The economic dispatch-based secondary controller aims to

reduce the cost of generation in the inductive grid by omitting the need for estimation-based algorithms to predict the load and renewable energy generation quantities, which causes prediction errors. The key features of the proposed controller can be summarized as:

- The active power was generated based on an economic dispatch algorithm subject to maximum active power capacity and nominal frequency constraints.
- The reactive power was managed in such a way that the reactive power values were maintained below their maximum capacity, and the voltages were maintained at their nominal values.
- The algorithm was performed in real-time on a 0.5 sec timescale such that the required power values were based on measurements to avoid prediction errors caused by the estimation of loads and renewable energy generation units.

## 7.2 Recommendation and Future work

The results using the controllers developed in this study have indicated the following areas for further investigation.

- **The generalized droop controller** used as coefficients for active and reactive powers, the  $f - P$  droop coefficient ( $\Delta\omega_{max}/P_{max}$ ) to control the frequency and the  $V - Q$  droop coefficient ( $\Delta V_{max}/Q_{max}$ ) to the voltage. A more precise representation of the power-sharing is to use ( $\Delta\omega_{max}/Q_{max}$ ) for ( $f - Q$ ) sharing and ( $\Delta V_{max}/P_{max}$ ) for ( $V - P$ ) sharing. However, a stability analysis is required to ensure the proper selection of these values.
- The proposed controller implements a linear relationship between frequency and voltage with active and reactive power. Therefore, coupling between variables can complicate the control objective for higher levels in a hierarchical control structure.
- The power-sharing in the proposed controller considers the average power over one cycle. A modification to share the power for non-linear load sharing would be considered.
- **For the optimization-based consensus secondary controller**, a study of the time of convergence to the consensus global average of power-sharing and its relation to the magnitude of line parameter mismatch is an important area for future research, especially with the use of an optimization-based approach.

- Further testing is required to validate the plug-and-play capabilities and behavior of the controller under pocket loss and communication link failure.
- **For the economic dispatch-based controller**, the distributed secondary controller is preferred in microgrid applications because it can reduce computation loading on the microgrid central controller and communication intensity while avoiding a single point of failure. Many distributed optimization algorithm methods can be utilized for the proposed controller.
- More investigation is needed under units reaching their rated active and reactive power to observe the behavior of the proposed controller under such conditions.
- The proposed controller assumes that the grid is inductive by utilizing a coupling inductance at the unit's terminal. For a mixed impedance grid, the coupling between the active and reactive power in controlling the frequency and voltage occurs. Therefore, a modification for the controller so it can provide its functionalities under a mixed impedance grid is preferred.
- **For overall hierarchical control structure**, the proposed controllers can be combined in a hierarchical control structure to satisfy each control objective addressed in this dissertation. However, the coupling between frequency and voltage with active and reactive power in the generalized droop control causes different control objectives for the same variables, i.e., frequency and voltage. Therefore, decoupling these variables improves the integration of the proposed controllers.
- When the frequency is decoupled from the reactive power and the voltage from active power, converting the economic dispatch-based controller to a distributed optimization problem allows an optimization function to provide unified reactive power-sharing and an economic dispatch for active power in a single optimization function.

## BIBLIOGRAPHY

- [1] M. Mahzarnia, M. P. Moghaddam, P. T. Baboli, and P. Siano, "A review of the measures to enhance power systems resilience," *IEEE Systems Journal*, vol. 14, no. 3, pp. 4059–4070, 2020.
- [2] A. Kenward and U. Raja, "Blackout: Extreme weather, climate change and power outages," technical report, Climate Central, Princeton, NJ 08542, 2014.
- [3] I. P. I. T. S. T. Force, "The definition and quantification of resilience," Technical Report PES-TR65, IEEE Power & Energy Society, Piscataway, NJ, USA, 2018.
- [4] G. Huang, J. Wang, C. Chen, J. Qi, and C. Guo, "Integration of preventive and emergency responses for power grid resilience enhancement," *IEEE Transactions on Power Systems*, vol. 32, no. 6, pp. 4451–4463, 2017.
- [5] Z. Wang and J. Wang, "Self-healing resilient distribution systems based on sectionalization into microgrids," *IEEE Transactions on Power Systems*, vol. 30, no. 6, pp. 3139–3149, 2015.
- [6] Z. Bie, Y. Lin, G. Li, and F. Li, "Battling the extreme: A study on the power system resilience," *Proceedings of the IEEE*, vol. 105, no. 7, pp. 1253–1266, 2017.
- [7] Y. Wu, Y. Wu, J. M. Guerrero, J. C. Vasquez, and J. Li, "Ac microgrid small-signal modeling: Hierarchical control structure challenges and solutions," *IEEE Electrification Magazine*, vol. 7, no. 4, pp. 81–88, 2019.
- [8] Guidehouse, "Global deployment of clean energy microgrids estimated to grow at a compound annual growth rate of 19 % through 2031." <https://guidehouseinsights.com>, accessed: August, 2022 [Online].
- [9] D. E. Olivares, A. Mehrizi-Sani, A. H. Etemadi, C. A. Cañizares, R. Iravani, M. Kazerani, A. H. Hajimiragha, O. Gomis-Bellmunt, M. Saadifard, R. Palma-Behnke, G. A. Jiménez-Estévez, and N. D. Hatziargyriou, "Trends in microgrid control," *IEEE Transactions on Smart Grid*, vol. 5, no. 4, pp. 1905–1919, 2014.
- [10] J. M. Guerrero, J. C. Vasquez, J. Matas, L. G. de Vicuna, and M. Castilla, "Hierarchical control of droop-controlled ac and dc microgrids—a general approach toward standardization," *IEEE Transactions on Industrial Electronics*, vol. 58, no. 1, pp. 158–172, 2011.
- [11] Y. W. Li and C.-N. Kao, "An accurate power control strategy for power-electronics-interfaced distributed generation units operating in a low-voltage multibus microgrid," *IEEE Transactions on Power Electronics*, vol. 24, no. 12, pp. 2977–2988, 2009.
- [12] R.-J. Wai, Q.-Q. Zhang, and Y. Wang, "A novel voltage stabilization and power sharing control method based on virtual complex impedance for an off-grid microgrid," *IEEE Transactions on Power Electronics*, vol. 34, no. 2, pp. 1863–1880, 2019.

- [13] J. M. Guerrero, J. Matas, L. Garcia de Vicuna, M. Castilla, and J. Miret, "Decentralized control for parallel operation of distributed generation inverters using resistive output impedance," *IEEE Transactions on Industrial Electronics*, vol. 54, no. 2, pp. 994–1004, 2007.
- [14] H. Han, X. Hou, J. Yang, J. Wu, M. Su, and J. M. Guerrero, "Review of power sharing control strategies for islanding operation of ac microgrids," *IEEE Transactions on Smart Grid*, vol. 7, no. 1, pp. 200–215, 2016.
- [15] B. John, A. Ghosh, and F. Zare, "Load sharing in medium voltage islanded microgrids with advanced angle droop control," *IEEE Transactions on Smart Grid*, vol. 9, no. 6, pp. 6461–6469, 2018.
- [16] Q.-C. Zhong and Y. Zeng, "Universal droop control of inverters with different types of output impedance," *IEEE Access*, vol. 4, pp. 702–712, 2016.
- [17] R. Han, L. Meng, G. Ferrari-Trecate, E. A. A. Coelho, J. C. Vasquez, and J. M. Guerrero, "Containment and consensus-based distributed coordination control to achieve bounded voltage and precise reactive power sharing in islanded ac microgrids," *IEEE Transactions on Industry Applications*, vol. 53, no. 6, pp. 5187–5199, 2017.
- [18] S. M. Mohiuddin and J. Qi, "Optimal distributed control of ac microgrids with coordinated voltage regulation and reactive power sharing," *IEEE Transactions on Smart Grid*, vol. 13, no. 3, pp. 1789–1800, 2022.
- [19] J. S. Gómez, D. Sáez, J. W. Simpson-Porco, and R. Cárdenas, "Distributed predictive control for frequency and voltage regulation in microgrids," *IEEE Transactions on Smart Grid*, vol. 11, no. 2, pp. 1319–1329, 2020.
- [20] X. Wu, C. Shen, and R. Iravani, "A distributed, cooperative frequency and voltage control for microgrids," *IEEE Transactions on Smart Grid*, vol. 9, no. 4, pp. 2764–2776, 2018.
- [21] Y. Liu, Z. Qu, H. Xin, and D. Gan, "Distributed real-time optimal power flow control in smart grid," *IEEE Transactions on Power Systems*, vol. 32, no. 5, pp. 3403–3414, 2017.
- [22] Y. C. Cassandra Wong, C. Shen Lim, A. J. Cruden, M. D. Rotaru, and K. Xin, "Semi-distributed optimal secondary control based on decoupled linearized power flow for large-area droop-controlled microgrids," in *2021 International Conference on Green Energy, Computing and Sustainable Technology (GECOST)*, pp. 1–7, 2021.
- [23] V. Suresh and P. Janik, "Optimal power flow in microgrids using genetic algorithm," in *2019 2nd International Conference on Power and Embedded Drive Control (ICPEDC)*, pp. 483–487, 2019.
- [24] D. K. Molzahn and I. A. Hiskens, *A Survey of Relaxations and Approximations of the Power Flow Equations*. 2019.
- [25] L. Xiaoping, D. Ming, H. Jianghong, H. Pingping, and P. Yali, "Dynamic economic dispatch for microgrids including battery energy storage," in *The 2nd International Symposium on Power Electronics for Distributed Generation Systems*, pp. 914–917, 2010.

- [26] W. Zheng, W. Wu, B. Zhang, H. Sun, Q. Guo, and C. Lin, "Dynamic economic dispatch for microgrids: A fully distributed approach," in *2016 IEEE/PES Transmission and Distribution Conference and Exposition (T D)*, pp. 1–3, 2016.
- [27] Z. Li, Z. Cheng, J. Liang, J. Si, L. Dong, and S. Li, "Distributed event-triggered secondary control for economic dispatch and frequency restoration control of droop-controlled ac microgrids," *IEEE Transactions on Sustainable Energy*, vol. 11, no. 3, pp. 1938–1950, 2020.
- [28] NATE, "Transmission resilience overview." <https://www.natf.net/docs/natf/documents/resources/resiliency/transmission-resilience-overview.pdf>, accessed: August, 2022 [Online].
- [29] G. M. initiative, "Grid modernization updated gmi strategy 2020," Technical Report PES-TR83, Department of Energy, Washington, D.C., U.S., 2020.
- [30] W. P. Zarakas, S. Sergici, H. Bishop, J. Zahniser-Word, and P. Fox-Penner, "Utility investments in resiliency: Balancing benefits with cost in an uncertain environment," *The Electricity Journal*, vol. 27, no. 5, pp. 31–41, 2014.
- [31] Y. Wang, C. Chen, J. Wang, and R. Baldick, "Research on resilience of power systems under natural disasters—a review," *IEEE Transactions on Power Systems*, vol. 31, no. 2, pp. 1604–1613, 2016.
- [32] G. Davis, A. F. Snyder, and J. Mader, "The future of distribution system resiliency," in *2014 Clemson University Power Systems Conference*, pp. 1–8, 2014.
- [33] Y. Xu, C.-C. Liu, K. P. Schneider, and D. T. Ton, "Toward a resilient distribution system," in *2015 IEEE Power & Energy Society General Meeting*, pp. 1–5, 2015.
- [34] T. I. P. . E. S. I. T. S. L. C. T. Force, "Resilience framework, methods, and metrics for the electricity sector," Technical Report PES-TR83, IEEE Power & Energy Society, 2020.
- [35] A. M. Nakiganda, S. Dehghan, U. Markovic, G. Hug, and P. Aristidou, "A stochastic-robust approach for resilient microgrid investment planning under static and transient islanding security constraints," *IEEE Transactions on Smart Grid*, vol. 13, no. 3, pp. 1774–1788, 2022.
- [36] H. Ren and N. N. Schulz, "A clustering-based microgrid planning for resilient restoration in power distribution system," in *2020 IEEE/PES Transmission and Distribution Conference and Exposition (T & D)*, pp. 1–5, 2020.
- [37] H. Masrur, M. Shafie-Khah, M. J. Hossain, and T. Senjyu, "Multi-energy microgrids incorporating ev integration: Optimal design and resilient operation," *IEEE Transactions on Smart Grid*, vol. 13, no. 5, pp. 3508–3518, 2022.
- [38] E. Taherian-Fard, T. Niknam, R. Sahebi, M. Javidsharifi, A. Kavousi-Fard, and J. Aghaei, "A software defined networking architecture for ddos-attack in the storage of multimicrogrids," *IEEE Access*, vol. 10, pp. 83802–83812, 2022.

- [39] K. S. A. Sedzro, A. J. Lamadrid, and L. F. Zuluaga, "Allocation of resources using a microgrid formation approach for resilient electric grids," *IEEE Transactions on Power Systems*, vol. 33, no. 3, pp. 2633–2643, 2018.
- [40] S. Chanda and A. K. Srivastava, "Defining and enabling resiliency of electric distribution systems with multiple microgrids," *IEEE Transactions on Smart Grid*, vol. 7, no. 6, pp. 2859–2868, 2016.
- [41] K. P. Schneider, F. K. Tuffner, M. A. Elizondo, C.-C. Liu, Y. Xu, and D. Ton, "Evaluating the feasibility to use microgrids as a resiliency resource," *IEEE Transactions on Smart Grid*, vol. 8, no. 2, pp. 687–696, 2017.
- [42] B. Papari, C. S. Edrington, M. Ghadamyari, M. Ansari, G. Ozkan, and B. Chowdhury, "Metrics analysis framework of control and management system for resilient connected community microgrids," *IEEE Transactions on Sustainable Energy*, vol. 13, no. 2, pp. 704–714, 2022.
- [43] X. Liu, M. Shahidehpour, Z. Li, X. Liu, Y. Cao, and Z. Bie, "Microgrids for enhancing the power grid resilience in extreme conditions," *IEEE Transactions on Smart Grid*, vol. 8, no. 2, pp. 589–597, 2017.
- [44] C. Chen, J. Wang, F. Qiu, and D. Zhao, "Resilient distribution system by microgrids formation after natural disasters," *IEEE Transactions on Smart Grid*, vol. 7, no. 2, pp. 958–966, 2016.
- [45] J. Li, X.-Y. Ma, C.-C. Liu, and K. P. Schneider, "Distribution system restoration with microgrids using spanning tree search," *IEEE Transactions on Power Systems*, vol. 29, no. 6, pp. 3021–3029, 2014.
- [46] Y. Du and D. Wu, "Deep reinforcement learning from demonstrations to assist service restoration in islanded microgrids," *IEEE Transactions on Sustainable Energy*, vol. 13, no. 2, pp. 1062–1072, 2022.
- [47] T. Zhao and J. Wang, "Learning sequential distribution system restoration via graph-reinforcement learning," *IEEE Transactions on Power Systems*, vol. 37, no. 2, pp. 1601–1611, 2022.
- [48] M. A. Igder, X. Liang, and M. Mitolo, "Service restoration through microgrid formation in distribution networks: A review," *IEEE Access*, vol. 10, pp. 46618–46632, 2022.
- [49] A. S. Kahnamouei and S. Lotfifard, "Enhancing resilience of distribution networks by coordinating microgrids and demand response programs in service restoration," *IEEE Systems Journal*, vol. 16, no. 2, pp. 3048–3059, 2022.
- [50] M. Khederzadeh and S. Zandi, "Enhancement of distribution system restoration capability in single/multiple faults by using microgrids as a resiliency resource," *IEEE Systems Journal*, vol. 13, no. 2, pp. 1796–1803, 2019.
- [51] D. T. Ton and M. A. Smith, "The U.S. Department of Energy's Microgrid Initiative," *The Electricity Journal*, vol. 25, no. 8, pp. 84–94, 2012.

- [52] S. Parhizi, H. Lotfi, A. Khodaei, and S. Bahramirad, "State of the art in research on microgrids: A review," *IEEE Access*, vol. 3, pp. 890–925, 2015.
- [53] A. Muhtadi, D. Pandit, N. Nguyen, and J. Mitra, "Distributed energy resources based microgrid: Review of architecture, control, and reliability," *IEEE Transactions on Industry Applications*, vol. 57, no. 3, pp. 2223–2235, 2021.
- [54] H. Jiayi, J. Chuanwen, and X. Rong, "A review on distributed energy resources and microgrid," *Renewable and Sustainable Energy Reviews*, vol. 12, no. 9, pp. 2472–2483, 2008.
- [55] A. Banerji, D. Sen, A. K. Bera, D. Ray, D. Paul, A. Bhakat, and S. K. Biswas, "Microgrid: A review," in *2013 IEEE Global Humanitarian Technology Conference: South Asia Satellite (GHTC-SAS)*, pp. 27–35, 2013.
- [56] M. H. Saeed, W. Fangzong, B. A. Kalwar, and S. Iqbal, "A review on microgrids' challenges & perspectives," *IEEE Access*, vol. 9, pp. 166502–166517, 2021.
- [57] B. M. Eid, N. A. Rahim, J. Selvaraj, and A. Elkhateb, "Control methods and objectives for electronically coupled distributed energy resources in microgrids: A review," *IEEE Systems Journal*, vol. 10, no. 2, pp. 446–458, 2016.
- [58] M. Ahmed, L. Meegahapola, A. Vahidnia, and M. Datta, "Stability and control aspects of microgrid architectures—a comprehensive review," *IEEE Access*, vol. 8, pp. 144730–144766, 2020.
- [59] J. Rocabert, A. Luna, F. Blaabjerg, and P. Rodríguez, "Control of power converters in ac microgrids," *IEEE Transactions on Power Electronics*, vol. 27, no. 11, pp. 4734–4749, 2012.
- [60] N. Salehi, H. Martínez-García, G. Velasco-Quesada, and J. M. Guerrero, "A comprehensive review of control strategies and optimization methods for individual and community microgrids," *IEEE Access*, vol. 10, pp. 15935–15955, 2022.
- [61] S. Ghosh, C. K. Chanda, and J. K. Das, "A comprehensive survey on communication technologies for a grid connected microgrid system," in *2021 International Conference on Artificial Intelligence and Smart Systems (ICAIS)*, pp. 1525–1528, 2021.
- [62] M. W. Altaf, M. T. Arif, S. N. Islam, and M. E. Haque, "Microgrid protection challenges and mitigation approaches—a comprehensive review," *IEEE Access*, vol. 10, pp. 38895–38922, 2022.
- [63] A. Hooshyar and R. Iravani, "Microgrid protection," *Proceedings of the IEEE*, vol. 105, no. 7, pp. 1332–1353, 2017.
- [64] H. Zou, S. Mao, Y. Wang, F. Zhang, X. Chen, and L. Cheng, "A survey of energy management in interconnected multi-microgrids," *IEEE Access*, vol. 7, pp. 72158–72169, 2019.
- [65] A. Dagar, P. Gupta, and V. Niranjana, "Microgrid protection: A comprehensive review," *Renewable and Sustainable Energy Reviews*, vol. 149, p. 111401, 2021.

- [66] S. Monesha, S. G. Kumar, and M. Rivera, "Methodologies of energy management and control in microgrid," *IEEE Latin America Transactions*, vol. 16, no. 9, pp. 2345–2353, 2018.
- [67] M. A. Jirdehi, V. S. Tabar, S. Ghassemzadeh, and S. Tohidi, "Different aspects of microgrid management: A comprehensive review," *Journal of Energy Storage*, vol. 30, p. 101457, 2020.
- [68] G. F. Reed, "Dc technologies: Solutions to electric power system advancements [guest editorial]," *IEEE Power and Energy Magazine*, vol. 10, no. 6, pp. 10–17, 2012.
- [69] D. J. Hammerstrom, "Ac versus dc distribution systems did we get it right?," in *2007 IEEE Power Engineering Society General Meeting*, pp. 1–5, 2007.
- [70] U. Manandhar, A. Ukil, and T. K. Kiat Jonathan, "Efficiency comparison of dc and ac microgrid," in *2015 IEEE Innovative Smart Grid Technologies - Asia (ISGT ASIA)*, pp. 1–6, 2015.
- [71] P. C. Loh, D. Li, Y. K. Chai, and F. Blaabjerg, "Autonomous operation of hybrid microgrid with ac and dc subgrids," *IEEE Transactions on Power Electronics*, vol. 28, no. 5, pp. 2214–2223, 2013.
- [72] A. Gupta, S. Doolla, and K. Chatterjee, "Hybrid ac–dc microgrid: Systematic evaluation of control strategies," *IEEE Transactions on Smart Grid*, vol. 9, no. 4, pp. 3830–3843, 2018.
- [73] I. S. 1547, "Ieee standard for interconnection and interoperability of distributed energy resources with associated electric power systems interfaces," *IEEE Std 1547-2018 (Revision of IEEE Std 1547-2003)*, pp. 1–138, 2018.
- [74] P. Basak, S. Chowdhury, S. Halder nee Dey, and S. Chowdhury, "A literature review on integration of distributed energy resources in the perspective of control, protection and stability of microgrid," *Renewable and Sustainable Energy Reviews*, vol. 16, no. 8, pp. 5545–5556, 2012.
- [75] H. Chen, T. N. Cong, W. Yang, C. Tan, Y. Li, and Y. Ding, "Progress in electrical energy storage system: A critical review," *Progress in Natural Science*, vol. 19, no. 3, pp. 291–312, 2009.
- [76] U. D. of Energy, "Benefits of demand response in electricity markets and recommendations for achieving them. a report to the united states congress pursuant to section 1252 of the energy policy act of 2005," technical report, Department of Energy, Washington, D.C., U.S., 2005.
- [77] H. Suyanto and R. Irawati, "Study trends and challenges of the development of microgrids," in *2017 6th IEEE International Conference on Advanced Logistics and Transport (ICALT)*, pp. 160–164, 2017.
- [78] H. Xu, X. Zhang, F. Liu, D. Zhu, R. Shi, H. Ni, and W. Cao, "Synchronization strategy of microgrid from islanded to grid-connected mode seamless transfer," in *2013 IEEE International Conference of IEEE Region 10 (TENCON 2013)*, pp. 1–4, 2013.

- [79] F. Tang, J. M. Guerrero, J. C. Vasquez, D. Wu, and L. Meng, "Distributed active synchronization strategy for microgrid seamless reconnection to the grid under unbalance and harmonic distortion," *IEEE Transactions on Smart Grid*, vol. 6, no. 6, pp. 2757–2769, 2015.
- [80] S. D'silva, M. Shadmand, S. Bayhan, and H. Abu-Rub, "Towards grid of microgrids: Seamless transition between grid-connected and islanded modes of operation," *IEEE Open Journal of the Industrial Electronics Society*, vol. 1, pp. 66–81, 2020.
- [81] A. D. Paquette and D. M. Divan, "Providing improved power quality in microgrids: Difficulties in competing with existing power-quality solutions," *IEEE Industry Applications Magazine*, vol. 20, no. 5, pp. 34–43, 2014.
- [82] S. F. Contreras, C. A. Cortes, and J. M. A. Myrzik, "Optimal microgrid planning for enhancing ancillary service provision," *Journal of Modern Power Systems and Clean Energy*, vol. 7, no. 4, pp. 862–875, 2019.
- [83] E. Dehghanpour, H. K. Karegar, and R. Kheirollahi, "Under frequency load shedding in inverter based microgrids by using droop characteristic," *IEEE Transactions on Power Delivery*, vol. 36, no. 2, pp. 1097–1106, 2021.
- [84] A. Bidram and A. Davoudi, "Hierarchical structure of microgrids control system," *IEEE Transactions on Smart Grid*, vol. 3, no. 4, pp. 1963–1976, 2012.
- [85] A. Timbus, A. Oudalov, and C. N. Ho, "Islanding detection in smart grids," in *2010 IEEE Energy Conversion Congress and Exposition*, pp. 3631–3637, 2010.
- [86] D. D. Reigosa, F. Briz, C. Blanco Charro, and J. M. Guerrero, "Passive islanding detection using inverter nonlinear effects," *IEEE Transactions on Power Electronics*, vol. 32, no. 11, pp. 8434–8445, 2017.
- [87] M. Seyedi, S. A. Taher, B. Ganji, and J. Guerrero, "A hybrid islanding detection method based on the rates of changes in voltage and active power for the multi-inverter systems," *IEEE Transactions on Smart Grid*, vol. 12, no. 4, pp. 2800–2811, 2021.
- [88] H. Laaksonen, "Advanced islanding detection functionality for future electricity distribution networks," *IEEE Transactions on Power Delivery*, vol. 28, no. 4, pp. 2056–2064, 2013.
- [89] J. Tao, H. Han, Z. Wang, Y. Shu, W. Fang, and Y. Li, "An advanced islanding detection strategy coordinating the newly proposed v detection and the rocof detection," in *2018 IEEE Innovative Smart Grid Technologies - Asia (ISGT Asia)*, pp. 1204–1208, 2018.
- [90] D. Reigosa, F. Briz, C. Blanco, P. García, and J. Manuel Guerrero, "Active islanding detection for multiple parallel-connected inverter-based distributed generators using high-frequency signal injection," *IEEE Transactions on Power Electronics*, vol. 29, no. 3, pp. 1192–1199, 2014.
- [91] I. S. 2030.7, "Ieee standard for the specification of microgrid controllers," *IEEE Std 2030.7-2017*, pp. 1–43, 2018.

- [92] M. Farrokhhabadi, C. A. Cañizares, J. W. Simpson-Porco, E. Nasr, L. Fan, P. A. Mendoza-Araya, R. Tonkoski, U. Tamrakar, N. Hatzargyriou, D. Lajos, R. W. Wies, M. Paolone, M. Liserre, L. Meegahapola, M. Kabalan, A. H. Hajimiragha, D. Peralta, M. A. Elizondo, K. P. Schneider, F. K. Tuffner, and J. Reilly, "Microgrid stability definitions, analysis, and examples," *IEEE Transactions on Power Systems*, vol. 35, no. 1, pp. 13–29, 2020.
- [93] A. Maitra, A. Pratt, T. Hubert, D. Wang, K. Prabakar, R. Handa, M. Baggu, and M. McGranaghan, "Microgrid controllers : Expanding their role and evaluating their performance," *IEEE Power and Energy Magazine*, vol. 15, no. 4, pp. 41–49, 2017.
- [94] S. Ansari, A. Chandel, and M. Tariq, "A comprehensive review on power converters control and control strategies of ac/dc microgrid," *IEEE Access*, vol. 9, pp. 17998–18015, 2021.
- [95] A. Srivastava, R. Mohanty, M. A. F. Ghazvini, L. A. Tuan, D. Steen, and O. Carlson, "A review on challenges and solutions in microgrid protection," in *2021 IEEE Madrid PowerTech*, pp. 1–6, 2021.
- [96] M. N. Naz, S. Imtiaz, M. K. L. Bhatti, W. Q. Awan, M. Siddique, and A. Riaz, "Dynamic stability improvement of decentralized wind farms by effective distribution static compensator," *Journal of Modern Power Systems and Clean Energy*, vol. 9, no. 3, pp. 516–525, 2021.
- [97] S. F. Zarei and M. Parniani, "A comprehensive digital protection scheme for low-voltage microgrids with inverter-based and conventional distributed generations," *IEEE Transactions on Power Delivery*, vol. 32, no. 1, pp. 441–452, 2017.
- [98] S. F. Zarei, H. Mokhtari, and F. Blaabjerg, "Fault detection and protection strategy for islanded inverter-based microgrids," *IEEE Journal of Emerging and Selected Topics in Power Electronics*, vol. 9, no. 1, pp. 472–484, 2021.
- [99] E. Dehghanpour, M. Normandeau, G. Joós, and Y. Brissette, "A protection system for inverter interfaced microgrids," *IEEE Transactions on Power Delivery*, vol. 37, no. 3, pp. 2314–2325, 2022.
- [100] F. Mumtaz, K. Imran, S. B. A. Bukhari, K. K. Mehmood, A. Abusorrah, M. A. Shah, and S. A. A. Kazmi, "A kalman filter-based protection strategy for microgrids," *IEEE Access*, vol. 10, pp. 73243–73256, 2022.
- [101] S. Wang, Z. Li, L. Wu, M. Shahidehpour, and Z. Li, "New metrics for assessing the reliability and economics of microgrids in distribution system," *IEEE Transactions on Power Systems*, vol. 28, no. 3, pp. 2852–2861, 2013.
- [102] T. Som and N. Chakraborty, "Studies on economic feasibility of an autonomous power delivery system utilizing alternative hybrid distributed energy resources," *IEEE Transactions on Power Systems*, vol. 29, no. 1, pp. 172–181, 2014.
- [103] S. Abu-Elzait and R. Parkin, "Economic and environmental advantages of renewable-based microgrids over conventional microgrids," in *2019 IEEE Green Technologies Conference (GreenTech)*, pp. 1–4, 2019.

- [104] A. Litchy, C. Young, S. Pourmousavi, and M. Nehrir, "Technology selection and unit sizing for a combined heat and power microgrid: Comparison of webopt and homer application programs," in *2012 North American Power Symposium (NAPS)*, pp. 1–6, 2012.
- [105] T. Ersal, C. Ahn, D. L. Peters, J. W. Whitefoot, A. R. Mechtenberg, I. A. Hiskens, H. Peng, A. G. Stefanopoulou, P. Y. Papalambros, and J. L. Stein, "Coupling between component sizing and regulation capability in microgrids," *IEEE Transactions on Smart Grid*, vol. 4, no. 3, pp. 1576–1585, 2013.
- [106] J. Mitra and M. R. Vallem, "Determination of storage required to meet reliability guarantees on island-capable microgrids with intermittent sources," *IEEE Transactions on Power Systems*, vol. 27, no. 4, pp. 2360–2367, 2012.
- [107] Y. Li, P. Wang, H. B. Gooi, J. Ye, and L. Wu, "Multi-objective optimal dispatch of microgrid under uncertainties via interval optimization," *IEEE Transactions on Smart Grid*, vol. 10, no. 2, pp. 2046–2058, 2019.
- [108] W. Yuan, Y. Wang, and Z. Chen, "New perspectives on power control of ac microgrid considering operation cost and efficiency," *IEEE Transactions on Power Systems*, vol. 36, no. 5, pp. 4844–4847, 2021.
- [109] A. Khodaei, "Microgrid optimal scheduling with multi-period islanding constraints," *IEEE Transactions on Power Systems*, vol. 29, no. 3, pp. 1383–1392, 2014.
- [110] W. Shi, X. Xie, C.-C. Chu, and R. Gadh, "Distributed optimal energy management in microgrids," *IEEE Transactions on Smart Grid*, vol. 6, no. 3, pp. 1137–1146, 2015.
- [111] Y. Zhang, N. Gatsis, and G. B. Giannakis, "Robust energy management for microgrids with high-penetration renewables," *IEEE Transactions on Sustainable Energy*, vol. 4, no. 4, pp. 944–953, 2013.
- [112] Q. Jiang, M. Xue, and G. Geng, "Energy management of microgrid in grid-connected and stand-alone modes," *IEEE Transactions on Power Systems*, vol. 28, no. 3, pp. 3380–3389, 2013.
- [113] N. Liu, Q. Chen, J. Liu, X. Lu, P. Li, J. Lei, and J. Zhang, "A heuristic operation strategy for commercial building microgrids containing evs and pv system," *IEEE Transactions on Industrial Electronics*, vol. 62, no. 4, pp. 2560–2570, 2015.
- [114] M. J. Rana, F. Zaman, T. Ray, and R. Sarker, "Heuristic enhanced evolutionary algorithm for community microgrid scheduling," *IEEE Access*, vol. 8, pp. 76500–76515, 2020.
- [115] F. Garcia-Torres, C. Bordons, J. Tobajas, R. Real-Calvo, I. Santiago, and S. Grieu, "Stochastic optimization of microgrids with hybrid energy storage systems for grid flexibility services considering energy forecast uncertainties," *IEEE Transactions on Power Systems*, vol. 36, no. 6, pp. 5537–5547, 2021.

- [116] T. Samad, E. Koch, and P. Stluka, "Automated demand response for smart buildings and microgrids: The state of the practice and research challenges," *Proceedings of the IEEE*, vol. 104, no. 4, pp. 726–744, 2016.
- [117] N. D. Tuyen, N. S. Quan, V. B. Linh, V. Van Tuyen, and G. Fujita, "A comprehensive review of cybersecurity in inverter-based smart power system amid the boom of renewable energy," *IEEE Access*, vol. 10, pp. 35846–35875, 2022.
- [118] M. Amin, F. F. M. El-Sousy, G. A. A. Aziz, K. Gaber, and O. A. Mohammed, "Cps attacks mitigation approaches on power electronic systems with security challenges for smart grid applications: A review," *IEEE Access*, vol. 9, pp. 38571–38601, 2021.
- [119] T. V. Vu, B. L. Nguyen, Z. Cheng, M.-Y. Chow, and B. Zhang, "Cyber-physical microgrids: Toward future resilient communities," *IEEE Industrial Electronics Magazine*, vol. 14, no. 3, pp. 4–17, 2020.
- [120] H.-M. Chung, W.-T. Li, C. Yuen, W.-H. Chung, and C.-K. Wen, "Local cyber-physical attack with leveraging detection in smart grid," in *2017 IEEE International Conference on Smart Grid Communications (SmartGridComm)*, pp. 461–466, 2017.
- [121] K. Manandhar, X. Cao, F. Hu, and Y. Liu, "Detection of faults and attacks including false data injection attack in smart grid using kalman filter," *IEEE Transactions on Control of Network Systems*, vol. 1, no. 4, pp. 370–379, 2014.
- [122] S. Sahoo, S. Mishra, J. C.-H. Peng, and T. Dragičević, "A stealth cyber-attack detection strategy for dc microgrids," *IEEE Transactions on Power Electronics*, vol. 34, no. 8, pp. 8162–8174, 2019.
- [123] T. R. B. Kushal, K. Lai, and M. S. Illindala, "Risk-based mitigation of load curtailment cyber attack using intelligent agents in a shipboard power system," *IEEE Transactions on Smart Grid*, vol. 10, no. 5, pp. 4741–4750, 2019.
- [124] S.-C. Yip, K. Wong, W.-P. Hew, M.-T. Gan, R. C.-W. Phan, and S.-W. Tan, "Detection of energy theft and defective smart meters in smart grids using linear regression," *International Journal of Electrical Power & Energy Systems*, vol. 91, pp. 230–240, 2017.
- [125] M. Esmalifalak, L. Liu, N. Nguyen, R. Zheng, and Z. Han, "Detecting stealthy false data injection using machine learning in smart grid," *IEEE Systems Journal*, vol. 11, no. 3, pp. 1644–1652, 2017.
- [126] K. Sun, W. Qiu, W. Yao, S. You, H. Yin, and Y. Liu, "Frequency injection based hvdc attack-defense control via squeeze-excitation double cnn," *IEEE Transactions on Power Systems*, vol. 36, no. 6, pp. 5305–5316, 2021.
- [127] J. L. Viegas and S. M. Vieira, "Clustering-based novelty detection to uncover electricity theft," in *2017 IEEE International Conference on Fuzzy Systems (FUZZ-IEEE)*, pp. 1–6, 2017.

- [128] M. N. Kurt, O. Ogundijo, C. Li, and X. Wang, "Online cyber-attack detection in smart grid: A reinforcement learning approach," *IEEE Transactions on Smart Grid*, vol. 10, no. 5, pp. 5174–5185, 2019.
- [129] U. Adhikari, T. H. Morris, and S. Pan, "Applying non-nested generalized exemplars classification for cyber-power event and intrusion detection," *IEEE Transactions on Smart Grid*, vol. 9, no. 5, pp. 3928–3941, 2018.
- [130] A. Fahad and E.-R. Ayman, "Functions of microgrid hierarchal control structure," in *2019 IEEE 7th International Conference on Smart Energy Grid Engineering (SEGE)*, pp. 17–25, 2019.
- [131] Y. Han, H. Li, P. Shen, E. A. A. Coelho, and J. M. Guerrero, "Review of active and reactive power sharing strategies in hierarchical controlled microgrids," *IEEE Transactions on Power Electronics*, vol. 32, no. 3, pp. 2427–2451, 2017.
- [132] F. de Bosio, L. A. De S. Ribeiro, M. S. Lima, F. Freijedo, J. M. Guerrero, and M. Pastorelli, "Inner current loop analysis and design based on resonant regulators for isolated microgrids," in *2015 IEEE 13th Brazilian Power Electronics Conference and 1st Southern Power Electronics Conference (COBEP/SPEC)*, pp. 1–6, 2015.
- [133] F. Blaabjerg, R. Teodorescu, M. Liserre, and A. Timbus, "Overview of control and grid synchronization for distributed power generation systems," *IEEE Transactions on Industrial Electronics*, vol. 53, no. 5, pp. 1398–1409, 2006.
- [134] J. Lopes, C. Moreira, and A. Madureira, "Defining control strategies for microgrids islanded operation," *IEEE Transactions on Power Systems*, vol. 21, no. 2, pp. 916–924, 2006.
- [135] H. Bevrani, T. Ise, and Y. Miura, "Virtual synchronous generators: A survey and new perspectives," *International Journal of Electrical Power & Energy Systems*, vol. 54, pp. 244–254, 2014.
- [136] M. Guan, W. Pan, J. Zhang, Q. Hao, J. Cheng, and X. Zheng, "Synchronous generator emulation control strategy for voltage source converter (vsc) stations," *IEEE Transactions on Power Systems*, vol. 30, no. 6, pp. 3093–3101, 2015.
- [137] J. Morren, J. Pierik, and S. W. de Haan, "Inertial response of variable speed wind turbines," *Electric Power Systems Research*, vol. 76, no. 11, pp. 980–987, 2006.
- [138] S. Anwar, A. Elrayyah, and Y. Sozer, "Efficient single-phase harmonics elimination method for microgrid operations," *IEEE Transactions on Industry Applications*, vol. 51, no. 4, pp. 3394–3403, 2015.
- [139] F. Nejabatkhah, Y. Li, and B. Wu, "Control strategies of three-phase distributed generation inverters for grid unbalanced voltage compensation," in *2015 IEEE Energy Conversion Congress and Exposition (ECCE)*, pp. 6467–6474, 2015.
- [140] M. Savaghebi, A. Jalilian, J. C. Vasquez, and J. M. Guerrero, "Autonomous voltage unbalance compensation in an islanded droop-controlled microgrid," *IEEE Transactions on Industrial Electronics*, vol. 60, no. 4, pp. 1390–1402, 2013.

- [141] Y. W. Li, D. M. Vilathgamuwa, and P. C. Loh, "A grid-interfacing power quality compensator for three-phase three-wire microgrid applications," *IEEE Transactions on Power Electronics*, vol. 21, no. 4, pp. 1021–1031, 2006.
- [142] P.-T. Cheng, C.-A. Chen, T.-L. Lee, and S.-Y. Kuo, "A cooperative imbalance compensation method for distributed-generation interface converters," *IEEE Transactions on Industry Applications*, vol. 45, no. 2, pp. 805–815, 2009.
- [143] M. M. A. Abdelaziz, M. F. Shaaban, H. E. Farag, and E. F. El-Saadany, "A multistage centralized control scheme for islanded microgrids with pevs," *IEEE Transactions on Sustainable Energy*, vol. 5, no. 3, pp. 927–937, 2014.
- [144] A. K. Basu, A. Bhattacharya, S. Chowdhury, and S. P. Chowdhury, "Planned scheduling for economic power sharing in a chp-based micro-grid," *IEEE Transactions on Power Systems*, vol. 27, no. 1, pp. 30–38, 2012.
- [145] P. Hasanpor Divshali, S. H. Hosseini, and M. Abedi, "A novel multi-stage fuel cost minimization in a vsc-based microgrid considering stability, frequency, and voltage constraints," *IEEE Transactions on Power Systems*, vol. 28, no. 2, pp. 931–939, 2013.
- [146] T. Caldognetto and P. Tenti, "Microgrids operation based on master–slave cooperative control," *IEEE Journal of Emerging and Selected Topics in Power Electronics*, vol. 2, no. 4, pp. 1081–1088, 2014.
- [147] G. G. Talapur, H. M. Suryawanshi, A. B. Shitole, and P. Nachankar, "Combined droop and master-slave method for load sharing in stand-alone ac microgrid," in *IECON 2018 - 44th Annual Conference of the IEEE Industrial Electronics Society*, pp. 1705–1710, 2018.
- [148] X. Sun, Y.-S. Lee, and D. Xu, "Modeling, analysis, and implementation of parallel multi-inverter systems with instantaneous average-current-sharing scheme," *IEEE Transactions on Power Electronics*, vol. 18, no. 3, pp. 844–856, 2003.
- [149] V. Nasirian, Q. Shafiee, J. M. Guerrero, F. L. Lewis, and A. Davoudi, "Droop-free distributed control for ac microgrids," *IEEE Transactions on Power Electronics*, vol. 31, no. 2, pp. 1600–1617, 2016.
- [150] A. Bidram, A. Davoudi, and F. L. Lewis, "A multiobjective distributed control framework for islanded ac microgrids," *IEEE Transactions on Industrial Informatics*, vol. 10, no. 3, pp. 1785–1798, 2014.
- [151] K. Yu, Q. Ai, S. Wang, J. Ni, and T. Lv, "Analysis and optimization of droop controller for microgrid system based on small-signal dynamic model," *IEEE Transactions on Smart Grid*, vol. 7, no. 2, pp. 695–705, 2016.
- [152] Y. Li and L. Fan, "Stability analysis of two parallel converters with voltage–current droop control," *IEEE Transactions on Power Delivery*, vol. 32, no. 6, pp. 2389–2397, 2017.

- [153] M. A. Hassan and M. A. Abido, "Optimal design of microgrids in autonomous and grid-connected modes using particle swarm optimization," *IEEE Transactions on Power Electronics*, vol. 26, no. 3, pp. 755–769, 2011.
- [154] C. Sao and P. Lehn, "Autonomous load sharing of voltage source converters," *IEEE Transactions on Power Delivery*, vol. 20, no. 2, pp. 1009–1016, 2005.
- [155] Y. Zhou and C. Ngai-Man Ho, "A review on microgrid architectures and control methods," in *2016 IEEE 8th International Power Electronics and Motion Control Conference (IPEMC-ECCE Asia)*, pp. 3149–3156, 2016.
- [156] J. Hu, Y. Shan, K. W. Cheng, and S. Islam, "Overview of power converter control in microgrids—challenges, advances, and future trends," *IEEE Transactions on Power Electronics*, vol. 37, no. 8, pp. 9907–9922, 2022.
- [157] C. K. Sao and P. W. Lehn, "Control and power management of converter fed microgrids," *IEEE Transactions on Power Systems*, vol. 23, no. 3, pp. 1088–1098, 2008.
- [158] B. Fan, Q. Li, W. Wang, G. Yao, H. Ma, X. Zeng, and J. M. Guerrero, "A novel droop control strategy of reactive power sharing based on adaptive virtual impedance in microgrids," *IEEE Transactions on Industrial Electronics*, vol. 69, no. 11, pp. 11335–11347, 2022.
- [159] J. He, Y. W. Li, J. M. Guerrero, F. Blaabjerg, and J. C. Vasquez, "An islanding microgrid power sharing approach using enhanced virtual impedance control scheme," *IEEE Transactions on Power Electronics*, vol. 28, no. 11, pp. 5272–5282, 2013.
- [160] A. Moawwad, V. Khadkikar, and J. L. Kirtley, "A new P-Q-V droop control method for an interline photovoltaic (i-pv) power system," *IEEE Transactions on Power Delivery*, vol. 28, no. 2, pp. 658–668, 2013.
- [161] W. Yao, M. Chen, J. Matas, J. M. Guerrero, and Z.-M. Qian, "Design and analysis of the droop control method for parallel inverters considering the impact of the complex impedance on the power sharing," *IEEE Transactions on Industrial Electronics*, vol. 58, no. 2, pp. 576–588, 2011.
- [162] J. Guerrero, L. G. de Vicuna, J. Matas, M. Castilla, and J. Miret, "Output impedance design of parallel-connected ups inverters with wireless load-sharing control," *IEEE Transactions on Industrial Electronics*, vol. 52, no. 4, pp. 1126–1135, 2005.
- [163] K. De Brabandere, B. Bolsens, J. Van den Keybus, A. Woyte, J. Driesen, and R. Belmans, "A voltage and frequency droop control method for parallel inverters," *IEEE Transactions on Power Electronics*, vol. 22, no. 4, pp. 1107–1115, 2007.
- [164] Y. Li and Y. W. Li, "Virtual frequency-voltage frame control of inverter based low voltage microgrid," in *2009 IEEE Electrical Power & Energy Conference (EPEC)*, pp. 1–6, 2009.

- [165] M. Golshan, "Adaptive voltage droop scheme for voltage source converters in an islanded multibus microgrid," *IET Generation, Transmission & Distribution*, vol. 4, pp. 562–578(16), May 2010.
- [166] H. Mahmood, D. Michaelson, and J. Jiang, "Reactive power sharing in islanded microgrids using adaptive voltage droop control," *IEEE Transactions on Smart Grid*, vol. 6, no. 6, pp. 3052–3060, 2015.
- [167] Y. Zhang and H. Ma, "Theoretical and experimental investigation of networked control for parallel operation of inverters," *IEEE Transactions on Industrial Electronics*, vol. 59, no. 4, pp. 1961–1970, 2012.
- [168] M. Marwali, J.-W. Jung, and A. Keyhani, "Control of distributed generation systems - part ii: Load sharing control," *IEEE Transactions on Power Electronics*, vol. 19, no. 6, pp. 1551–1561, 2004.
- [169] A. Tuladhar, H. Jin, T. Unger, and K. Mauch, "Control of parallel inverters in distributed ac power systems with consideration of line impedance effect," *IEEE Transactions on Industry Applications*, vol. 36, no. 1, pp. 131–138, 2000.
- [170] E. Espina, M. Espinoza, and R. Cárdenas, "Active power angle droop control per phase for unbalanced 4-wire microgrids," in *2017 IEEE Southern Power Electronics Conference (SPEC)*, pp. 1–6, 2017.
- [171] R. Majumder, B. Chaudhuri, A. Ghosh, R. Majumder, G. Ledwich, and F. Zare, "Improvement of stability and load sharing in an autonomous microgrid using supplementary droop control loop," *IEEE Transactions on Power Systems*, vol. 25, no. 2, pp. 796–808, 2010.
- [172] C.-T. Lee, C.-C. Chu, and P.-T. Cheng, "A new droop control method for the autonomous operation of distributed energy resource interface converters," *IEEE Transactions on Power Electronics*, vol. 28, no. 4, pp. 1980–1993, 2013.
- [173] Y. Khayat, Q. Shafiee, R. Heydari, M. Naderi, T. Dragičević, J. W. Simpson-Porco, F. Dörfler, M. Fathi, F. Blaabjerg, J. M. Guerrero, and H. Bevrani, "On the secondary control architectures of ac microgrids: An overview," *IEEE Transactions on Power Electronics*, vol. 35, no. 6, pp. 6482–6500, 2020.
- [174] B. de Nadai Nascimento, A. C. Zambroni de Souza, D. Marujo, J. E. Sarmiento, C. A. Alvez, F. M. Portelinho Jr, and J. G. de Carvalho Costa, "Centralised secondary control for islanded microgrids," *IET Renewable Power Generation*, vol. 14, no. 9, pp. 1502–1511, 2020.
- [175] A. Micallef, M. Apap, C. Spiteri-Staines, J. M. Guerrero, and J. C. Vasquez, "Reactive power sharing and voltage harmonic distortion compensation of droop controlled single phase islanded microgrids," *IEEE Transactions on Smart Grid*, vol. 5, no. 3, pp. 1149–1158, 2014.
- [176] A. Milczarek, M. Malinowski, and J. M. Guerrero, "Reactive power management in islanded microgrid—proportional power sharing in hierarchical droop control," *IEEE Transactions on Smart Grid*, vol. 6, no. 4, pp. 1631–1638, 2015.

- [177] M. Yazdani and A. Mehrizi-Sani, "Washout filter-based power sharing," *IEEE Transactions on Smart Grid*, vol. 7, no. 2, pp. 967–968, 2016.
- [178] M. Castilla, A. Camacho, J. Miret, M. Velasco, and P. Martí, "Local secondary control for inverter-based islanded microgrids with accurate active power sharing under high-load conditions," *IEEE Transactions on Industrial Electronics*, vol. 66, no. 4, pp. 2529–2539, 2019.
- [179] W. Gu, G. Lou, W. Tan, and X. Yuan, "A nonlinear state estimator-based decentralized secondary voltage control scheme for autonomous microgrids," *IEEE Transactions on Power Systems*, vol. 32, no. 6, pp. 4794–4804, 2017.
- [180] Q. Shafiee, c. Stefanovic, T. Dragicevic, P. Popovski, J. C. Vasquez, and J. M. Guerrero, "Robust networked control scheme for distributed secondary control of islanded microgrids," *IEEE Transactions on Industrial Electronics*, vol. 61, no. 10, pp. 5363–5374, 2014.
- [181] Q. Shafiee, J. M. Guerrero, and J. C. Vasquez, "Distributed secondary control for islanded microgrids—a novel approach," *IEEE Transactions on Power Electronics*, vol. 29, no. 2, pp. 1018–1031, 2014.
- [182] J. W. Simpson-Porco, Q. Shafiee, F. Dörfler, J. C. Vasquez, J. M. Guerrero, and F. Bullo, "Secondary frequency and voltage control of islanded microgrids via distributed averaging," *IEEE Transactions on Industrial Electronics*, vol. 62, no. 11, pp. 7025–7038, 2015.
- [183] J. Lai, X. Lu, X. Li, and R.-L. Tang, "Distributed multiagent-oriented average control for voltage restoration and reactive power sharing of autonomous microgrids," *IEEE Access*, vol. 6, pp. 25551–25561, 2018.
- [184] Q. Shafiee, V. Nasirian, u. C. Vasquez, J. M. Guerrero, and A. Davoudi, "A multi-functional fully distributed control framework for ac microgrids," *IEEE Transactions on Smart Grid*, vol. 9, no. 4, pp. 3247–3258, 2018.
- [185] J. Schiffer, T. Seel, J. Raisch, and T. Sezi, "Voltage stability and reactive power sharing in inverter-based microgrids with consensus-based distributed voltage control," *IEEE Transactions on Control Systems Technology*, vol. 24, no. 1, pp. 96–109, 2016.
- [186] Y. Zhang, A. M. Shotorbani, L. Wang, and B. Mohammadi-Ivatloo, "Distributed secondary control of a microgrid with a generalized pi finite-time controller," *IEEE Open Access Journal of Power and Energy*, vol. 8, pp. 57–67, 2021.
- [187] M. Shi, X. Chen, J. Zhou, Y. Chen, J. Wen, and H. He, "Pi-consensus based distributed control of ac microgrids," *IEEE Transactions on Power Systems*, vol. 35, no. 3, pp. 2268–2278, 2020.
- [188] J. Lai, H. Zhou, X. Lu, X. Yu, and W. Hu, "Droop-based distributed cooperative control for microgrids with time-varying delays," *IEEE Transactions on Smart Grid*, vol. 7, no. 4, pp. 1775–1789, 2016.

- [189] S. Weng, D. Yue, C. Dou, J. Shi, and C. Huang, "Distributed event-triggered cooperative control for frequency and voltage stability and power sharing in isolated inverter-based microgrid," *IEEE Transactions on Cybernetics*, vol. 49, no. 4, pp. 1427–1439, 2019.
- [190] X. Ge and Q.-L. Han, "Distributed formation control of networked multi-agent systems using a dynamic event-triggered communication mechanism," *IEEE Transactions on Industrial Electronics*, vol. 64, no. 10, pp. 8118–8127, 2017.
- [191] J. Choi, S. I. Habibi, and A. Bidram, "Distributed finite-time event-triggered frequency and voltage control of ac microgrids," *IEEE Transactions on Power Systems*, vol. 37, no. 3, pp. 1979–1994, 2022.
- [192] Z. Wang, H. Jiang, H. He, and Y. L. Sun, "Distributed finite-time economic dispatch for islanded microgrids," in *2020 IEEE Power & Energy Society General Meeting (PESGM)*, pp. 1–5, 2020.
- [193] C. Zhou and C. Zheng, "Economic optimization model of islanded microgrid considering the benefit of energy storage charge and discharge," in *2020 15th IEEE Conference on Industrial Electronics and Applications (ICIEA)*, pp. 839–844, 2020.
- [194] Z. Tang, D. J. Hill, and T. Liu, "A novel consensus-based economic dispatch for microgrids," *IEEE Transactions on Smart Grid*, vol. 9, no. 4, pp. 3920–3922, 2018.
- [195] H. Xia, Q. Li, R. Xu, T. Chen, J. Wang, M. A. S. Hassan, and M. Chen, "Distributed control method for economic dispatch in islanded microgrids with renewable energy sources," *IEEE Access*, vol. 6, pp. 21802–21811, 2018.
- [196] F. Alshammari and A. El-Refaie, "Generalized droop control for mixed impedance microgrid," in *2021 IEEE PES Innovative Smart Grid Technologies - Asia (ISGT Asia)*, pp. 1–5, 2021.
- [197] S. A. R. Konakalla, A. Valibeygi, and R. A. de Callafon, "Microgrid dynamic modeling and islanding control with synchrophasor data," *IEEE Transactions on Smart Grid*, vol. 11, no. 1, pp. 905–915, 2020.
- [198] F. Alshammari and A. El-Refaie, "Distributed averaging optimization-based technique for microgrid secondary control," in *2020 IEEE Energy Conversion Congress and Exposition (ECCE)*, pp. 1343–1350, 2020.
- [199] F. Alshammari and A. El-Refaie, "Time-varying optimization-based consensus control for microgrid's secondary control," in *2021 IEEE Power & Energy Society Innovative Smart Grid Technologies Conference (ISGT)*, pp. 1–5, 2021.
- [200] S. Boyd and L. Vandenberghe, *Convex Optimization*. Cambridge University Press, mar 2004.
- [201] S. Rahili and W. Ren, "Distributed continuous-time convex optimization with time-varying cost functions," *IEEE Transactions on Automatic Control*, vol. 62, pp. 1590–1605, apr 2017.

- [202] J. Mattingley and S. Boyd, "CVXGEN: a code generator for embedded convex optimization," *Optimization and Engineering*, vol. 13, no. 1, pp. 1–27, 2012.
- [203] F. Alshammari and A. El-Refai, ""economic dispatch-based secondary control for islanded microgrid"." "unpublished", "2022".
- [204] *Benchmark systems for network integration of renewable and distributed energy resources*. No. April, 2014.
- [205] J. L. López-Prado, J. W. González-Sánchez, J. I. Vélez, and G. A. Garcia-Llinás, "Reliability assessment in rural distribution systems with microgrids: A computational- based approach," *IEEE Access*, vol. 10, pp. 43327–43340, 2022.
- [206] R. A. Osama, A. F. Zobaa, and A. Y. Abdelaziz, "A planning framework for optimal partitioning of distribution networks into microgrids," *IEEE Systems Journal*, vol. 14, no. 1, pp. 916–926, 2020.
- [207] Z. Zhang, D. Yue, C. Dou, and H. Zhang, "Multiagent system-based integrated design of security control and economic dispatch for interconnected microgrid systems," *IEEE Transactions on Systems, Man, and Cybernetics: Systems*, vol. 51, no. 4, pp. 2101–2112, 2021.
- [208] A. Cagnano, E. De Tuglie, and P. Gibilisco, "Assessment and control of microgrid impacts on distribution networks by using experimental tests," *IEEE Transactions on Industry Applications*, vol. 55, no. 6, pp. 7157–7164, 2019.
- [209] J. Zhang, D. Qin, Y. Ye, Y. He, X. Fu, J. Yang, G. Shi, and H. Zhang, "Multi-time scale economic scheduling method based on day-ahead robust optimization and intraday mpc rolling optimization for microgrid," *IEEE Access*, vol. 9, pp. 140315–140324, 2021.
- [210] Y. Gao and Q. Ai, "Demand-side response strategy of multi-microgrids based on an improved co-evolution algorithm," *CSEE Journal of Power and Energy Systems*, vol. 7, no. 5, pp. 903–910, 2021.
- [211] F. L. Lewis, H. Zhang, K. Hengster-Movric, and A. Das, *Cooperative control of multi-agent systems: optimal and adaptive design approaches*. Springer Science & Business Media, 2013.
- [212] S. Diamond, "Disciplined convex programming." <https://dcp.stanford.edu>, accessed: August, 2022 [Online].

APPENDIX A  
PRELIMINARY ON GRAPH THEORY

In Chapter 4, the communication network is modeled as a graph with directed edges corresponding to the information flow between units. Units are modeled as nodes on the graph, called agents. The overall dynamical system representing these nodes is called a multi-agent dynamical system. The dynamical system interacts with the agents' local feedback control protocols to produce the interconnected nodes' overall behaviors. This appendix is based mainly on [211].

### A.1 Definitions and Connectivity

A graph is made up of the pair  $\mathcal{G}(\mathcal{V}, \mathcal{E})$  where  $\mathcal{V} = \{\mathcal{V}_1, \dots, \mathcal{V}_N\}$  is a collection of  $N$  nodes or vertices and  $E$  is a collection of arcs or edges. Elements of  $E$  are depicted as an arrow with a tail at  $\mathcal{V}_i$  and a head at  $\mathcal{V}_j$  and are labeled as  $(\mathcal{V}_i, \mathcal{V}_j)$ , which is known as an edge or arc from  $\mathcal{V}_i$  to  $\mathcal{V}_j$ . The graph is assumed to be simple for the sake of this study, meaning that there are no self-loops and no duplicate edges connecting the same pairs of nodes  $(\mathcal{V}_i, \mathcal{V}_i)$ , i.e.,  $(\mathcal{V}_i, \mathcal{V}_i) \notin \mathcal{E}, \forall i$ . For an edge  $(\mathcal{V}_i, \mathcal{V}_j)$ , node  $\mathcal{V}_i$  is referred to as the parent and node  $\mathcal{V}_j$  as the child, and edge  $(\mathcal{V}_i, \mathcal{V}_j)$  is said to be outgoing with respect to node  $\mathcal{V}_i$  and incoming with respect to node  $\mathcal{V}_j$ . The in-degree of  $\mathcal{V}_i$  is the number of edges having  $\mathcal{V}_i$  as a head, and the out-degree of a node  $\mathcal{V}_i$  is the number of edges having  $\mathcal{V}_i$  as a tail. The set of (in-degree) neighbors of a node  $\mathcal{V}_i$  is denoted as  $N_i = \{\mathcal{V}_j : (\mathcal{V}_j, \mathcal{V}_i) \in \mathcal{E}\}$ , i.e., the set of nodes with edges incoming to  $\mathcal{V}_i$ . The in-degree of the node  $\mathcal{V}_i$  is equal to the number of neighbors  $|N_i|$ .

When the in-degree for each node  $\mathcal{V}_i \in \mathcal{V}$  equals the out-degree, the graph is said to be balanced. The graph is referred to as bidirectional if  $(\mathcal{V}_i, \mathcal{V}_j) \in \mathcal{E} \Rightarrow (\mathcal{V}_j, \mathcal{V}_i) \in \mathcal{E}, \forall i, j$ , otherwise as a directed graph or digraph. The weight  $a_{ij}$  is associated with each edge  $(\mathcal{V}_j, \mathcal{V}_i) \in \mathcal{E}$ . The nonzero weights in this analysis are presumed to be strictly positive. A graph is said to be undirected if  $a_{ij} = a_{ji}, \forall i, j$ , i.e. if it is bidirectional and the weights of edges  $(\mathcal{V}_i, \mathcal{V}_j)$  and  $(\mathcal{V}_j, \mathcal{V}_i)$  are the same.

A sequence of nodes  $\mathcal{V}_0, \mathcal{V}_1, \dots, \mathcal{V}_r$  such that  $(\mathcal{V}_i, \mathcal{V}_{i+1}) \in \mathcal{E}, i \in \{0, 1, \dots, r-1\}$  is known as a directed path. The node  $\mathcal{V}_i$  is connected to the node  $\mathcal{V}_j$  if there is a directed path from  $\mathcal{V}_i$  to  $\mathcal{V}_j$ . The distance from  $\mathcal{V}_i$  to  $\mathcal{V}_j$  is the length of the shortest path from  $\mathcal{V}_i$  to  $\mathcal{V}_j$ . Graph  $\mathcal{G}$  is strongly connected if  $\mathcal{V}_i, \mathcal{V}_j$  are connected for all distinct nodes  $\mathcal{V}_i, \mathcal{V}_j \in \mathcal{V}$ . For both bidirectional and undirected graphs, when there is a directed path from  $\mathcal{V}_i$  to  $\mathcal{V}_j$ , then there is a directed path from  $\mathcal{V}_j$  to  $\mathcal{V}_i$ .

A directed tree is a connected digraph in which each node except one, called a root, has an in-degree equal to 1. A spanning tree of a digraph is a directed tree formed by graph edges that connects all graph nodes. A graph is said to have a spanning tree if a subset of the edges creates a directed tree. This implies that all nodes in the graph can be reached from a single node, the root, by following the edge arrows. A graph may have more than one spanning tree. Define the root set or the leader set of a graph as the set of nodes that are the roots of all spanning trees. The graph is strongly connected if it at least contains one spanning tree. If a graph is strongly connected, then all nodes are root nodes.

## A.2 Graph Matrices

Given the edge weights  $a_{ij}$ , an adjacency or connectivity matrix of a graph  $A = [a_{ij}]$  can be represented with weights  $a_{ij} > 0$  if  $(\mathcal{V}_j, \mathcal{V}_i) \in E$  and  $a_{ij} = 0$  otherwise. Self-edges are not allowed (i.e.,  $a_{ii}=0$ ) unless otherwise indicated. Define the weighted in-degree of node  $\mathcal{V}_i$  as the  $i^{th}$  row sum of  $A$

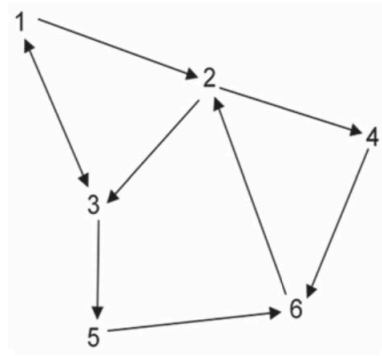
$$d_i = \sum_{j=1}^N a_{ij} \quad (\text{A.1})$$

And the weighted out-degree of node  $\mathcal{V}_i$  as the  $i^{th}$  column sum of  $A$

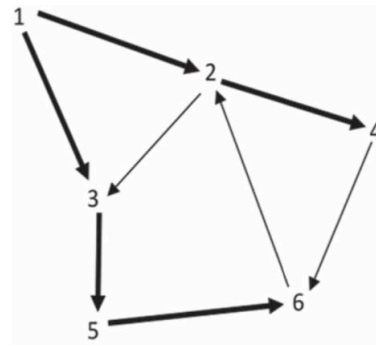
$$d_i^o = \sum_{j=1}^N a_{ji} \quad (\text{A.2})$$

The in-degree and out-degree are local properties of the graph. The adjacency matrix  $A$  of an undirected graph is symmetric, such that  $A = A^T$ . If the weighted in-degree is equal to the weighted out-degree for all  $i$ , then the graph is considered to be weighted balanced. If all the nonzero edge weights are equal to 1, this is similar to the definition of a balanced graph. An undirected graph is weight balanced since if  $A = A^T$ , then the  $i^{th}$  row sum equals the  $i^{th}$  column sum.

Defining the diagonal in-degree matrix  $D = \text{diag}(d_i)$ , the weighted graph Laplacian matrix is given as  $\mathcal{L} = D - A$ . Note that, the graph Laplacian matrix  $\mathcal{L}$  has all row sums equal to zero. The graph Laplacian matrix is essential in the study of dynamical multi-agent systems on graphs. Many properties of a graph are studied in terms of the graph Laplacian matrix.



(a) A directed graph.



(b) Spanning tree in the directed graph.

Figure A.1: An example of a directed graph.

### A.3 Directed Graph Example

Consider the directed graph shown in Figure A.1 with all edge weights equal to 1. The graph is strongly connected since there is a path between any two nodes. A spanning tree with root node 1 is shown in bold in Figure A.1. There are other spanning trees in the graph. Every node is a root node since the graph is strongly connected.

The adjacency matrix  $A$ , the diagonal in-degree matrix  $D$ , and graph Laplacian matrix  $\mathcal{L}$  are given by.

$$A = \begin{bmatrix} 0 & 0 & 1 & 0 & 0 & 0 \\ 1 & 0 & 0 & 0 & 0 & 1 \\ 1 & 1 & 0 & 0 & 0 & 0 \\ 0 & 1 & 0 & 0 & 0 & 0 \\ 0 & 0 & 1 & 0 & 0 & 0 \\ 0 & 0 & 0 & 1 & 1 & 0 \end{bmatrix} \quad D = \begin{bmatrix} 1 & 0 & 0 & 0 & 0 & 0 \\ 0 & 2 & 0 & 0 & 0 & 0 \\ 0 & 0 & 2 & 0 & 0 & 0 \\ 0 & 1 & 0 & 1 & 0 & 0 \\ 0 & 0 & 1 & 0 & 1 & 0 \\ 0 & 0 & 0 & 0 & 0 & 2 \end{bmatrix} \quad \mathcal{L} = \begin{bmatrix} 1 & 0 & -1 & 0 & 0 & 0 \\ -1 & 2 & 0 & 0 & 0 & -1 \\ -1 & -1 & 2 & 0 & 0 & 0 \\ 0 & -1 & 0 & 1 & 0 & 0 \\ 0 & 0 & -1 & 0 & 1 & 0 \\ 0 & 0 & 0 & -1 & -1 & 2 \end{bmatrix}$$

## APPENDIX B CVX/CVXGEN

In Chapters 4 and 5, a convex optimization solver is used to provide functionalities of the secondary control level. CVX/CVXGEN software tool generates a real-time custom solver with high-speed capabilities suitable for secondary control applications. In this appendix, the CVX/CVXGEN software tool is introduced to transform the convex optimization problem to C-code. Furthermore, the optimization problems, given in Chapter 4 and Chapter 5, are shown.

### B.1 An Overview

CVX/ CVXGEN is a software tool that takes high-level descriptions of convex optimization problems and generates custom C-Code to create a reliable and fast solver for a class of convex optimization problems. Using disciplined convex programming (DCP) techniques, convex optimization problems are reduced into small convex quadratic programs. CVX/CVXGEN generates code that is simple and library-free, making it suited for embedding in real-time applications. Because the produced code is branch-free, its runtime behavior is predictable. The combination of static and dynamic regularization, as well as iterative refinement in the search direction computation, results in a high-performance solver [202].

The CVX/CVXGEN code generator creates source code based on a problem family description generated using disciplined convex programming. The source code is then compiled into a customized embedded solution. Finally, in a real-time application, the input is directly fed into the embedded solution, yielding an optimal point  $x^*$  as shown in Figure B.1.

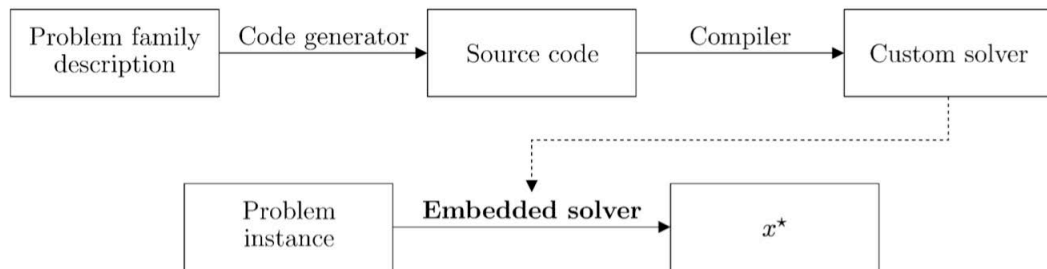


Figure B.1: The process of generating a custom solver in CVX/CVXGEN.

## B.2 Generating the Custom Code

The optimization function is required to be converted to disciplined convex programming before it is processed in the CVX/CVXGEN to generate the custom code. Figure B.2 and Figure B.3 show the problems given in Chapters 4 and 5, correspondingly.

```

1
2 parameters
3   Wnom
4   Vnom
5   Vmin
6   Vmax
7   P
8   Q
9   W
10  V
11  Kp
12  Kq
13  Xw
14  Xv
15 end
16
17 variables
18   ew
19   ev
20 end
21
22 minimize
23   quad(Wnom-W+ew-Xw) + quad(Vnom-V+ev-Xv)
24 subject to
25   ew == Kp*P
26   Vmin <= Vnom-Kq*Q+ev <= Vmax
27 end

```

Figure B.2: Optimization problem of Chapter 4 converted to DCP.

CVX/CVXGEN conducts syntax, dimension, and convexity checks on each problem description. Then, it converts the description into a custom C solver. CVX/CVXGEN requires no configuration more than the problem description to generate the solver. Several settings, including the duality gap boundaries, equality and inequality residuals, maximum number of iterations, and other settings, can be modified for the designed solver.

```

1 dimensions
2   n=4
3 end
4
5 parameters
6   ai(n,n) symmetric psd
7   bi(n)
8   Pmax(n)
9   Qmax(n)
10  dw(n)
11  dv(n)
12  Kpi(n,n)
13  Kqi(n,n)
14  Pg(n)
15  Qg(n)
16  I(n)
17 end
18
19 variables
20   P(n)
21   Q(n)
22 end
23
24 minimize
25   quad(Kpi*dw+P,ai) + bi'*(Kpi*dw+P)
26 subject to
27   Kpi*dw+P <= Pmax
28   Q <= Qmax
29   sum(Pg) == sum(P)
30   Qg==Q
31 end

```

Figure B.3: Optimization problem of Chapter 5 converted to DCP.

## APPENDIX C CIGRE NORTH AMERICA MICROGRID BENCHMARK

In Chapter 6, the North America LV distribution system CIGRE benchmark is used to validate the proposed controllers. The CIGRE distribution system includes three feeder types; residential, industrial, and commercial. The commercial subnetwork is selected in this dissertation for its suitability for the proposed controllers' features, including balanced three phases and the voltage level. In this appendix, the North America LV distribution system CIGRE benchmark for commercial application, used in Chapter 6 is discussed in terms of specifications and system parameters.

### C.1 An Overview

The CIGRE benchmark network for low-voltage distribution (LV) reflects a real-world LV network that supports user flexibility for studying DER integration. The benchmark for the LV distribution system is specified for residential, industrial, and commercial feeders; however, any combination of these feeders can be utilized to model a particular study. Figure C.1 shows the single-line diagram of the LV distribution network for the North America benchmark, including residential, industrial, and commercial feeders.

### C.2 System specifications

The structure and specifications of the North American LV distribution network benchmark differ from those of the European one. The North American LV distribution network has a system frequency of 60Hz, and the nominal voltage varies depending on the feeder type. The LV distribution system is radial in design, with consumers connecting anywhere along the lines. Because the residential feeder contains single-phase loads, it is intrinsically imbalanced. The lines can be underground or overhead. Underground lines are typically found in densely populated urban areas, while overhead lines are found in rural areas.

### C.3 Network Data

The commercial LV distribution network benchmark for North America is used as a microgrid benchmark in this dissertation, where the point of common coupling (PCC) is located at C0 in Figure C.1. In Table C.3, the line installation data, including connections and line types for the commercial feeder is shown where OH stands for the overhead line and UG for the underground line.

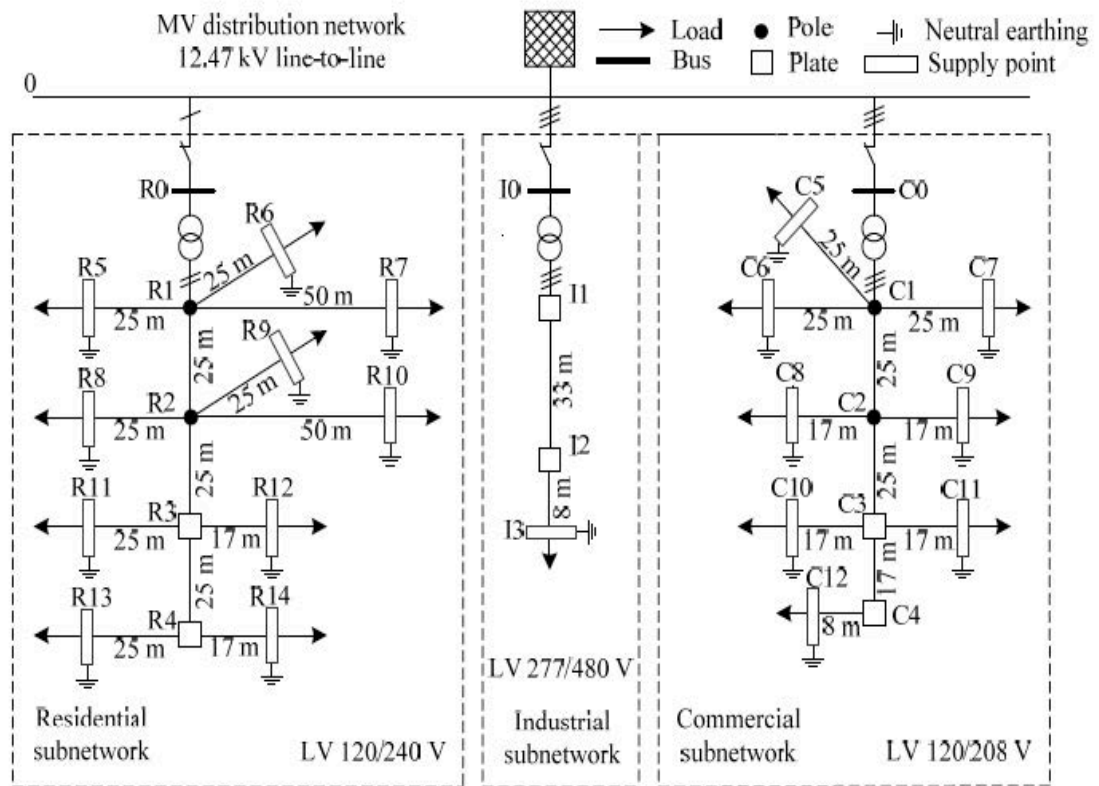


Figure C.1: CIGRE North America LV distribution network benchmark

The primitive impedance matrices for overhead lines are shown in Table C.3 and for underground in Table C.3. The coupling impedance between phases is not considered in Chapter 6. These data are accommodated to 3-ph and  $\Omega/m$  to be used on the system in MATLAB/SIMULINK.

#### C.4 Loads Data

Table C.4 shows the values of the peak loads for all nodes of the commercial feeder benchmark. The single-phase values assume 120 V. Each load represents a group of users. The data is presented in terms of apparent power and corresponding power factor.

Table C.1: Connections and line parameters of the commercial feeder of North American LV distribution network benchmark

Line segment	Node from	Node to	Conductor ID/[m]	Installation	
1	C1	C2	OH1	25	OH 3-ph
2	C2	C3	UG3	25	UG 3-ph
3	C3	C4	UG3	17	UG 3-ph
4	C1	C5	OH3	25	OH 3-ph
5	C1	C6	OH3	25	OH 3-ph
6	C1	C7	OH3	25	OH 3-ph
7	C2	C8	OH3	17	OH 3-ph
8	C2	C9	OH3	17	OH 3-ph
9	C3	C10	UG4	17	UG 3-ph
10	C3	C11	UG4	17	UG 3-ph
11	C4	C12	UG4	8	UG 3-ph

Table C.2: Primitive impedance matrices of three-phase overhead lines of North American LV distribution network benchmark

Conductor ID/ Installation		The primitive impedance matrix [ $\Omega/km$ ]			
		A	B	C	N
OH1 / 3-ph	A	$0.161 + j0.859$	$0.059 + j0.780$	$0.059 + j0.754$	$0.059 + j0.780$
	B	$0.059 + j0.780$	$0.161 + j0.859$	$0.059 + j0.780$	$0.059 + j0.754$
	C	$0.059 + j0.754$	$0.059 + j0.780$	$0.161 + j0.859$	$0.059 + j0.780$
	N	$0.059 + j0.780$	$0.059 + j0.754$	$0.059 + j0.780$	$0.161 + j0.859$
OH3 / 3-ph	A	$1.151 + j0.955$	$0.059 + j0.860$	$0.059 + j0.834$	$0.059 + j0.860$
	B	$0.059 + j0.860$	$1.151 + j0.955$	$0.059 + j0.860$	$0.059 + j0.834$
	C	$0.059 + j0.834$	$0.059 + j0.860$	$1.151 + j0.955$	$0.059 + j0.860$
	N	$0.059 + j0.860$	$0.059 + j0.834$	$0.059 + j0.860$	$1.151 + j0.955$

Table C.3: Primitive impedance matrices of three-phase underground lines of North American LV distribution network benchmark

Conductor ID/ Installation		The primitive impedance matrix [ $\Omega/km$ ]			
		A	B	C	N
UG3 / 3-ph	A	$0.402 + j0.908$	$0.059 + j0.823$	$0.059 + j0.797$	$0.059 + j0.823$
	B	$0.059 + j0.823$	$0.402 + j0.908$	$0.059 + j0.823$	$0.059 + j0.797$
	C	$0.059 + j0.797$	$0.059 + j0.823$	$0.402 + j0.908$	$0.059 + j0.823$
	N	$0.059 + j0.823$	$0.059 + j0.797$	$0.059 + j0.823$	$0.402 + j0.908$
UG4 / 3-ph	A	$1.151 + j0.955$	$0.059 + j0.860$	$0.059 + j0.834$	$0.059 + j0.860$
	B	$0.059 + j0.860$	$1.151 + j0.955$	$0.059 + j0.860$	$0.059 + j0.834$
	C	$0.059 + j0.834$	$0.059 + j0.860$	$1.151 + j0.955$	$0.059 + j0.860$
	N	$0.059 + j0.860$	$0.059 + j0.834$	$0.059 + j0.860$	$1.151 + j0.955$

Table C.4: Load parameters of North American LV distribution network benchmark

Node	Apparent Power, S [KVAS]	Power Factor, $pf$
C5	10.1	0.90
C6	13.5	0.90
C7	16.9	0.85
C8	13.5	0.90
C9	16.9	0.95
C10	10.1	0.95
C11	16.9	0.95
C12	10.1	0.9